DEVELOPMENT OF MULTIDIMENSIONAL SEPARATIONS USING MICROFLUIDIC DEVICES FOR PROTEOMICS APPLICATIONS

Andrew George Chambers

A dissertation submitted to the faculty of the University of North Carolina at Chapel Hill in partial fulfillment of the requirements for the degree of Doctor of Philosophy in the Department of Chemistry.

Chapel Hill
2010

Approved by:

Professor J. Michael Ramsey

Professor James W. Jorgenson

Professor Gary L. Glish

Professor Dorothy A. Erie

Professor Christopher J. Fecko

ABSTRACT

Andrew George Chambers

DEVELOPMENT OF MULTIDIMENSIONAL SEPARATIONS USING MICROFLUIDIC DEVICES FOR PROTEOMICS APPLICATIONS
(Under the direction of J. Michael Ramsey)

This work describes the development of novel microfluidic tools for the analysis of complex peptide mixtures. Gradient elution electrochromatography utilizing a reversed-phase monolith stationary phase is demonstrated on a microchip device. Porous polymer monoliths were patterned within glass microchips by photopolymerization of acrylate monomers. Mobile phase gradients were readily produced on-chip by computer-controlled mixing of solvents. Isocratic and gradient separations of protein digests were preformed to evaluate this device.

Several two-dimensional (2D) separation systems were constructed for online coupling of liquid chromatography (LC) and capillary electrophoresis (CE). First, a hybrid 2D LC-CE system was constructed to perform LC in a capillary column and transfer the effluent to a microchip for CE with laser-induced fluorescence (LIF) detection. This basic hybrid 2D LC-CE system was then directly interfaced with mass spectrometry (MS) detection by microfabricating an electrospray ionization (ESI) emitter on the microchip device. This system new was used for rapid peptide mass fingerprinting of monoclonal antibody digests to confirm antibody identity and modification. In a third 2D system, the LC dimension was also integrated to produce a microchip device capable

of performing LC-CE-ESI. This microchip incorporated a sample-trapping region and an LC channel packed with reversed-phase particles. In addition to LC-CE-ESI, this device was used for LC-ESI without any instrumental modifications.

Finally, a dual microfluidic ESI source will be discussed for increasing the mass accuracy of microchip ESI measurements. This device featured two independent ESI emitters that were used to sequentially introduce ions from two solutions into a mass spectrometer. Using the second emitter to introduce a reference compound for internal calibration, accurate mass measurements (< 3 ppm mass error) were obtained with the microchip dual ESI device and time-of-flight MS.

ACKNOWLEDGEMENTS

I would like to thank Dr. J. Michael Ramsey for his support and guidance of my research. In addition, I thank all of the Ramsey group members for their help and camaraderie over the years. In particular, I am grateful to J.P. Alarie for getting me up to speed with all of the instrumentation when I joined the group. I would also like to recognize Dr. J. Scott Mellors for his contributions to many of the 2D LC-CE projects. Finally, I would like to thank my family and friends for all their love and support during the last five years.

TABLE OF CONTENTS

LIST OF FIGURES

LIST OF ABBERVIATIONS

1D	one-dimensional
2D	two-dimensional
2D-PAGE	two-dimensional polyacrylamide gel electrophoresis
AIBN	2,2'-azobisisobutyronitrile
AMPS	2-acrylamido-2-methyl-1-propanesulfonic acid
BGE	background electrolyte
BPI	base peak index
BSA	bovine serum albumin
CCD	charge-coupled device
CE	capillary electrophoresis
CEC	capillary electrochromatography
cm	centimeter
°C	degrees Celsius
Da	dalton
EOF	electroosmotic flow
ESI	electrospray ionization
HPLC	high performance liquid chromatography
Hz	Hertz
i.d.	inner diameter
IEF	isoelectric focusing
kV	kilovolt
LC	liquid chromatography

LIF	laser-induced fluorescence
lys-C	lysyl endopeptidase
m	meter
MEKC	micellar electrokinetic chromatography
mg	milligram
min	minute
mL	milliliter
mm	millimeter
mM	millimolar
mAb	monoclonal antibody
ms	millisecond
MS	mass spectrometry
mW	milliwatt
MW	molecular weight
m/z	mass to charge ratio
µL	microliter
µm	micrometer
µM	micromolar
nL	nanoliter
nm	nanometer
o.d.	outer diameter
PLGS	ProteinLynx Global Server
PTFE	polytetrafluoroethylene

QTof	quadrupole-time of flight
RSD	relative standard deviation
s	seconds
SDS	sodium dodecyl sulfate
SEM	scanning electron microscope
SMO	statistical model of overlap
Tof	time of flight
TRITC	tetramethylrhodamine isothiocyanate
UV	ultra-violet
V	volt

LIST OF SYMBOLS

E	electric field strength
ϵ	dielectric constant
ϵ_o	permittivity of free space
H	height equivalent theoretical plate
L	length
m	total number of components in sample
N	number of theoretical plates
n_c	peak capacity
η	viscosity
p	probability of separating all components in a sample
R_s	resolution
s	number of separated components
σ	standard deviation
t_{run}	elapsed time from injection to detection of last peak
t_{window}	elapsed time for the separation window
u_{eo}	electroosmotic velocity
μ_{eo}	electroosmotic mobility
μ_{ep}	electrophoretic mobility
ζ	zeta potential

CHAPTER 1: Introduction to Multidimensional Separations for Proteomics

1.1 Motivation

1.1.1 Proteomics and the Complexity of Biological Samples

Proteomics is the global study of all proteins in an organism to determine how protein expression and interaction regulate biological pathways. This information is crucial to improving our fundamental understanding of physiology and has immediate application in the diagnosis, monitoring and treatment of disease. One key step in deciphering the proteome is the ability to identify and quantify proteins and peptides in biological samples. This task is extremely challenging due to the complexity of biological systems. For example, the human genome codes for approximately 20,000 to 25,000 proteins.[1] The actual number of proteins expressed is likely orders of magnitude higher due to several factors including alternative messenger ribonucleic acid splicing[2] and post-translational modifications.[3] In addition, the range of protein concentration in some samples is a least ten orders of magnitude.[4] To further complicate matters, protein expression changes in with time and in response to various environmental stimuli.

The comprehensive analysis of proteins in biological samples is dominated by mass spectrometry (MS)-based analytical methods because of their ability to unambiguously identify species by providing accurate mass and structural information.[5-6] There are two distinct strategies known as “bottom-up” and “top-down” proteomics. In the bottom-up approach, proteins are enzymatically cleaved into their constituent

peptides prior to separation and MS analysis. The MS data is then used to search protein sequence databases to identify the original proteins in the sample. Alternatively, top-down approaches focus on the separation and MS analysis of intact proteins. There are many advantages and disadvantages to each approach that depend on the specific data desired. A comprehensive approach combines data from both top-down and bottom-up approaches to obtain the most complete data set from the sample. Regardless of which approach is selected, one of the largest obstacles in identifying proteins is sample complexity, which must be reduced prior to introduction into a mass spectrometer.

1.1.2 The Necessity for High Peak Capacity

It may be useful to review a few metrics for assessing the performance of an analytical separation to further define what is necessary to separate complex biological samples. The broadening of an analyte band as it travels through the separation space can be described using the height equivalent theoretical plate, H, which is calculated by,[7]

$$H = \sigma^2 / L \tag{1-1}$$

where σ is the standard deviation of the peak width and L is the length that the peak is displaced. The total number of plates, N, is the number of H units contained in the separation path,[7]

$$N = L / H \tag{1-2}$$

The separation efficiency is typically reported in units of theoretical plates per meter (N/m). High separation efficiency results in narrower peak widths and therefore less peak separation will be needed to resolve them. While separation efficiency is an important metric, it does not fully define the ability to separate a large number of

components. For this purpose, it may be better to use peak capacity, n_c, which is defined as the maximum number of peaks that can theoretically fit in a given separation space,[7]

$$n_c = L/(4\,\sigma\,R_s) \tag{1-3}$$

where L is the space over which the peak may be distributed and the last peak and R_s is the resolution between adjacent peaks. This equation assumes that peaks of equal width are evenly spaced at the highest density that allowed for a given resolution. In practice, peaks are rarely spaced at even intervals and are often overlapped. Thus a peak capacity value of 100 is not sufficient to resolve a mixture of 100 components. The peak capacity required to resolve all components in a complex mixture for a given confidence interval can be described using the statistical model of overlap (SMO).[8] This model assumes that peaks are randomly distributed throughout the given separation space. Using SMO theory the probability that any given component will be resolved by a one-dimensional (1D) separation can be calculated by[8]

$$p = s/m = e^{-2(m/n_c)} \tag{1-4}$$

where s is the number of successfully resolved components and m is the total number components in the sample. Figure 1-1 illustrates this probability as a percentage of components that are resolved ($s/m * 100$) for mixtures containing 100, 250, 500 and 1,000 components. This shows that a peak capacity of 500 is expected to resolve 67% of components in a 100 component mixture. However, this same peak capacity is only capable of resolving 1.8% of a 1,000 component mixture. If the goal is to resolve 950 components in a 1,000 component mixture ($s/m * 100 = 95\%$), then the peak capacity required is 39,000.

Current 1D separation methods lack the peak capacity to separate even moderately complex biological mixtures. For example, reversed-phase liquid chromatography (LC) is among the best 1D separation methods for proteins and peptides. The highest reported peak capacity to date for reversed-phase LC separations of peptides is 1,500.[9] Using Equation 1-4, a peak capacity of 1,500 will only resolve 0.13% a sample that contained 5,000 peptides. It is readily apparent that this level of separation power is inadequate to resolve highly complex samples that may contain hundreds of thousands of peptides. The inability to resolve peaks results in a loss of information as overlapping peaks prevents identification and quantification when using a general detection scheme, such as ultraviolet (UV)-absorbance. MS detection can differentiate between several components introduced simultaneously; however, efficient sample ionization and data interpretation becomes problematic when large numbers of components are introduced together. In general, increasing the resolving power of the separation will increase the number of proteins identified in the original sample. The development of analytical instrumentation that can rapidly generate larger peak capacities is a critical step to advancing proteomic research.

1.2 Multidimensional Separations

1.2.1 Theory

Multidimensional separations are one strategy for dramatically increasing peak capacity. The illustration of a two-dimensional (2D) separation in Figure 1-2 can be used to describe the basic concept for improving the overall resolution. A 1D separation of a complex sample results in peaks that contain multiple components and in reality these peaks will also be overlapped as discussed in the preceding section. Subjecting these

peaks to a second separation provides another opportunity for components to be resolved. Giddings described two general criteria for maximizing the peak capacity of a multidimensional separation method.[10] First, separations to be coupled should be orthogonal so that there is no correlation in selectivity. Generally, different separation mechanisms are coupled so each separates the sample based on a different set of chemical or physical properties. The need for othogonality is illustrated using a 2D separation in Figure 1-3. If the selectivity is the same in both dimensions, then the peaks will fall along a diagonal line without increasing resolution as shown in Figure 1-3A. Conversely, a large difference in selectivity will result in peaks being distributed across the entire 2D separation space as shown in Figure 1-3B. This additional resolution may also allow multiple components within the original peaks to be resolved. The second criterion for multidimensional separations states that the resolution obtained in any dimension must be retained. If these two criteria are met, then the maximum peak capacity is the product of the peak capacity in each dimension,[10]

$$n_{c_{total}} = n_{c_1} \times n_{c_2} \times n_{c_3} \cdots \tag{1-5}$$

For example, a two dimensional (2D) separation method with a modest peak capacity of 150 in the first dimension and 50 in the second dimension could be coupled to produce a total peak capacity of 7,500.

It is important to point out that peak capacities generated by 1D and 2D separations are not equivalent. An extension of SMO theory reveals that the probability of resolving any given component by a 2D separation is[11]

$$p = s/m = e^{-4(m/n_c)} \tag{1-6}$$

This equation shows that twice the peak capacity is needed for a 2D separation to resolve the same number of components as a 1D separation. Figure 1-4 illustrates this difference by comparing the peak capacity required to separate 50% of the components ($s/m * 100 = 50\%$) in a 100 component mixture using 1D and 2D methods. Fortunately, 2D separation methods often increase the peak capacity by many fold to provide a large net gain in the ability to resolve complex mixtures.

1.2.2 Conventional 2D Separations

Two-dimensional polyacrylamide gel electrophoresis (2D-PAGE) is the most common multidimensional separation method used in the analysis of proteins.[12] This method utilizes isoelectric focusing (IEF) to separate proteins by their isoelectric point followed by sodium dodecyl sulfate polyacrylamide gel electrophoresis (SDS-PAGE) to further resolve proteins essentially by size. 2D-PAGE is a very powerful protein separation method as it can routinely resolve thousands of proteins.[13] Following the separation, proteins of interest are typically excised from the gel and enzymatically digested prior to analysis by MS. Although 2D-PAGE can provide a high resolving power, this method suffers from key limitations.[13-15] This method is not well suited to the analysis of several classes of proteins as very large or hydrophobic proteins do not efficiently load into the gel and alkaline proteins are often poorly resolved. The separation often takes days to complete and is difficult to automate. The reproducibility of 2D-PAGE is poor due to considerable variation in polyacrylamide gel preparation and this is especially problematic for quantitative analysis. Finally, protein identification generally requires each resolved spot to be excised from the gel, prepared, and introduced

into the mass spectrometer individually. This laborious procedure makes comprehensive identification of complex samples largely impractical.

To address some of the limitations of 2D-PAGE, several column-based 2D separation methods have been developed. These 2D methods couple linear separation columns by collecting fractions from the first dimension and injecting this material onto the second dimension. One large advantage of column-based 2D separations is that they are readily coupled with MS detection via electrospray ionization (ESI).[16] Columns may be coupled using an offline or online strategy. Offline column coupling requires fractions from the first dimension to be stored for later analysis by the second dimension. In online column coupling, fractions from the first column are immediately injected onto the second column for analysis. The main advantage of online column coupling is that the entire analysis is completed in the time required for the first dimension. This requires that the separation in second dimension is completed rapidly to prevent undersampling of the first dimension. In theory, peaks from the first dimension should be sampled 3-4 times by the second dimension to preserve the resolution already obtained.[17]

The majority of online 2D methods utilize LC in both dimensions (LC-LC), such as ion exchange chromatography followed by reversed-phase chromatography.[18-22] This is largely due to the relative ease in coupling these separations as a standard LC valve can readily transfer fractions from the first column onto the second. However, it is generally difficult to complete the second dimension fast enough to keep up with the peaks eluting from the first dimension. Several alterative separation methods involving capillary electrophoresis (CE) have also been explored including LC-CE, CE-LC, and CE-CE.[23-26]

1.2.3 Microfluidic 2D Separations

Microfluidic devices provide a fundamentally different platform for performing chemical analysis.[27-28] These microfabricated devices, also known as Lab-on-a-Chip or Micro Total Analysis Systems, are characterized by a network of interconnecting fluidic channels created in a single planer substrate. Typical channels have dimensions in the micron range and are readily fabricated using well established technologies borrowed from the semi-conductor industry. These properties give microfluidic devices inherent advantages over traditional instrumentation for chemical analysis. The confined channel environment enables precise manipulation of fluid volumes in the picoliter to microliter range. The reduced length scale also decreases sample and reagent consumption and often leads to shorter analysis time. Parallel fabrication can reduce instrumentation cost and enable highly multiplexed systems, increasing sample throughput. The most important advantage is the ability to integrate several fluidic operations on the same device. This enables minute samples to be rapidly transported between several sequential processing steps with near zero band broadening. Integration can also reduce the complexity of the instrumentation and facilitate automation. Over the last two decades, numerous fluidic operations have been successfully implemented on microfluidic devices to enable a wide range of chemical analyses to be performed.[29-34] In addition, there have been many strategies reported for coupling these devices with MS detection via ESI.[35-37]

There has been considerable development of 2D separations on microfluidic devices.[38-39] Nearly all reports have coupled two electrokinetically-driven separation mechanisms due to the ease at which electroosmotic flow (EOF) can be controlled. One of the first microfluidic 2D separations described used micellar electrokinetic

chromatography (MEKC) coupled with CE.[40] Later improvements to this device allowed for a peak capacity of approximately 4,000 to be generated for protein digests in less than 15 min.[41] Shadpour and coworkers coupled gel CE with MEKC resulting in a peak capacity of over 1,000 for proteins in 12 min.[42] Multiple groups have reported devices that perform IEF-CE that are able to generate peak capacities in excess of 1,700 for proteins in less than 15 min.[43-44] This represents a reduction in analysis time of approximately two orders of magnitude when compared with conventional 2D-PAGE. These examples clearly demonstrate the power of microfluidic 2D separation systems to rapidly separate biological samples. The next crucial step towards comprehensive analysis of biological samples using microfluidic devices is the development of 2D separations that can be directly integrated with MS detection.

1.3 Figures

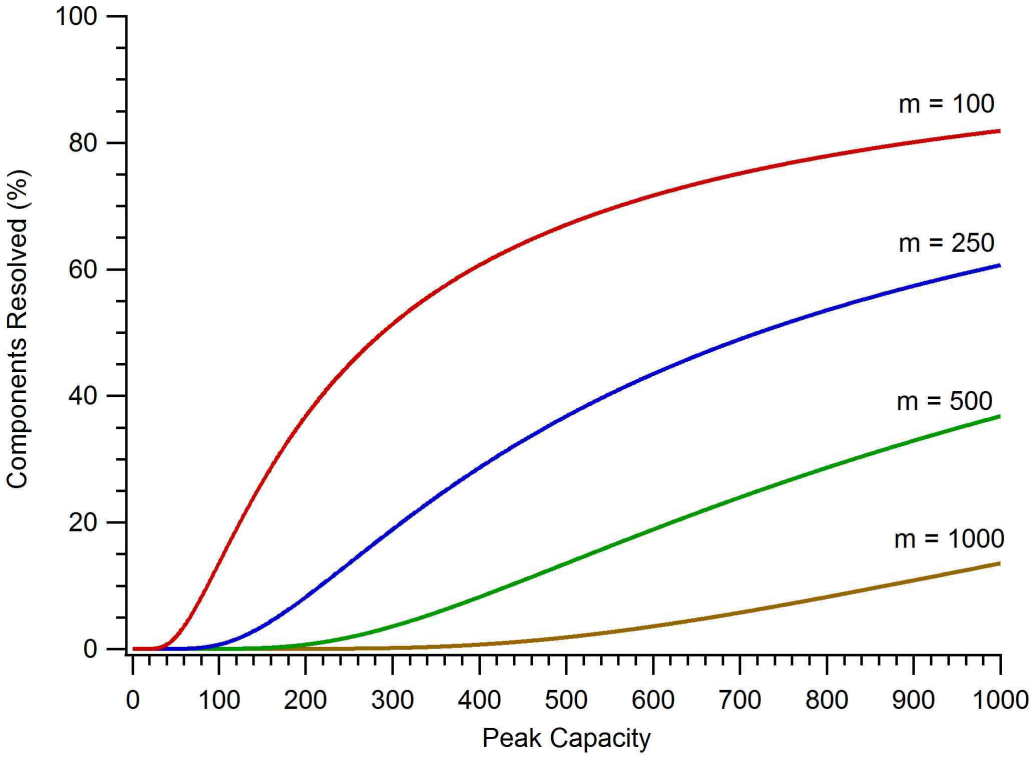

Figure 1-1. The percentage of components resolved as a function of peak capacity for a 1D separation using SMO theory. Traces are shown for mixtures containing 100, 250, 500, and 1,000 components.

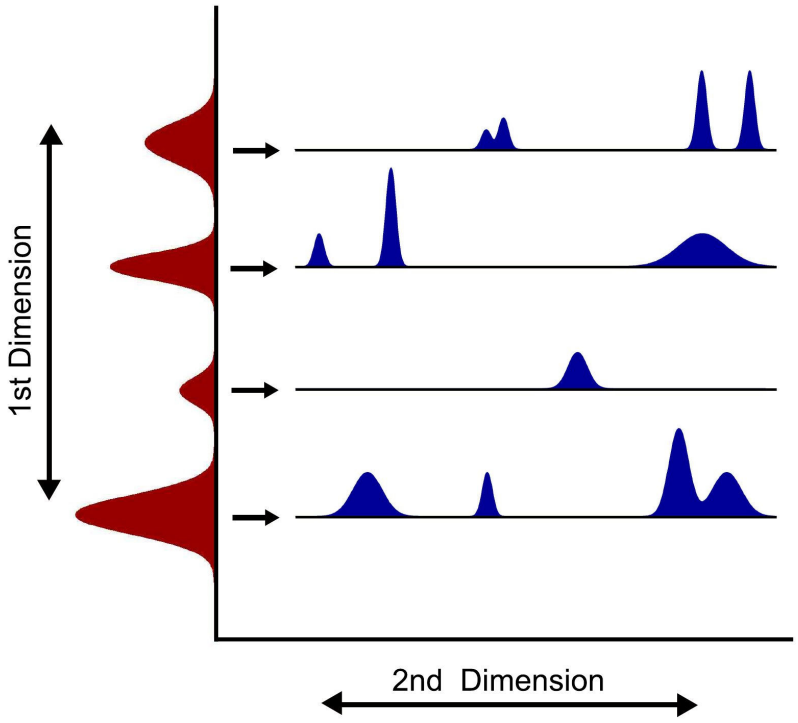

Figure 1-2. General strategy for 2D separations. Peaks from the first dimension are subjected to a second dimension of separation to increase the overall resolving power.

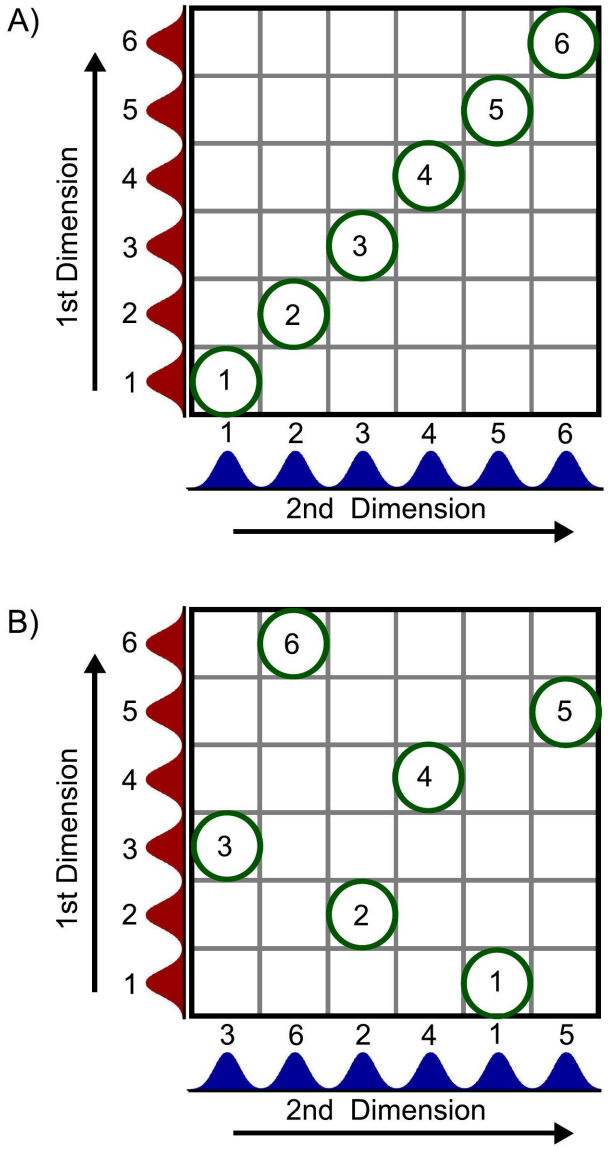

Figure 1-3. Illustration of the need for orthogonality in 2D separation methods. A) non-orthogonal, B) orthogonal

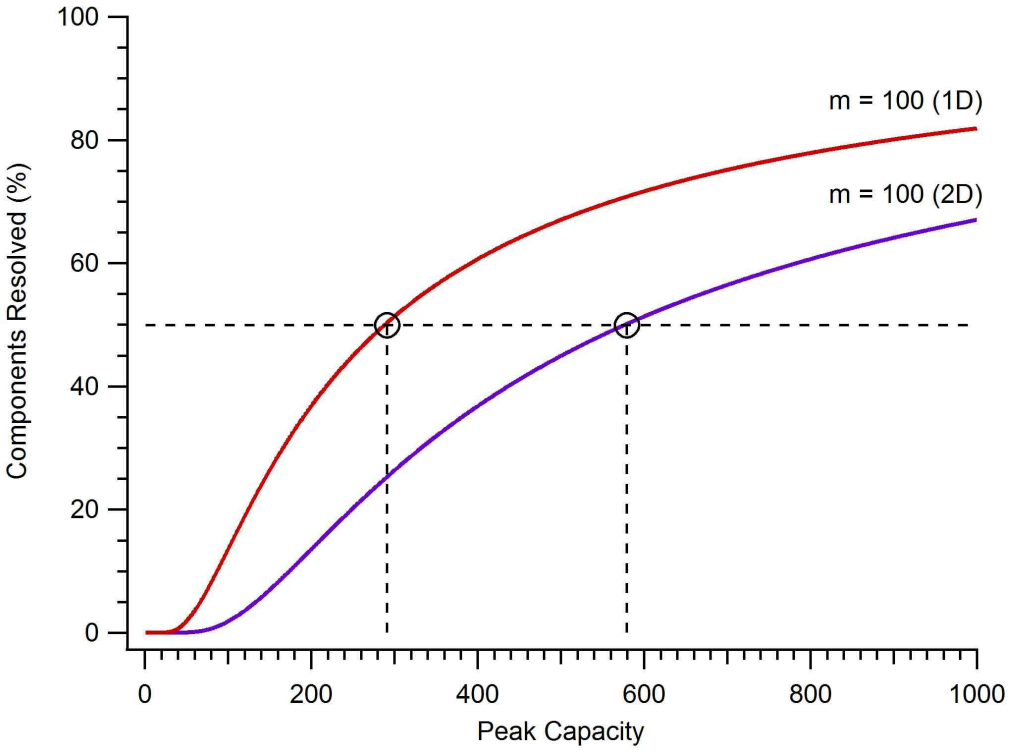

Figure 1-4. The percentage of components resolved as a function of peak capacity for a 1D and 2D separation of a 100 component mixture using SMO theory.

1.4 References

1. Collins, F. S.; Lander, E. S.; Rogers, J.; Waterston, R. H.; Int Human Genome Sequencing, C. Finishing the euchromatic sequence of the human genome. *Nature* **2004**, *431*, 931.

2. Matlin, A. J.; Clark, F.; Smith, C. W. J. Understanding alternative splicing: Towards a cellular code. *Nat. Rev. Mol. Cell Bio.* **2005**, *6*, 386.

3. Uy, R.; Wold, F. Post-translational covalent modification of proteins. *Science* **1977**, *198*, 890.

4. Anderson, N. L.; Anderson, N. G. The human plasma proteome - History, character, and diagnostic prospects. *Mol. Cell Proteomics* **2002**, *1*, 845.

5. Domon, B.; Aebersold, R. Review - Mass spectrometry and protein analysis. *Science* **2006**, *312*, 212.

6. Yates, J. R.; Ruse, C. I.; Nakorchevsky, A. Proteomics by mass spectrometry: Approaches, advances, and applications. *Annu. Rev. Biomed. Eng.* **2009**, *11*, 49.

7. Giddings, J. C. *Unified Separation Science*; John Wiley & Sons, Inc.: New York, NY, 1991.

8. Davis, J. M.; Giddings, J. C. Statistical-theory of component overlap in multicomponent chromatograms *Anal. Chem.* **1983**, *55*, 418.

9. Shen, Y. F.; Zhang, R.; Moore, R. J.; Kim, J.; Metz, T. O.; Hixson, K. K.; Zhao, R.; Livesay, E. A.; Udseth, H. R.; Smith, R. D. Automated 20 kpsi RPLC-MS and MS/MS with chromatographic peak capacities of 1000-1500 and capabilities in proteomics and metabolomics. *Anal. Chem.* **2005**, *77*, 3090.

10. Giddings, J. C. Two-dimensional separations - concept and promise. *Anal. Chem.* **1984**, *56*, 1258A.

11. Davis, J. M. Statistical-theory of spot overlap in 2-dimensional separations *Anal. Chem.* **1991**, *63*, 2141.

12. Ofarrell, P. H. High-resolution 2-dimensional electrophoresis of proteins. *J. Biol. Chem.* **1975**, *250*, 4007.

13. Lopez, J. L. Two-dimensional electrophoresis in proteome expression analysis. *J. Chromatogr. B* **2007**, *849*, 190.

14. Vercauteren, F. G. G.; Arckens, L.; Quirion, R. Applications and current challenges of proteomic approaches, focusing on two-dimensional electrophoresis. *Amino Acids* **2007**, *33*, 405.

15. Chevalier, F. Highlights on the capacities of "Gel-based" proteomics. *Proteome Sci.* **2010**, *8*.

16. Fenn, J. B.; Mann, M.; Meng, C. K.; Wong, S. F.; Whitehouse, C. M. Electrospray ionization for mass-spectrometry of large biomolecules *Science* **1989**, *246*, 64.

17. Murphy, R. E.; Schure, M. R.; Foley, J. P. Effect of sampling rate on resolution in comprehensive two-dimensional liquid chromatography. *Anal. Chem.* **1998**, *70*, 1585.

18. Stoll, D. R.; Li, X. P.; Wang, X. O.; Carr, P. W.; Porter, S. E. G.; Rutan, S. C. Fast, comprehensive two-dimensional liquid chromatography. *J. Chromatogr. A* **2007**, *1168*, 3.

19. Dugo, P.; Cacciola, F.; Kumm, T.; Dugo, G.; Mondello, L. Comprehensive multidimensional liquid chromatography: Theory and applications. *J. Chromatogr. A* **2008**, *1184*, 353.

20. Guiochon, G.; Marchetti, N.; Mriziq, K.; Shalliker, R. A. Implementations of two-dimensional liquid chromatography. *J. Chromatogr. A* **2008**, *1189*, 109.

21. Zhang, X.; Fang, A. Q.; Riley, C. P.; Wang, M.; Regnier, F. E.; Buck, C. Multi-dimensional liquid chromatography in proteomics-A review. *Anal. Chim. Acta* **2010**, *664*, 101.

22. Horvatovich, P.; Hoekman, B.; Govorukhina, N.; Bischoff, R. Multidimensional chromatography coupled to mass spectrometry in analysing complex proteomics samples. *J. Sep. Sci.* **2010**, *33*, 1421.

23. Cooper, J. W.; Wang, Y. J.; Lee, C. S. Recent advances in capillary separations for proteomics. *Electrophoresis* **2004**, *25*, 3913.

24. Evans, C. R.; Jorgenson, J. W. Multidimensional LC-LC and LC-CE for high-resolution separations of biological molecules. *Anal. Bioanal. Chem.* **2004**, *378*, 1952.

25. Stroink, T.; Ortiz, M. C.; Bult, A.; Lingeman, H.; de Jong, G. J.; Underberg, W. J. M. On-line multidimensional liquid chromatography and capillary electrophoresis systems for peptides and proteins. *J. Chromatogr. B* **2005**, *817*, 49.

26. Sandra, K.; Moshir, M.; D'Hondt, F.; Tuytten, R.; Verleysen, K.; Kas, K.; Francois, I.; Sandra, P. Highly efficient peptide separations in proteomics Part 2: Bi- and multidimensional liquid-based separation techniques. *J. Chromatogr. B* **2009**, *877*, 1019.

27. Whitesides, G. M. The origins and the future of microfluidics. *Nature* **2006**, *442*, 368.

28. Kutter, J. P.; Fintschenko, Y. *Separation Methods in Microanalytical Systems*; CRC Press Taylor and Francis Group: Boca Raton, FL, 2006.

29. Reyes, D. R.; Iossifidis, D.; Auroux, P. A.; Manz, A. Micro total analysis systems. 1. Introduction, theory, and technology. *Anal. Chem.* **2002**, *74*, 2623.

30. Auroux, P. A.; Iossifidis, D.; Reyes, D. R.; Manz, A. Micro total analysis aystems. 2. Analytical standard operations and applications. *Anal. Chem.* **2002**, *74*, 2637.

31. Vilkner, T.; Janasek, D.; Manz, A. Micro total analysis systems. Recent developments. *Anal. Chem.* **2004**, *76*, 3373.

32. Dittrich, P. S.; Tachikawa, K.; Manz, A. Micro total analysis systems. Latest advancements and trends. *Anal. Chem.* **2006**, *78*, 3887.

33. West, J.; Becker, M.; Tombrink, S.; Manz, A. Micro total analysis systems: Latest achievements. *Anal. Chem.* **2008**, *80*, 4403.

34. Arora, A.; Simone, G.; Salieb-Beugelaar, G. B.; Kim, J. T.; Manz, A. Latest developments in micro total analysis systems. *Anal. Chem.* **2010**, *82*, 4830.

35. Lazar, I. M.; Grym, J.; Foret, F. Microfabricated devices: A new sample introduction approach to mass spectrometry. *Mass Spectrom. Rev.* **2006**, *25*, 573.

36. Foret, F.; Kusy, P. Microfluidics for multiplexed MS analysis. *Electrophoresis* **2006**, *27*, 4877.

37. Koster, S.; Verpoorte, E. A decade of microfluidic analysis coupled with electrospray mass spectrometry: An overview. *Lab Chip* **2007**, *7*, 1394.

38. Chen, H.; Fan, Z. H. Two-dimensional protein separation in microfluidic devices. *Electrophoresis* **2009**, *30*, 758.

39. Tia, S.; Herr, A. E. On-chip technologies for multidimensional separations. *Lab Chip* **2009**, *9*, 2524.

40. Rocklin, R. D.; Ramsey, R. S.; Ramsey, J. M. A microfabricated fluidic device for performing two-dimensional liquid-phase separations. *Anal. Chem.* **2000**, *72*, 5244.

41. Ramsey, J. D.; Jacobson, S. C.; Culbertson, C. T.; Ramsey, J. M. High-efficiency, two-dimensional separations of protein digests on microfluidic devices. *Anal. Chem.* **2003**, *75*, 3758.

42. Shadpour, H.; Soper, S. A. Two-dimensional electrophoretic separation of proteins using poly(methyl methacrylate) microchips. *Anal. Chem.* **2006**, *78*, 3519.

43. Li, Y.; Buch, J. S.; Rosenberger, F.; DeVoe, D. L.; Lee, C. S. Integration of isoelectric focusing with parallel sodium dodecyl sulfate gel electrophoresis for multidimensional protein separations in a plastic microfludic network. *Anal. Chem.* **2004**, *76*, 742.

44. Yang, S.; Liu, J. K.; Lee, C. S.; Devoe, D. L. Microfluidic 2-D PAGE using multifunctional in situ polyacrylamide gels and discontinuous buffers. *Lab Chip* **2009**, *9*, 592.

CHAPTER 2: Gradient Elution Capillary Electrochromatography using Monolith Stationary Phases on a Microfluidic Device

2.1 Introduction

In capillary electrochromatography (CEC), the mobile phase is driven through separation column or channel by electroosmosis. The velocity of this electroosmotic flow (EOF), u_{eo}, can be determined by,

$$u_{\text{eo}} = \frac{\zeta \epsilon_o \epsilon E}{\eta} \tag{2-1}$$

where ζ is the zeta potential, ϵ_o is the permittivity of free space, ϵ is the dielectric constant of the electrolyte solution, E is the electric field strength and η is the viscosity of the solution. There are important considerations that arise when the mobile phase is driven by EOF as opposed to an applied pressure driven system as in LC. The presence of the electric field will separate molecules by electrophoresis and thus CEC is a combination of electrophoretic and chromatographic separation mechanisms. The main advantage of CEC over LC is that the flat flow profile of EOF introduces less band broadening than pressure-driven flow.[1-2] In addition, velocity of the EOF is independent of column diameter or geometry of the stationary phase support under common operating conditions. This means that very small packing material may be used to improve mass transfer efficiency. The use of pressure-driven flow with this material may be challenging due to the high hydrodynamic resistance. The elimination of high-pressure pumps may also reduce the instrumentation complexity and cost of CEC compared to LC.

Microfluidic devices are well suited to performing CEC separations due to the ease at which EOF can be precisely controlled.[3-4]

In early microchip CEC work, an open-channel design was used where the stationary phase was created by simply functionalizing the channel surface.[5] Although efficiencies over 500,000 plates/m for isocratic separations were achieved,[6] the mass loading capacity of open-channel devices is relatively low.[7-8] Reducing the mass of the injected sample is not always feasible as the concentration of analytes may fall below the limit of detection. Mass loading is an especially important consideration when samples are highly complex or when analytes are present over a wide range of concentrations. Consequently, there have been numerous studies focused on increasing the mass loading capacity by incorporating three-dimensional solid supports within the channels to increase the surface area of the stationary phase. Several different strategies have been explored including packing channels with particles, synthesizing organic or inorganic monoliths, and fabricating micro pillar arrays within the channels. [9]

One attractive approach for fabricating porous polymer monoliths in channels is to photopolymerize acrylate monomers in situ.[10-11] By careful selection of the acrylate monomers and porogenic solvents, the monolith's chemical and physical properties can be tailored for a given application. The photopolymerization process allows for localized monolith formation since regions may be masked prior to irradiation. In addition, these porous polymer monoliths can be electrokinetically flushed immediately after formation, eliminating the need for any external pumps at any point in the fabrication or operation.[12] Monolithic materials have been successfully used in microfluidic devices for various functions including solid phase extraction, separation, enzymatic digestion, microvalving

and ESI.[13-14] There have been many reports on photopolymerized acrylate-based monoliths employed for microchip CEC separations.[15-19]

Gradient elution in CEC provides the same advantages as in LC, specifically reducing analysis times while increasing the overall resolution and sensitivity. Previously, we have demonstrated gradient elution integrated with MEKC[20] and open-channel CEC on microchips.[6,8] At the time of this research, all previous microchip CEC with three-dimensional stationary phase supports utilized isocratic mobile phase elution. Some recent research by Watson and coworkers has explored this technique with some success.[21] In this chapter, CEC with monolithic stationary phases is combined with gradient elution for improving separations of protein digests.

2.2 Experimental

2.2.1 Reagents

All water used in this experiment was deionized and filtered through a Nanopure Diamond purification system (Barnstead, Dubuque, IA). The following materials were obtained from Sigma-Aldrich Chemical Co. (St. Louis, MO): 1,3-butanediol diacrylate, 2-acrylamido-2-methyl-1-propanesulfonic acid (AMPS), 2,2'-azobisisobutyronitrile (AIBN), 3-trimethoxysilylpropyl acrylate , bovine serum albumin (BSA), butyl acrylate, rhodamine B and trypsin from bovine pancreas. The following peptides were purchased from American Peptide Co. (Sunnyvale, CA): G-P-R, G-F-R, bradykinin (1-6) and enkephalin [Met5, Arg6]. The fluorescent labels tetramethylrhodamine-5(and 6)-isothiocyanate (5(6)-TRITC) and tetramethylrhodamine-5-isothiocyanate (5-TRITC) were purchased from Molecular Probes (Eugene, OR). All other chemicals were purchased from Fisher Chemicals (Fairlawn, NJ) and used without further purification.

Stock buffer solutions were prepared by combining sodium phosphate monobasic and dibasic to give a concentration of 100 mM and a pH of 7. For all experiments, the buffer was diluted with water and acetonitrile to a final concentration of 10 mM.

2.2.2 Sample Preparation

Preparation of fluorescently-labeled peptides was adapted from a previously reported procedure.[7] Individual peptides where dissolved in 100 mM sodium bicarbonate (pH 9) at a concentration of 10 mg/mL. For the digest, BSA was dissolved in 100 mM sodium bicarbonate (pH 9) at a concentration of 20 mg/mL, thermally denatured at 80 °C for 45min and then cooled to room temperature for subsequent digestion. Trypsin was dissolved in 100 mM sodium bicarbonate (pH 9) at a concentrated of 2 mg/mL. The BSA and trypsin solutions were then combined at a 40:1 ratio (substrate/trypsin) by weight and allowed to react overnight at 37 °C.

Digest peptide mixtures and single peptides were fluorescently labeled using the following procedure. TRITC was dissolved in dimethyl sulfoxide at 10 mg/mL, combined with the peptides at approximately a 1:1 molar ratio, and allowed to react between 3-5 hours at room temperature. All peptides were labeled with 5-TRITC except G-P-R and G-F-R, which were labeled with the mixed isomers 5(6)-TRITC. The chemical structure for 5-TRITC and the general scheme for the labeling reaction are shown in Figure 2-1. Individual labeled peptides were diluted approximately 8-fold with water. All samples were frozen until needed. Just prior to use, samples were diluted with run buffer to a final concentration of 10 μM for individual peptides and 5 μM for the BSA digest.

2.2.3 Microchip Fabrication

Microchips were fabricated from glass substrates (White Crown B-270; Telic Co., Valencia, CA) using standard photolithography, wet chemical etching, and bonding procedures.[22] Figure 2-2A shows the basic layout of the channels and reservoirs for the microchip device. Glass cylinders were attached to the access ports at the channel termini using chemically resistant epoxy (Hysol E-120HP; Loctite, Rocky Kill, CT) and were used as fluid reservoirs. The serpentine separation channel incorporated asymmetric turns to minimize band broadening as previously discussed.[23-25] All channels were 13 μm deep and 96 μm wide at full width except for the asymmetric turns that were 37 μm wide at full width and exhibited the expected edge profile of an isotopic etch with good mask integrity. The separation channel was 192 mm in length; however, the effective separation distance was defined by the point of laser-induced fluorescence (LIF) detection (see microchip operation). The distance from the "T" intersection to the injection cross was 5 mm. A photograph of the microchip is shown in Figure 2-2B.

2.2.4 Monolith Synthesis

The monolith synthesis within the microchannels was adapted from a previously reported procedure.[16] The channels were first functionalized with an acrylate that was later incorporated into the monolith structure during the photopolymerization to provide attachment to the channel walls. The channels were prepared by sequentially flushing with the following solutions: 1 N sodium hydroxide, water, 1 M hydrochloric acid, water, and methanol. The chip was then dried in a vacuum oven at 50 °C for 6 hours. The glass channel walls were functionalized by continuous flushing with 1% 3-trimethoxysilylpropyl acrylate in dry toluene for 1 hour. All percentages are

volumetric unless otherwise noted. Afterwards, the chip was flushed with dry toluene, and then acetonitrile, before being briefly dried under vacuum.

Figure 2-3 shows the chemical structure of the acrylate monomers and the general mechanism for polymerization.[26] The acrylate monomers were filtered through basic activated alumina to remove inhibitors before use. The monomer mixture consisted of 69% butyl acrylate as the hydrophobic monomer, 30% 1,3-butanediol diacrylate as the crosslinker, 0.25% AMPS to provide the negative surface charge, and 0.30% 3-trimethoxysilylpropyl acrylate for enhanced surface attachment and structural stability. This concentration of AMPS corresponds to half the amount stated in the previously reported procedure. The free-radical initiator, AIBN, was added at 0.5% (w/w) of the monomers. The monomer casting solvent was created from 5 mM sodium phosphate (pH 7), ethanol, and acetonitrile in a 1:1:3 ratio. The monomers and casting solvent were then combined at a ratio of 1:2 (monomers : casting solvent). This solution was sonnicated for 5 min before use to ensure uniform distribution. Note that excessive sonication will heat the solution and initiate free radical production prematurely.

Monolith formation was only desirable in the separation channel therefore all other regions were masked off with general purpose laboratory tape. The final 9 mm of the separation channel was also masked off to provide an open channel region for LIF detection. Care was taken to fill all reservoirs equally with the combined monomer and casting solvent solution to avoid generating fluid flow by hydrostatic pressure. The chip was then exposed to UV radiation from a 100 W UV lamp (Blak-Ray, San Gabriel, CA) from below at a distance of 7.5 cm for 25 min. After polymerization, the chip was electrokinetically flushed for 2 hours with a solution containing 2.5 mM sodium

phosphate, pH 7 and 75% acetontirile. The distance between the injection cross and the monolith in the separation channel was 1 mm. The microchip was stored with buffer in the channels; however, the reservoirs were filled with water to prevent the acetonitrile from diminishing the epoxy's structural integrity. The chip was placed in a sealed container to prevent the monolith from drying out when not in use.

2.2.5 Microchip Operation

The schematic for the complete experimental setup is shown in Figure 2-4. The EOF was controlled by varying the voltages applied to each reservoir. The mobile phase gradient was formed by the mixing of two electroosmotic flows with different organic composition at a "T" intersection as previously described.[20] This was accomplished by adjusting the voltages applied to buffer A and buffer B to select the desired solvent composition delivered to the injection cross. Buffer A was composed of 10 mM sodium phosphate (pH 7) in water and buffer B was 10 mM sodium phosphate (pH 7) in 1:1 ratio of water and acetonitrile. All sample injections were performed using the gated injection scheme.[27] Four positive high voltages were supplied by a +10 kV power supply (2866A; Bertan, Hicksville, NY) and one negative high voltage lead was supplied by a custom-built, -10 kV power supply (Ultravolt, Ronkonkoma, NY). Both power supplies were controlled by a Power Macintosh G5 via an I/O board (PCI-6713; National Instruments, Austin, TX). Analytes were detected by LIF in the open channel region immediately following the monolith in the separation channel, defining a separation length of 183 mm. An argon ion laser (543-AP-A01; Melles Griot, Carlsbad, CA) supplied a continuous power of 10 mW of 514.5 nm light that was focused at the microchip by a 150-mm focal length lens (Newport Corp., Irvine, Ca). Fluorescence emission was collected by a 40x

microscope objective (CD-240-M40; Creative Devices, Neshanic Station, NJ), spatially filtered with a 800-μm diameter pinhole, filtered spectrally by a long pass filter (LP02-514RU-25; Semrock, Rochestor, NY), and detected by a photomultiplier tube (R928; Hamamatsu, Bridgewater, NY). The photomultiplier signal was amplified by a low-noise current amplifier (SR570; Stanford Research Systems, Sunnyvale, CA) and read into the computer by a second I/O board (PCI-6251; National Instruments, Austin, TX).

2.2.6 Data Analysis

Peak capacity values were calculated using open source software (Peak Finder, available at http://omics.pnl.gov/software). This program fits the peaks with a Gaussian curve and then calculates the median peak width (4σ). The peak capacity is then calculated by Equation 1-3 using a resolution of 1.

2.3 Results and Discussion

2.3.1 Photopatterned Monolith Material

Negatively charged porous polymer monoliths were fabricated in glass microchips by photopolymerization of acrylate monomers following established procedures.[16] No gaps or voids were observed in the monolith material when inspected with a light microscope. For a closer look, scanning electron microscope (SEM) images of a microchip filled with this material were obtained. To expose the monolith for SEM imaging, a microchip was scored with a diamond tipped scribe and cleaved into two pieces. Two SEM images of the channel cross-section are shown in Figure 2-5. The globular structure of the monolith appears to be more dense here than in a previous report.[12] A difference in UV irradiance during the monolith synthesis will change the rate of polymerization and this may account for the small difference in the monolith

structure. This material has been previously characterized and found to have a average pore size of 1 μm (by mercury porosimetry) and a surface area ~1-3 m^2/g (by the BET method).[12] As previously noted, the monolith material could be readily removed from the device by thermal decomposition.[17] A 6 hr dwell time at 400 °C was sufficient to completely remove the material without damaging the microchip device. Thus a single microchip device could be used to evaluate several different monolith formulations.

By simply masking off areas to be irradiated, the monolith formation was easily localized to the separation channel. There are several advantages to photopatterning the monolith material in the separation channel as opposed to filling the entire device. First, an open sample channel reduces the loading time required for hydrophobic analytes to travel to the injection cross. This is especially important when one desires to load an aqueous sample as often done in gradient elution separations. Secondly, an open injection cross reduces the injection bias based on the analyte's hydrophobicity.

However, a photopatterned device has both open and monolith filled regions that may lead to significant drawbacks. A change in the surface charge at the interface between the open channel and monolith will result in a different zeta potential and by Equation 2-1 the velocity of the EOF will be different. This difference in EOF will create a pressure gradient that will produce recirculating flow.[28-29] It is advantageous to eliminate pressure-driven flow as it complicates fluid control in the device and introduces axial dispersion, lowering separation efficiency. In this study, the previously reported monolith formulation was found to have a larger EOF than the open channel regions.[16] This created an area of low pressure in the separation channel near the injection cross. This induced hydrodynamic flow forced sample into the separation channel, making it

difficult to establish the gated injection scheme. To correct this mismatch in EOF, the amount of AMPS in the monomer solution was reduced to lower the EOF in the monolith. The new monolith produced an EOF velocity approximately equal to the open-channel regions. This was verified qualitatively by fluorescence imaging of rhodamine B injections.

2.3.2 Isocratic Separations

Although the separation mechanism for electrochromatography is a combination of electrophoresis and chromatography, neutral molecules are separated solely by chromatographic partitioning. As test analytes, four short peptides were chosen that had a net charge after labeling with TRITC near zero. CE separations using an identical microchip without the monolith could not resolve these labeled peptides with a field strength of 0.45 kV/cm. In addition, CEC separations were not able to separate these peptides when the mobile phase contained over 50% acetonitrile. Figure 2-6 shows an isocratic separation of three of these peptides using 30% acetonitrile. Since these molecules are only separated by chromatographic partitioning, the optimal linear velocity for the mobile phase can be determined by constructing a van Deemter plot. However, there was difficultly in determining the mobile phase velocity in these experiments. In LC experiments, the mobile phase velocity is generally determined by measuring the dead time, meaning the time required for an unretained molecule to elute. Commonly used dead time markers for reversed-phase LC with UV-absorbance detection are hydrophilic, low molecular weight organic molecules that are not charged such as thiourea or uracil. Dead time markers for CEC-LIF must also have a high quantum yield to be compatible with LIF detection. A fluorescent dye that was sufficiently hydrophilic

without being charged was not readily available. However, the mobile phase velocity is directly proportional to the applied field strength as shown in Equation 2-1. Figure 2-7A shows that the velocity for each peptide is linearly related to the applied field strength. This data suggests that the mobile phase velocity is also linearly related to the applied field strength. Therefore plotting the plate height as a function of the field strength produces a pseudo-van Deemter plot shown in Figure 2-7B. Although the linear velocity of the mobile phase was not known, the optimum conditions for reducing *H* could be readily obtained. A separation field strength of 0.38 kV/cm produces the optimum mobile phase linear velocity for these three peptides. Here, the separation efficiency for enkephalin [Met5, Arg6] was 570,000 plates/m, which corresponds to 105,000 plates generated on the device. This efficiency value compares well with previously reported isocratic electrochromatography results using a similar monolith material.[17]

2.3.3 Gradient Separations

The voltages applied to the buffer A and buffer B reservoirs for gradient production were determined experimentally. This was done by adding rhodamine B to the buffer B reservoir and monitoring the "T" intersection by fluorescence imaging. Figure 2-8A shows a light field image of the "T" intersection. The three other images in the figure show fluorescence images of buffer mixing at 0%, 50%, and 100% buffer B. Note that there is no significant fluid flow from the buffer A channel into the buffer B channel and vice-versa. The fluorescence of rhodamine B across the channel width was approximately uniform at the injection cross. This suggests that the buffers were well mixed before the separation channel, especially considering that the diffusion coefficient of a molecule of acetonitrile is much larger than rhodamine B.

Figure 2-9A shows the separation of four TRITC-labeled peptides with a net charge near zero under isocratic elution conditions using 25% acetonitrile. As the solvent strength is increased in subsequent separations, resolution decreased until ultimately all four peptides coelute at 50% acetonitrile shown in Figure 2-9B. Increasing the amount of acetonitrile slightly reduces the EOF as previously observed in CE experiments.[30] Figure 2-9C shows the separation of the same analytes employing a mobile phase gradient from 20% to 50% acetonitrile. The resolution between the first two peptides is maintained while the time necessary to elute the later eluting peptides is decreased considerably. In addition, the last two peptides are greatly focused by the gradient, which increased their signal-to-noise ratio.

A BSA tryptic digest was analyzed to further illustrate the advantage of gradient elution in microchip CEC. Figure 2-10A shows an isocratic separation of the BSA digest using 10% acetonitrile. Many of the earlier eluting peaks are overlapped while the later peaks are quite broad. It is likely that several components either remain on the separation column or their efficiency is so poor that their concentration is below the limit of detection. Figure 2-10B shows a gradient elution separation of the same sample. Here, the peak widths are more or less constant throughout the chromatogram and many more peaks are observed. The peak capacity for the isocratic and gradient elution separations were 50 and 115, respectively. To increase sample throughput, it is helpful to decrease the analysis time. Figure 2-11 shows an analysis of the same BSA digest where the field strength is increased by a factor of 3 and the slope of the gradient is increased 4 fold. Now the entire separation is complete in just over 8 min, although some loss in performance is observed as the peak capacity is now 72.

2.4 Conclusions

Porous polymer monoliths created by the photopolymerization of acrylate monomers are well suited for microchip CEC due to their ease of fabrication and the tunability of their chemical and physical properties. Adjusting the surface charge to balance the EOF between the monolith and open-channel regions largely avoided the drawbacks of pressure driven flow. The ability to perform gradient elution significantly increased the separation power of CEC, leading to high efficiency separations of protein digests. Gradient elution CEC is likely a good candidate to be coupled with CE for 2D microfluidic separations. Future work should also focus on the integration of mass spectrometry detection for comprehensive identification of peptides in complex mixtures.

2.5 Acknowledgements

Use of the Peak Finder software, written by Matthew Monroe, is acknowledged in the following statement. "*Portions of this research were supported by the NIH National Center for Research Resources (Grant RR018522), and the W.R. Wiley Environmental Molecular Science Laboratory (a national scientific user facility sponsored by the U.S. Department of Energy's Office of Biological and Environmental Research and located at PNNL). PNNL is operated by Battelle Memorial Institute for the U.S. Department of Energy under contract DE-AC05-76RL0 1830.*"

2.6 Figures

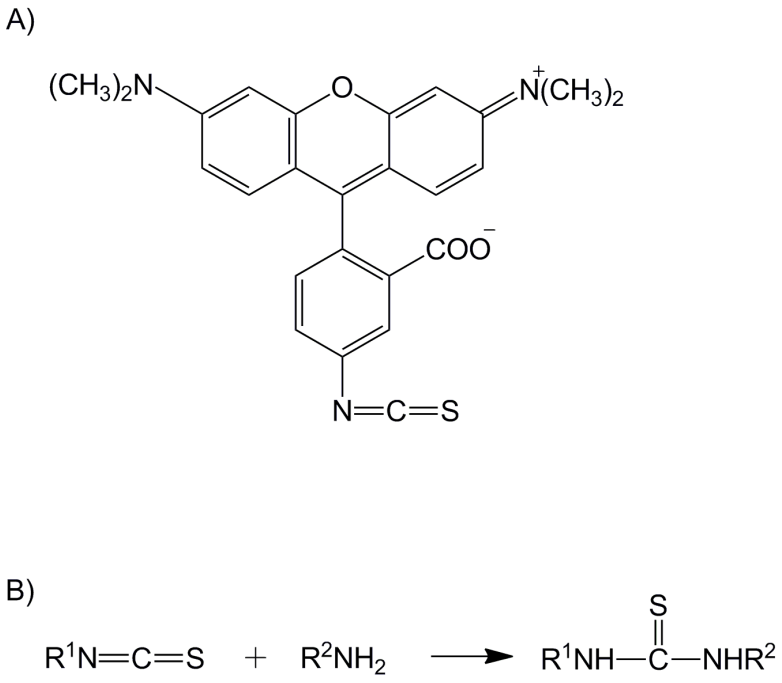

Figure 2-1. A) Chemical structure for 5-TRITC, B) Schematic for the labeling reaction involving an isothiocyanate and a primary amine.

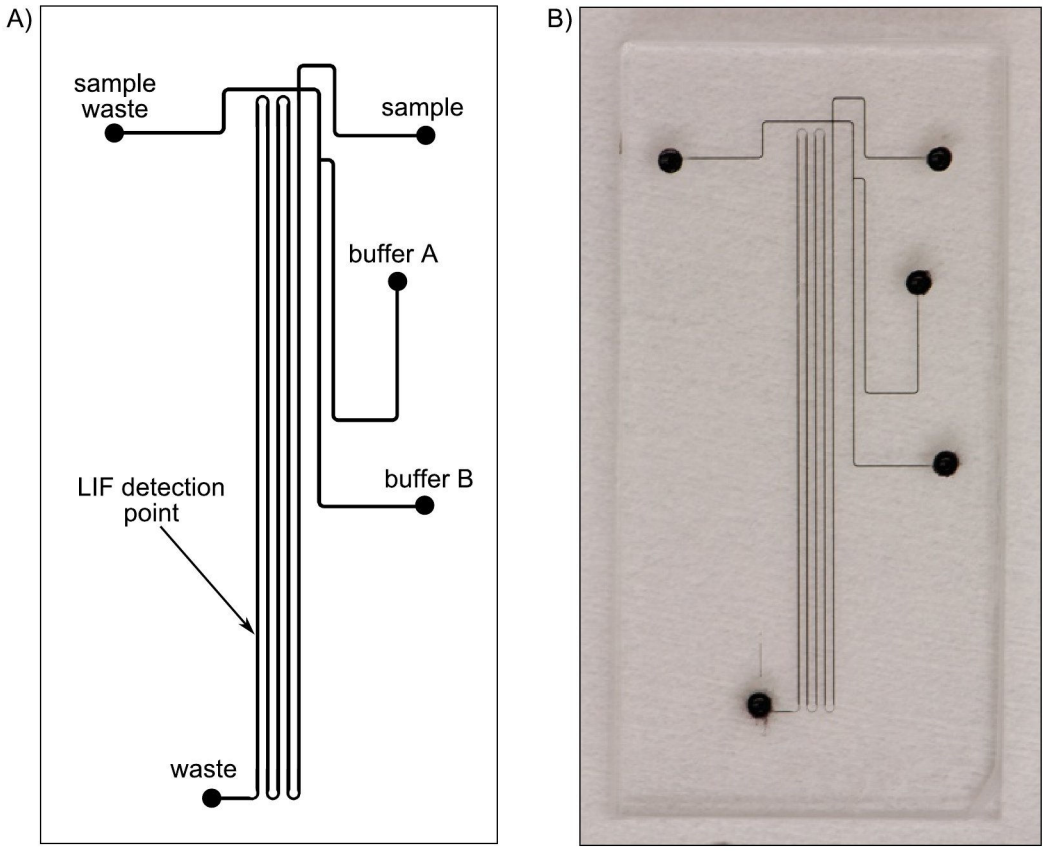

Figure 2-2. A) Channel layout for the gradient elution CEC microchip device. B) Photograph of the device with channels filled with ink for contrast. The dimensions of the microchip are 25 mm by 50 mm.

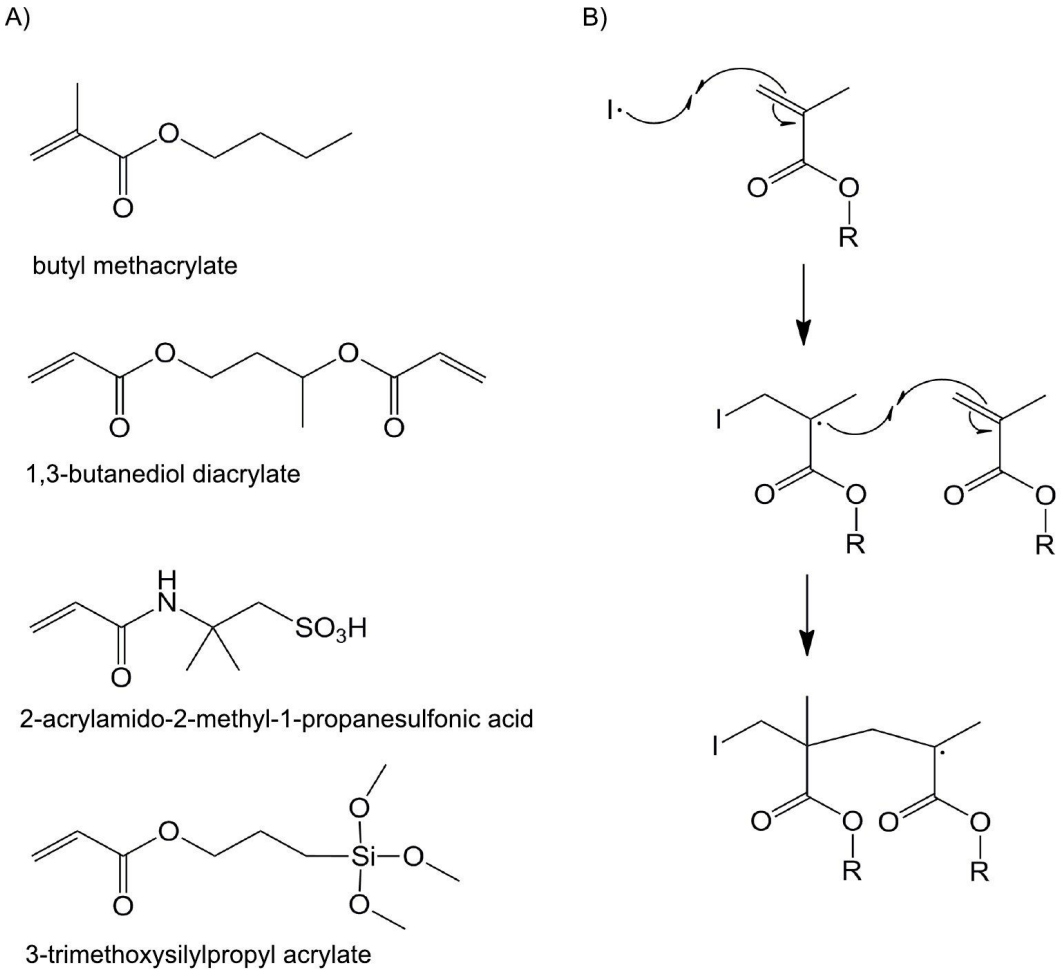

Figure 2-3. A) Chemical structures for the acrylates used in the monolith synthesis, B) mechanism for the polymerization of butyl methacrylate where I is the free radical initiator and R is a butyl group.

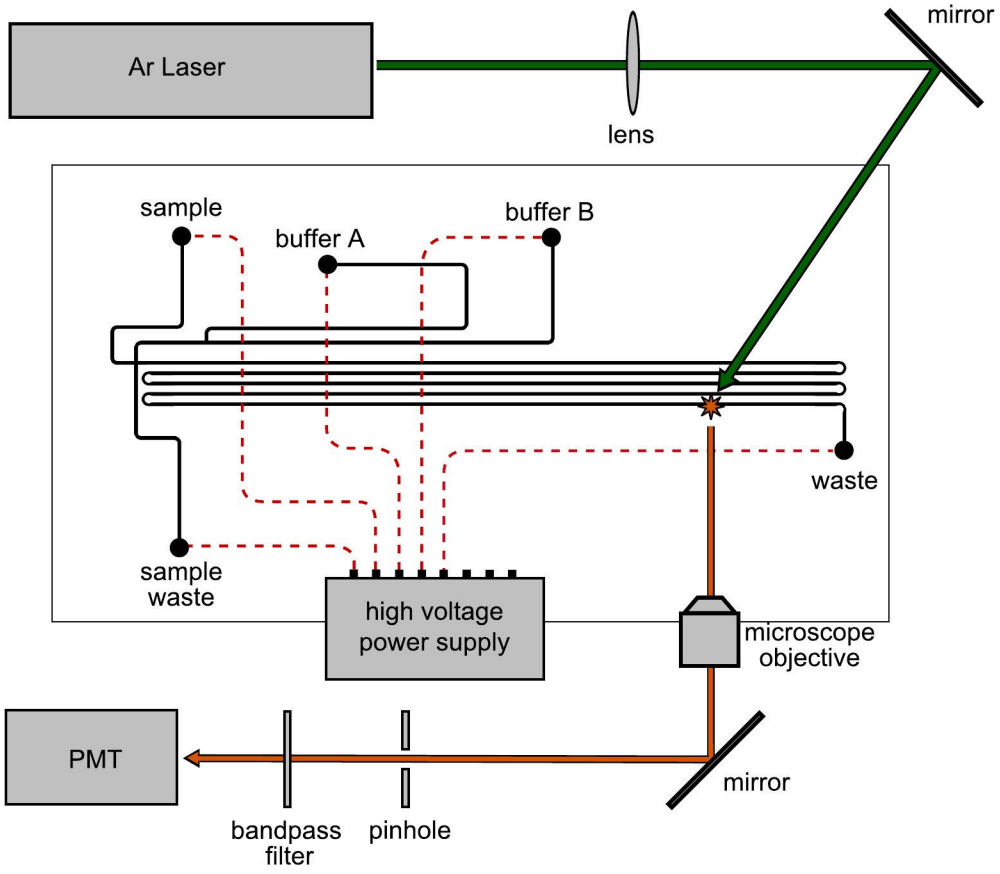

Figure 2-4. The schematic for the complete gradient elution CEC-LIF setup.

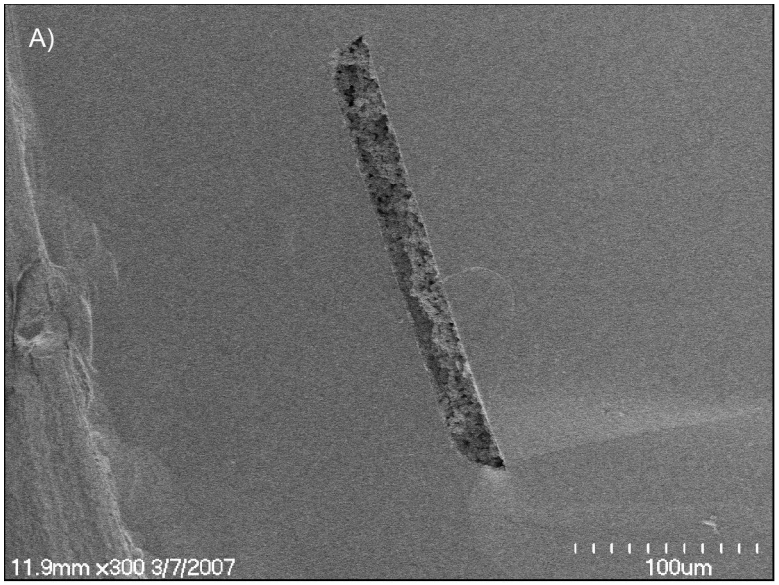

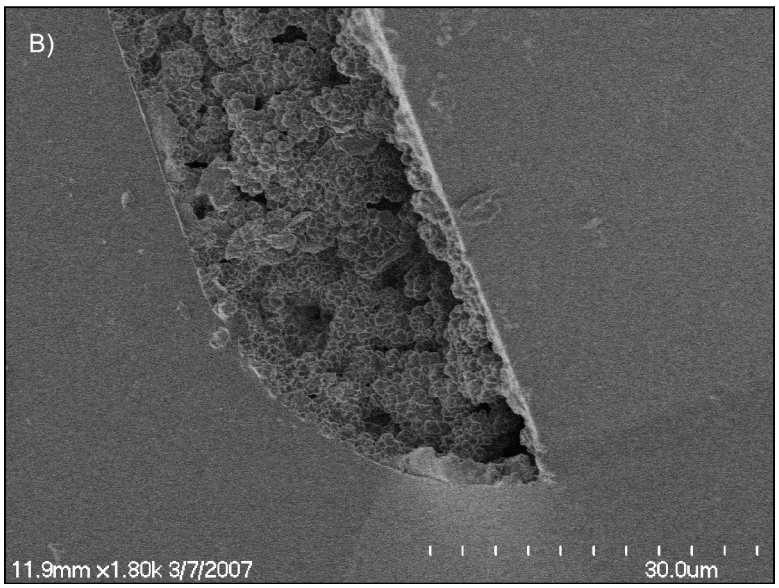

Figure 2-5. SEM images of a microchannel cross-section filled with the monolith material.

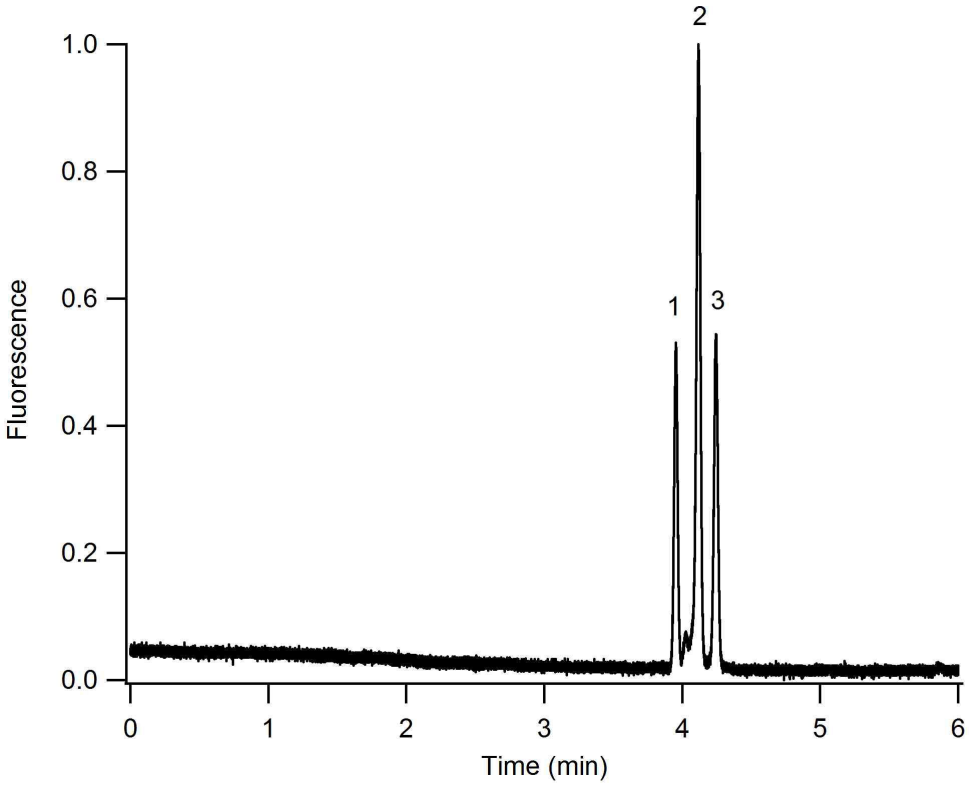

Figure 2-6. CEC separation of peptides under isocratic conditions. Mobile phase: 10 mM sodium phosphate, pH 7 with 30% acetonitrile. Analytes: 1) G-P-R, 2) Bradykinin (1-6), 3) Enkephalin [Met5, Arg6]. Field strength: 0.38 kV/cm.

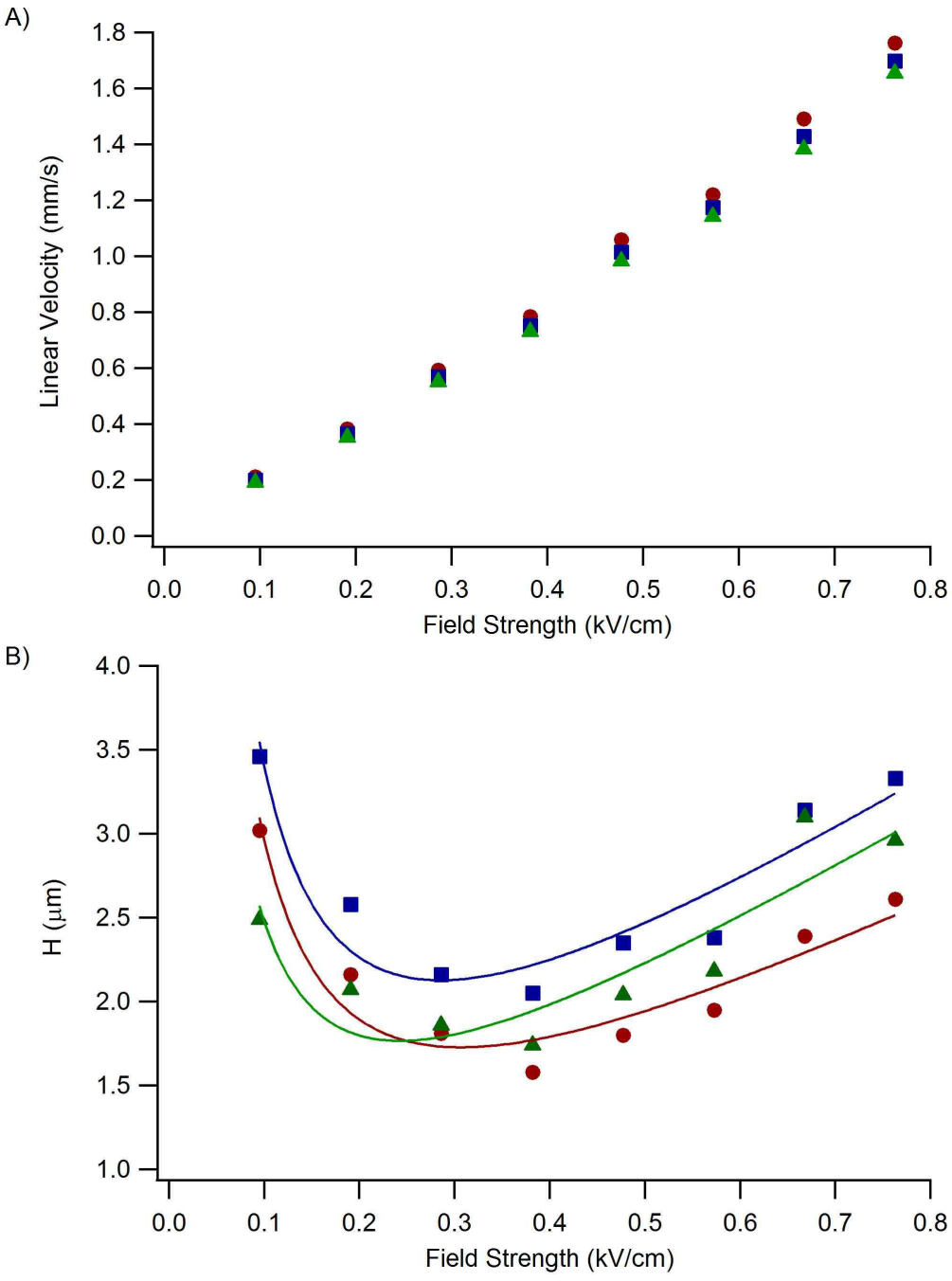

Figure 2-7. A) Linear velocity and B) plate height vs field strength. Mobile phase: 10 mM sodium phosphate, pH 7 with 30% acetonitrile. Analytes: G-P-R (cicles), Bradykinin (1-6) (squares), Enkephalin [Met5, Arg6] (triangles).

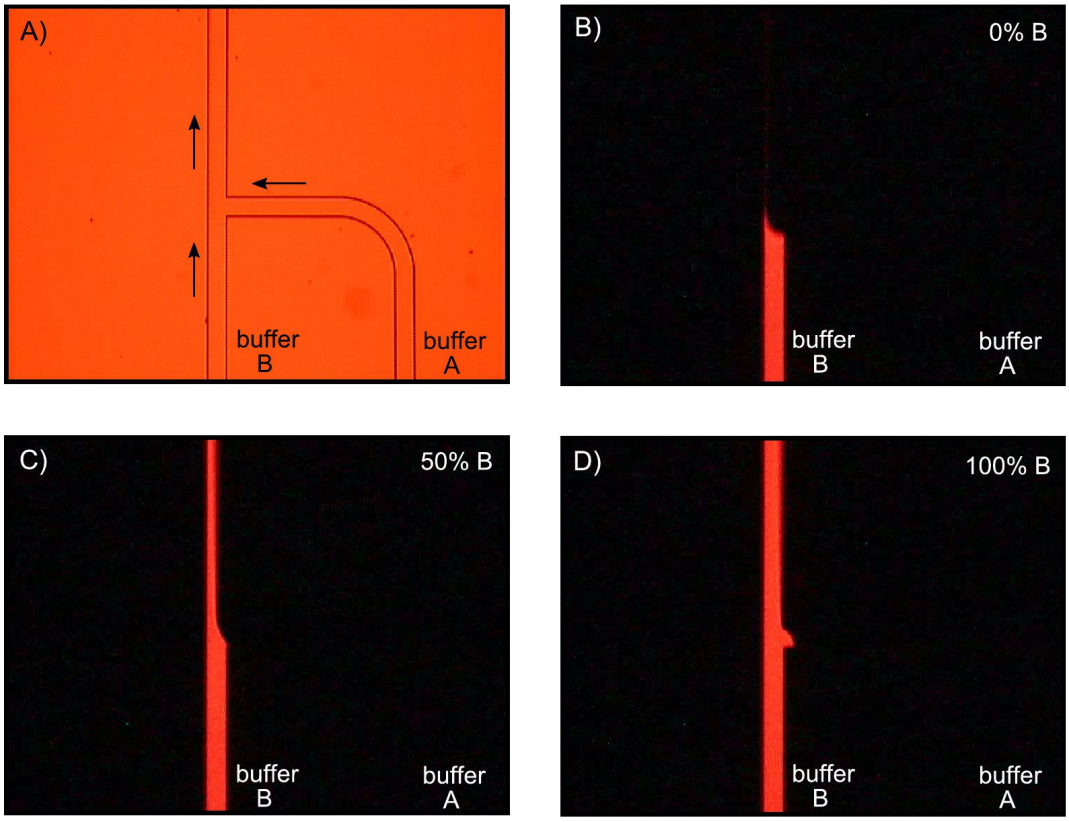

Figure 2-8. A) Photograph of the "T" intersection. The arrows denote the direction of the fluid flow. B-D) Flourescence imaging of buffer mixing at different compositions. Rhodamine B was added to buffer B.

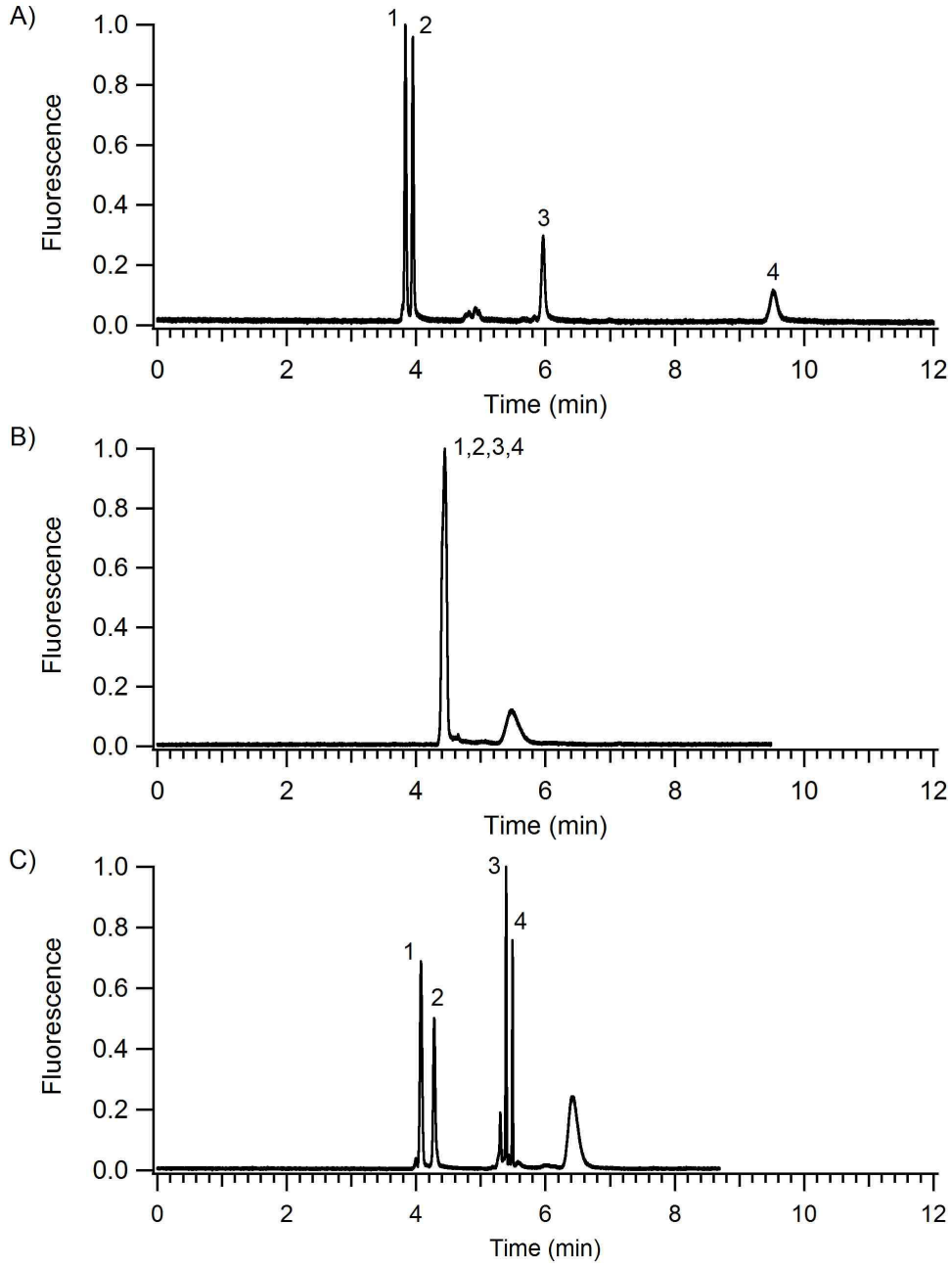

Figure 2-9. Isocratic and gradient elution CEC separations of peptides. Mobile phase: 10 mM sodium phosphate, pH 7 with A) 25% acetonitrile, B) 50% acetonitrile, C) 20% to 50% acetonitrile in 2 min. Analytes: 1) G-P-R , 2) G-F-R, 3) Bradykinin (1-6), and 4) Enkephalin [Met5, Arg6, Phe7]. Field strength: 0.42 kV/cm.

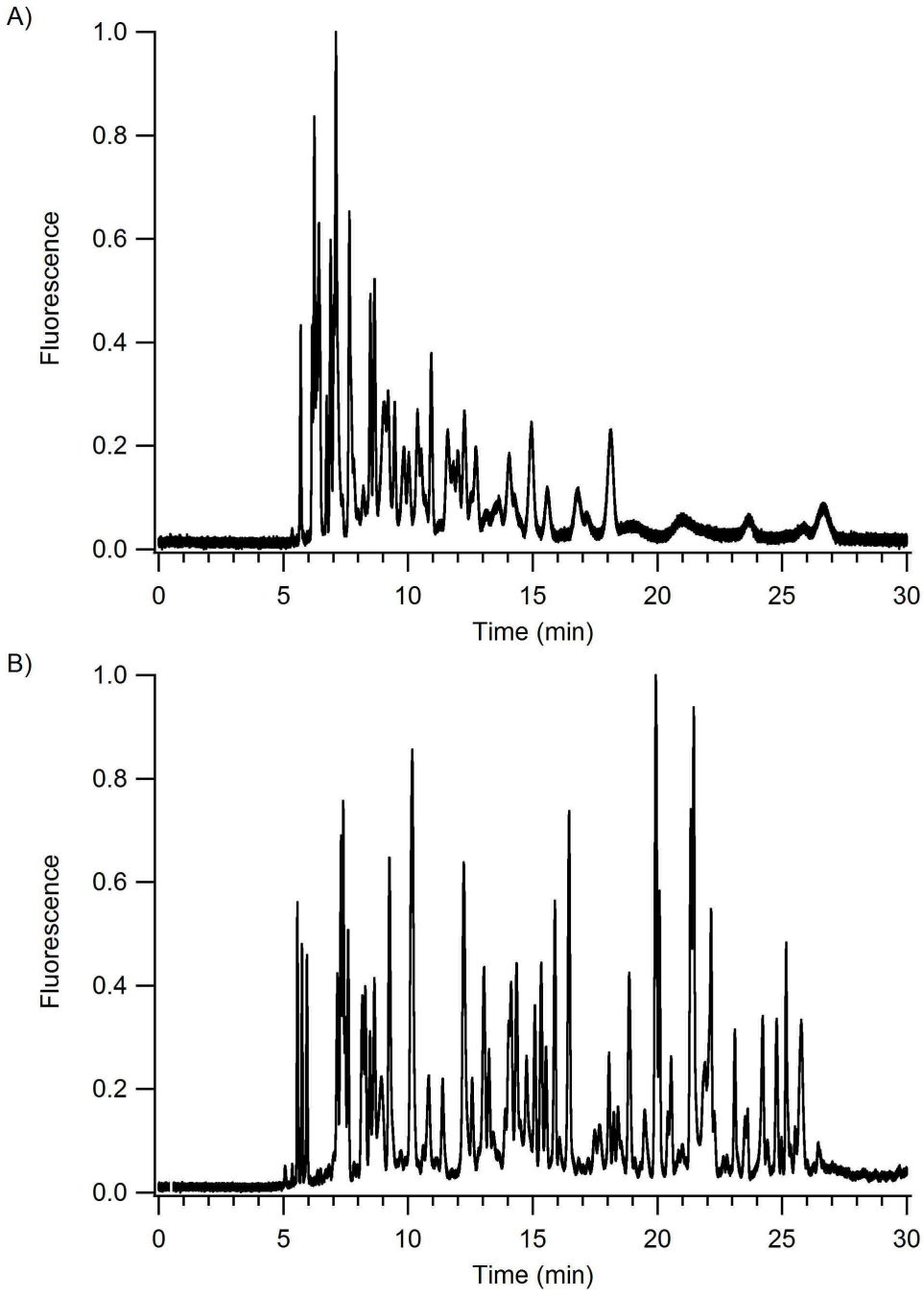

Figure 2-10. Isocratic and gradient elution CEC separation of a BSA trypic digest. Mobile phase: 10 mM sodium phosphate, pH 7 with A) 10% acetonitrile, B) 0% to 50% acetonitrile in 33 min. Field strength: 0.3 kV/cm.

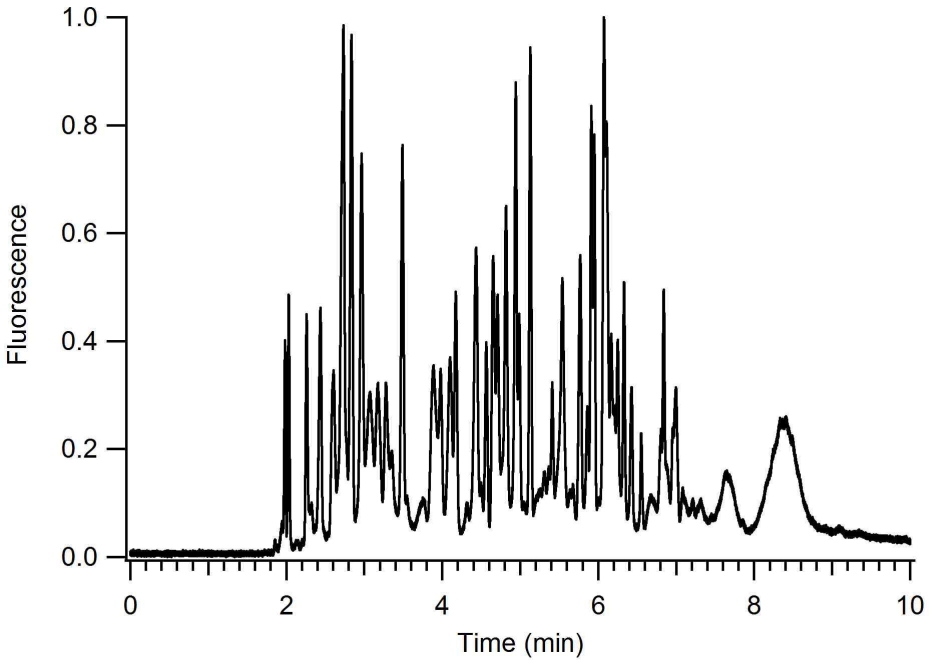

Figure 2-11. Fast gradient elution CEC separation of a BSA tryptic digest. Mobile phase: 10 mM sodium phosphate, pH 7 with 0% to 50% acetonitrile in 8 min. Field strength: 1.0 kV/cm.

2.7 References

1. Bartle, K. D.; Myers, P. Theory of capillary electrochromatograpy. *J. Chromatogr. A* **2001**, *916*, 3.

2. Rathore, A. S. Theory of electroosmotic flow, retention and separation efficiency in capillary electrochromatography. *Electrophoresis* **2002**, *23*, 3827.

3. Stachowiak, T. B.; Svec, F.; Frechet, J. M. J. Chip electrochromatography. *J. Chromatogr. A* **2004**, *1044*, 97.

4. Pumera, M. Microchip-based electrochromatography: designs and applications. *Talanta* **2005**, *66*, 1048.

5. Jacobson, S. C.; Hergenroder, R.; Koutny, L. B.; Ramsey, J. M. Open-channel electrochromatography on a microchip. *Anal. Chem.* **1994**, *66*, 2369.

6. Kutter, J. P.; Jacobson, S. C.; Matsubara, N.; Ramsey, J. M. Solvent-programmed microchip open-channel electrochromatography. *Anal. Chem.* **1998**, *70*, 3291.

7. Gottschlich, N.; Jacobson, S. C.; Culbertson, C. T.; Ramsey, J. M. Two-dimensional electrochromatography/capillary electrophoresis on a microchip. *Anal. Chem.* **2001**, *73*, 2669.

8. Broyles, B. S.; Jacobson, S. C.; Ramsey, J. M. Sample filtration, concentration, and separation integrated on microfluidic devices. *Anal. Chem.* **2003**, *75*, 2761.

9. Peterson, D. S. Solid supports for micro analytical systems. *Lab Chip* **2005**, *5*, 132.

10. Viklund, C.; Ponten, E.; Glad, B.; Irgum, K.; Horstedt, P.; Svec, F. "Molded" macroporous poly(glycidyl methacrylate-co-trimethylolpropane trimethacrylate) materials with fine controlled porous properties: Preparation of monoliths using photoinitiated polymerization. *Chemistry Of Materials* **1997**, *9*, 463.

11. Yu, C.; Svec, F.; Frechet, J. M. J. Towards stationary phases for chromatography on a microchip: Molded porous polymer monoliths prepared in capillaries by photoinitiated in situ polymerization as separation media for electrochromatography. *Electrophoresis* **2000**, *21*, 120.

12. Ngola, S. M.; Fintschenko, Y.; Choi, W. Y.; Shepodd, T. J. Conduct-as-cast polymer monoliths as separation media for capillary electrochromatography. *Anal. Chem.* **2001**, *73*, 849.

13. Svec, F.; Tennikova, T. B.; Deyl, Z. *Monolith Materials*; Elsevier New York, 2003.

14. Ro, K. W.; Nayalk, R.; Knapp, D. R. Monolithic media in microfluidic devices for proteomics. *Electrophoresis* **2006**, *27*, 3547.

15. Shediac, R.; Ngola, S. M.; Throckmorton, D. J.; Anex, D. S.; Shepodd, T. J.; Singh, A. K. Reversed-phase electrochromatography of amino acids and peptides using porous polymer monoliths. *J. Chromatogr. A* **2001**, *925*, 251.

16. Fintschenko, Y.; Choi, W. Y.; Ngola, S. M.; Shepodd, T. J. Chip electrochromatography of polycyclic aromatic hydrocarbons on an acrylate-based UV-initiated porous polymer monolith. *Frensen. J. Anal. Chem.* **2001**, *371*, 174.

17. Throckmorton, D. J.; Shepodd, T. J.; Singh, A. K. Electrochromatography in microchips: Reversed-phase separation of peptides and amino acids using photopatterned rigid polymer monoliths. *Anal. Chem.* **2002**, *74*, 784.

18. Lazar, I. M.; Li, L. J.; Yang, Y.; Karger, B. L. Microfluidic device for capillary electrochromatography-mass spectrometry. *Electrophoresis* **2003**, *24*, 3655.

19. Faure, K.; Bias, M.; Yassine, O.; Delaunay, N.; Cretier, G.; Albert, M.; Rocca, J. L. Electrochromatography in poly(dimethyl)siloxane microchips using organic monolithic stationary phases. *Electrophoresis* **2007**, *28*, 1668.

20. Kutter, J. P.; Jacobson, S. C.; Ramsey, J. M. Integrated microchip device with electrokinetically controlled solvent mixing for isocratic and gradient elution in micellar electrokinetic chromatography. *Anal. Chem.* **1997**, *69*, 5165.

21. Watson, M. W. L.; Mudrik, J. M.; Wheeler, A. R. Gradient elution in microchannel electrochromatography. *Anal. Chem.* **2009**, *81*, 3851.

22. Jacobson, S. C.; Hergenroder, R.; Koutny, L. B.; Ramsey, J. M. High-speed separations on a microchip. *Anal. Chem.* **1994**, *66*, 1114.

23. Griffiths, S. K.; Nilson, R. H. Low dispersion turns and junctions for microchannel systems. *Anal. Chem.* **2001**, *73*, 272.

24. Molho, J. I.; Herr, A. E.; Mosier, B. P.; Santiago, J. G.; Kenny, T. W.; Brennen, R. A.; Gordon, G. B.; Mohammadi, B. Optimization of turn geometries for microchip electrophoresis. *Anal. Chem.* **2001**, *73*, 1350.

25. Ramsey, J. D.; Jacobson, S. C.; Culbertson, C. T.; Ramsey, J. M. High-efficiency, two-dimensional separations of protein digests on microfluidic devices. *Anal. Chem.* **2003**, *75*, 3758.

26. Legido-Quigley, C.; Marlin, N. D.; Melin, V.; Manz, A.; Smith, N. W. Advances in capillary electrochromatography and micro-high performance liquid chromatography monolithic columns for separation science. *Electrophoresis* **2003**, *24*, 917.

27. Jacobson, S. C.; Koutny, L. B.; Hergenroder, R.; Moore, A. W.; Ramsey, J. M. Microchip capillary electrophoresis with an integrated postcolumn reactor. *Anal. Chem.* **1994**, *66*, 3472.

28. Potocek, B.; Gas, B.; Kenndler, E.; Stedry, M. Electroosmosis in capillary zone electrophoresis with nonuniform zeta-potential. *J. Chromatogr. A* **1995**, *709*, 51.

29. Rathore, A. S.; Horvath, C. Axial nonuniformities and flow in columns for capillary electrochromatography. *Anal. Chem.* **1998**, *70*, 3069.

30. Schwer, C.; Kenndler, E. Electrophoresis in fused-silica capillaries - The influence of organic-solvents on the electroosmotic velocity and the zeta-potential. *Anal. Chem.* **1991**, *63*, 1801.

CHAPTER 3: Hybrid 2D Liquid Chromatography-Capillary Electrophoresis with Laser-Induced Fluorescence Detection

3.1 Introduction

The Jorgenson group reported the first online system for comprehensive LC-CE separations.[1] This system utilized a 6-port valve and sample loop to interface the LC column and CE capillary. The valve was setup such that fresh buffer was presented to the CE capillary while the LC effluent filled the sample loop. To perform CE injections, the CE voltage was turned off and the valve was actuated to deliver the LC effluent in the sample loop to the CE capillary. After a short electrokinetic injection at low voltage, the valve was actuated to again present buffer to the CE capillary and the CE voltage was restored. All of the LC effluent in the sample loop was not injected but rather a very small fraction. The CE injections were performed frequently such that a fraction of every LC peak was injected at least once into the CE dimension. The large dead volume associated with the valve and loop setup prompted the same group to develop a "transverse flow gating" interface that sufficiently reduced the band broadening to allow capillary LC columns to be employed.[2] In this new system, the interface was constructed to position the end of the LC capillary on axis with the CE capillary but with a small gap between the two. A second LC pump was used to generate transverse flow that flushed this narrow gap to prevent the LC effluent from entering the CE capillary during CE separations. For each CE injection, the transverse flow and the CE voltage were stopped to allow the LC effluent to reach the CE capillary and electrokinetic sample injection at

low voltage. The transverse flow and the CE voltage were then turned back on to perform the CE separation. Additional modifications to this basic interface have improved performance and ease of use.[3]

One challenging aspect of the transverse flow gating system was that it relied upon the precise alignment of the LC and CE capillaries. The gap between the capillaries must be within tens of microns to prevent excessive dilution of the LC effluent before it reaches the CE capillary. More recently, Bergstrom and coworkers partially addressed this issue by designing a microfabricated interface from polydimethylsiloxane.[4-5] This created a confined region between the LC and CE capillaries to reduce the dilution of the LC effluent when performing CE injections. Unfortunately, this benefit was largely rescinded by the fact these injections were transported back to a capillary for the CE separation. The band broadening that occurs in the interface/CE capillary connection is much more critical than the LC capillary/interface connection due to the much smaller volumes of the CE peaks.

Another strategy for 2D LC-CE separations is to use a hybrid system where the capillary LC is coupled with CE performed on a microfluidic device. The interconnected channels of a microfluidic device enable extremely narrow CE injection plugs to be routinely realized. In addition, the CE separation is performed on the same device to maintain high separation efficiency throughout the analysis. Furthermore, the increased rate of heat transfer on microchips allows for higher electric field strengths to be used without encountering Joule heating which causes band broadening.[6] These advantages have allowed for microchip-based CE to outperform capillary-based CE in terms of both

speed and efficiency. For example, our group has demonstrated that microchip CE can generate over 18,000 plates/s which resulted in a peak capacity of 48 in only 0.8 s.[7]

The greatest challenge in a hybrid LC-CE system is overcoming the large dead-volume usually associated with transferring fluid from capillaries to microfluidic devices. If this can be overcome, a system would combine state of the art LC separations performed in capillaries at ultra high pressures with the speed and efficiency of microchip CE would be feasible. Yang and coworkers reported a hybrid system that coupled capillary-based LC with microchip-based CE.[8] They were able to couple a 250 μm i.d. capillary LC column operated at a flow rate of 1.5 μL/min to a simple cross channel microchip using a pinched injection scheme.[9] However, this injection scheme does not allow for rapid consecutive CE injections due to the time required to load sample at the injection cross after each injection.

This chapter will describe the development of a hybrid 2D LC-CE separation system. First, a custom fitting was developed to connect capillaries to microchips with limited dead volume. A modified version of the gated injection scheme is demonstrated for coupling LC and CE at flow rates that are an order of magnitude lower than those demonstrated in the work by Yang *et al*.[8] The hybrid 2D LC-CE system was then used for high efficiency separations of protein digests labeled with TRITC. Finally, the labeling of peptides with TRITC will be investigated by LC-LIF in an attempt to determine the source of the additional sample complexity.

3.2 Experimental

3.2.1 Reagents

Water used in this experiment was deionized and filtered (Nanopure Diamond, Barnstead International, Dubuque, IA). The following materials were purchased from Fisher Chemicals (Fairlawn, NJ): acetone (HPLC grade), acetonitrile (HPLC grade), acetic acid (HPLC grade), tetrahydrofuran (HPLC grade). The following materials were obtained from Sigma Chemical Co. (St. Louis, MO): 1,2-bis(3-aminopropylamino)ethane, bovine serum albumin, cytochrome c from horse heart, epichlorohydrin, formic acid (Acros Organics, 99%), trypsin from bovine pancreas, and rhodamine B. The 5-TRITC was purchased from Molecular Probes (Eugene, OR). The Kasil 2130 potassium silicate solution can be obtained from PQ Corp. (Valley Forge, PA). The PolyE-323 polymer was synthesized as previously described, adjusted to pH 7 with acetic acid, and diluted with water to 15% (by mass) polymer.[10]

3.2.2 Sample Preparation

Proteins were digested with trypsin and labeled with 5-TRITC as described in Chapter 2 and frozen until needed. Just prior to experiments, the digest was diluted with an aqueous solution of 0.1% (v/v) formic acid and 3% (v/v) acetronitrile to a final concentration of 1 μM.

3.2.3 Capillary LC Column

All LC separations were performed using an in-house packed capillary LC column. The fused-silica capillary (Polymicro Technologies Inc., Phoenix, AZ) had an internal diameter (i.d.) of 75 μm and an outer diameter (o.d.) of 360 μm. The outlet frit was prepared using glass microfibers from filter paper and a sol-gel mixture using a 1:1

ratio of Kasil 2130 to formamide.[11] The 2.5 μm diameter porous particles (X-Bridge C18, Waters Corp., Milford, MA) were suspended in tetrahydrofuran at 2.5 mg/mL and sonicated briefly. This slurry of particles was forced into the capillary at a pressure of 2000 bar using a previously described apparatus[12] with an updated capillary fitting.[13] After a sufficient length of the capillary was packed, the column was flushed with acetonitrile and then water. A temporary inlet frit was formed with a heated wire stripper while the column was flushed with an aqueous solution at a pressure of 700 bar. The packed capillary was cut to a length of 54 cm and a new inlet frit was prepared using the same sol-gel fused microfiber procedure mentioned above.

3.2.4 Capillary-to-Microchip Fittings

Fittings were developed to connect capillary tubing to microchips. Photographs of the fittings are displayed in Figure 3-1. A C-clamp was used to compress a modified LC fitting against a microchip. The C-clamp was machined from an 8-mm square stainless steel rod cut to a length of 20 mm. A 3-mm-wide slot was cut in one end of the rod to accept the microchip. A hole was drilled perpendicularly to the slot and tapped to match the thread of the fitting assembly. The fitting assembly consisted of a polyetheretherketone nut (F121-H, Upchurch Scientific, Oak Habor, WA) modified to hold a stainless steel coned insert. The cone of the insert was used to press a polytetrafluoroethylene (PTFE) ferrule against the surface of the microchip. The PTFE ferrule deformed easily to seal against both the capillary and the glass microchip surface. To install the fitting, a capillary was threaded through the loose fitting/C-clamp assembly and into the access port on the microchip. As the nut was finger tightened, the capillary would remain aligned with the access port on the microchip. The alignment could be

checked by inspecting the capillary's position through the hole drilled in the bottom of the C-clamp.

3.2.5 Microchip CE Device

Figure 3-2A shows a schematic of the simple cross channel microchip used for 2D LC-CE separations. Microchips were fabricated from 150-μm-thick glass substrates (Corning 0211 borosilicate, Erie Scientific Co., Portsmouth, NH) by standard photolithography, wet-chemical etching, and bonding procedures.[14] Microchips were attached to 0.9-mm-thick glass with UV epoxy (68, Norland Products Inc., Cranbury, NJ) to provide greater structural support. The 4-cm-long CE channel was 7 μm deep and 65 μm wide at full width as measured by profilometry (P15, KLA, Tencor Corp., San Jose, CA).

After the device fabrication was complete, all channel surfaces were coated with PolyE-323. PolyE-323 is a polyamine that adheres to the silanol groups on the glass by electrostatic interactions and hydrogen bonding to provide stable EOF when using acidic to neutral background electrolyte solutions.[10,15] The chemical structure for PolyE-323 is shown in Figure 3-2B. The coating procedure has been previously reported and will only be briefly described here.[14] Flushing the device was accomplished by applying vacuum to select fluid reservoirs. The channels were first cleaned by flushing with 1N sodium hydroxide for 30 min followed by a 5 min rinse with water. Next, the channels were coated by flushing with the PolyE-323 solution for 1 hr. Excess polymer was removed by flushing the channels with 60 mM ammonium acetate for 5 min and finally water for 5 min.

3.2.6 System Operation

Figure 3-2A shows the experimental setup for the 2D LC-CE separation system. The LC pump (nanoAcquity Binary Solvent Manager, Waters Corp., Milford, MA) delivered the mobile phase at 150 nL/min. Mobile phase A was 0.1% formic acid in water and mobile phase B was 0.1% formic acid in acetonitrile. A standard 6-port valve (C72, VICI Valco Intruments Co. Inc., Houston, TX) was used for sample injection onto the capillary LC column. The outlet of this column was connected to a 30 μm i.d. transfer capillary that was 3 cm-long using a PTFE sleeve. The transfer capillary was then connected to the microchip using the custom capillary-to-chip fittings. This transfer capillary was used to prevent potential damage to the LC capillary oulet frit in the capillary-to-microchip fitting. The LC effluent was directed towards the CE or sample waste channel by controlling the EOF within the device. Electric potentials were applied to the buffer, sample waste and waste reservoirs using a computer-controlled, high voltage power supply (2866A; Bertan, Hicksville, NY). The voltage rise and fall times (10-90%) were approximately 5 ms for this power supply. The background electrolyte (BGE) for CE separations was an aqueous solution with 1% or 0.1% formic acid and 25% acetonitrile. The CE injections were accomplished using a slight variation of the "gated" injection scheme[16] as described later.

Analytes were detected by the LIF system described in Chapter 2. For separations of flourescein and rhodamine B an excitation wavelength of 488 nm and a band pass emission filter (575 DF 50) were employed. Separations of 5-TRITC labeled peptides utilized a 514 nm excitation wavelength and a long pass emission filter (LP02-514RU-25; Semrock, Rochestor, NY). For LC-LIF analysis, a detection window

was made on the transfer capillary by removing the polyimide coating with a flame and cleaning the bare capillary with acetone. The data acquisition rate was 300 Hz with exception of the 2D separation where the rate was increased to 1000 Hz.

3.2.7 Data Analysis

Peak capacities for individual LC and CE separations were calculated using software described in Chapter 2. The 2D plot was created as follows: The linear string of 2D data was segmented according to the individual CE separation windows by an in-house written LabVIEW program (National Instruments, Austin, TX). This data was then loaded into Igor Pro (WaveMetrics, Lake Oswego, OR) to stack each CE run according to LC retention time and create an image.

3.3 Results and Discussion

3.3.1 Capillary-to-Microchip Fittings

A custom fitting connected the transfer column to the microchip as shown in Figure 3-1A. In this hybrid LC-CE-LIF system, the capillary-to-microchip connection is after the LC column and therefore this connection only experienced low pressure. The peaks eluting from the LC dimension must be efficiently transferred on the microchip to retain the resolution obtained in the first dimension. To minimize the dead volume in the capillary-to-microchip connection, care was taken to create a small access port at the LC inlet channel during microchip fabrication. The access ports powder blasted into the 150-μm-thick substrates had an i.d. of 400 μm. The cylindrical volume of the access port was 18 nL; however, the dead volume in the connection was less as the inserted capillary and compressed ferrule displaced some of this volume.

These fittings were convenient to use as the installation or removal took only 30 s. Since this is a low pressure connection, very little force was needed for the PTFE ferrule to reliably seal against the capillary and microchip. No damage to the end of the capillary in the fitting was observed as long as the capillary was cut with a clean edge that was perpendicular with its length.

The amount of band broadening caused by the capillary-to-microchip connection was then determined. For this experiment, the LC column was replaced with an open capillary and the six-port valve was used to perform injections of rhodamine B at 100 nL/min. LIF detection was performed in either the transfer capillary or the LC inlet channel on the microchip. Figure 3-3 shows 7 consecutive injections monitored by LIF at each location after the peak height for each trace was normalized. The peak tailing seen at the on-capillary detection location is likely a result of the dead volume in the valve used for injections and the PTFE sleeve connection to the transfer capillary. Any additional peak broadening in the on-microchip detection trace is a result of the capillary-to-microchip fitting. The average peak full width at half max was 20% greater for the on-microchip detection. A larger difference is observed at the base of the peaks where peak tailing resulting from the capillary-to-microchip fitting is evident. The average peak width at 10% of the peak height was 38% greater for the on-microchip detection.

3.3.2 CE Injection Interface

The CE injection strategy was similar to the gated injection scheme[16] that our group previously employed to perform MEKC-CE[17-18] and CEC-CE.[19] The fluid from the buffer channel was directed across the injection cross by controlling the EOF to gate the effluent from the first dimension to waste. A portion of the flow from the buffer

channel is also directed to the CE channel for the separation. Injections are made by adjusting the applied potentials to effectively stop the fluid flow in the buffer and waste channel. The material from the first dimension is then transported directly into the CE channel. The basic fluid routing path is similar to the transverse flow gate designed by the Jorgenson group except that we generate the transverse flow by EOF instead of pressure-driven flow. As a result, the microfluidic gated injection scheme can be performed at least an order of magnitude faster than the transverse flow gating interface which relies on a mechanical valve to start and stop the transverse flow.

For the microchip devices used in this work, there were no problems establishing the gated injection scheme when the LC flow rate was approximately equal to the CE flow rate. At lower LC flow rates, the LC effluent was diluted during CE injections unless the CE filed strength was reduced. At higher LC flow rates, the EOF-driven transverse flow was insufficient to gate the LC effluent to waste. If a different LC flow rate is desired, the microchip could be redesigned to accommodate the change. For example, if the LC flow rate was increased by a factor of two, then the cross-sectional area of the channels should be two fold larger to increase the EOF proportionally while using the same applied field strength.

Consecutive CE injections were performed to evaluate the stability of the microchip LC-CE injection interface. A 2 μL sample loop in the 6-port valve continuously delivered a solution containing 30 μM fluroescein and rhodamine B to the microchip at 120 nL/min via an open capillary. The microchip used in this experiment was similar to the device in Figure 3-2, except the CE channel was 10 cm long and featured two asymmetric turns described in Chapter 2. Figure 3-4 shows a plot for the

retention times for 80 consecutive separations of these fluorescent dyes. The relative standard deviation (RSD) for the fluorescein and rhodamine B retention time was 0.27% and 0.33%, respectively. The deviation in the migration times may largely be due to temperature changes as no attempt was made to control this variable. The peak area for both fluorescent dyes for each injection is shown in Figure 3-5. The RSD for the peak area was 5.8% for fluorescein and 6.5% for rhodamine B.

3.3.3 CE Injection Sequence

For a 2D separation to be considered comprehensive, each component that elutes from the first dimension must be analyzed by the second dimension. To preserve the resolution obtained in the first dimension using the gated injection scheme, 3-4 CE injections must be performed for each LC peak.[19] Given this criteria, efforts were made to increase the number of CE separations per unit time. A normal injection scheme for consecutive CE separations is shown in the top trace of Figure 3-6. Injections are represented by the red arrows and the resulting separation is indicated by the bracket above the peaks. Each injection and the corresponding separation is labeled with the same number. The run time, t_{run}, is the elapsed time from injection to the detection of the last peak. If the same sample is analyzed in each CE separation, then t_{run} is constant. However, t_{run} will vary in a 2D LC-CE analysis because the sample composition in the LC effluent varies with time. To take this into account we will modify the definition of t_{run} to refer to the elapsed time from injection to the detection of the last peak for the CE separation that requires the longest time to complete. Similarly, we will define the CE separation window, t_{window}, as the elapsed time from the peak with the earliest migration time to the latest migration time among any of the CE separations. These values for t_{run}

and t_{window} must be determined in advance to construct the optimal CE injection frequency. This information can readily be obtained from a single CE separation of the sample without performing the LC separation.

To maximize the number of CE separations using the normal injection scheme, the second injection is performed immediately after the previous run is completed as shown in the top trace of Figure 3-6. However, t_{window} is only half of t_{run} so there are no peaks being detected during the first half of any CE separation. As a result, this time is wasted as no information is obtained about the sample. Jorgenson and coworkers described the use of an injection technique known as "overlapping injections" to utilize this down time to analyze additional separations.[1-2] Using this technique, additional injections may be performed while the first separation is still in the column. For this example where t_{window} is half of t_{run}, the use of "overlapping injections" is shown in the second trace of Figure 3-6. As a result, twice as many separations are completed in the same amount of time. This increases the number of times a peak eluting from the first dimension is sampled by the second. In theory, the maximum use of the time in the second dimension will always occur when the injection frequency is equal to t_{window}. As long as t_{run} is divided evenly by t_{window}, the injection will fall between each separation window. This last consideration is only important if the injection method changes the CE field strength or some other condition which would impair the simultaneous detection of peaks. In this device the CE field strength is held constant even during the CE injections.

3.3.4 LC-CE-LIF System

The labeled BSA digest was first separated by LC to obtain 1D data to compare with subsequent 2D LC-CE separations. Here, LIF detection was performed in a detection window created within the transfer capillary attached to the capillary LC column. The chromatogram for this 1D separation is shown in Figure 3-7. The peak capacity was calculated to be 127 using a median peak width of 19.5 s. Due to the complexity of the sample there are few baseline resolved peaks.

Next a 2D LC-CE separation was performed using the same sample and LC conditions as the 1D separation. The LC effluent was transferred onto a microchip and repetitive CE injections were performed. The voltages applied to the buffer, sample waste and waste reservoirs for injection and separation were 0 kV, 0 kV, +7 kV and 0 kV, +4 kV, +10 kV, respectively. These voltages resulted in a CE field strength of 1.7 kV/cm during both the injection and separation configuration. The CE separations were monitored by LIF at a distance of 23.5 mm from the injection cross. Previous CE separations of the sample under these CE conditions resulted in a t_{window} that was approximately 3 s. Here, "overlapping injections" were performed at an interval of 3.2 s to ensure that peaks from adjacent CE separations did not mix. The duration of each CE injection was 20 ms which was the shortest injection time possible with the high voltage power supply. A total of 1,490 CE separations were performed during the 80 min analysis.

The fluorescence signal for all CE separations was recorded in a single data file and is shown in Figure 3-8A. At this time scale, the 2D chromato-electropherogram appears similar to the 1D chromatogram in Figure 3-7. Figure 3-8B shows an expanded

time axis for a segment of the run where 4 individual CE separations are shown in greater detail. The dashed lines represent the individual CE separation windows for injection number 832 to 835. The peaks were very narrow and fit well with a Gaussian function, which suggests that there was minimal peptide adsorption to the PolyE-323 surface. The median peak width for the 13 most intense peaks in Figure 3-8B was calculated to be 43 ms. Using an average migration time for these 13 peaks of 3.70 s, the number of plates generated was calculated to be 7404, which corresponds to 3.2×10^5 plates/m.

The data was then segmented according to the individual CE separation windows and stacked to produce the 2D image plot as shown in Figure 3-9. This 2D plot shows that a large number of components were isolated in this separation. The horizontal streaking observed at an LC retention time of 29 min is was likely caused by a component continuously leaking into the CE channel. Figure 3-10 an enlarged image of a spot taken from the 2D plot in Figure 3-9 as indicated by the box. The horizontal dashes indicate the individual CE separations that were stacked to produce this image. It is clearly seen that at least 6 CE injections were preformed of the same component eluting from the LC dimension. This high sampling rate ($\geq$4 CE injections per LC peak) allows the resolution attained in the first dimension to be maintained.

The maximum theoretical peak capacity for a 2D separation is the product of the single dimension peak capacities.[20] To estimate the peak capacity of the first dimension, the LC chromatogram was reconstructed form the 2D data. This was accomplished by summing the fluorescence intensity in each CE run to represent a single point in the LC chromatogram. The peak capacity of this reconstructed chromatogram was 134 using a median peak width of 21.3 s. The higher flow rate used in this 2D separation likely

reduced the effect of the band broadening caused by the capillary-to-microchip fittings. The peak capacity in the CE dimension was calculated to be 58 using a median CE peak width of 43 ms and a separation window of 2.5 s. Therefore the maximum peak capacity for this system would be 7772. However, Figure 3-8 shows a large amount of the total separation space is not occupied by peaks. This is especially apparent in the upper right corner of the 2D plot. To explain this phenomenon it is useful to estimate the properties of analytes likely to occupy this region of the separation space. The polyE-323 coated CE channel provided anodic (reversed) EOF and no TRITC-labeled peptides in the sample are not expected to have a net negative charge at pH 2.5. Therefore, peptides eluting early in the CE dimension (CE migration time near 3.25 s) have a relatively low electrophoretic mobility, μ_{ep}, against the EOF. Later eluting peptides (CE migration time near 5 s) have a relatively high μ_{ep} against the EOF. For a peptide to elute in the upper right hand corner it would have to be very hydrophobic and have a relatively high μ_{ep}. However, it is unlikely that a peptide would be both very hydrophobic and a high mobility (a high charge to hydrodynamic drag ratio). Thus there is some correlation in selectivity between reversed-phase LC and CE for TRITC-labeled peptides under these conditions. Since roughly one-third of the separation space is occupied by peaks, the practical peak capacity for this 2D separation may be estimated to be 2591 (one-third of the original estimate). Interestingly, a similar skew in the 2D pattern was also observed for a MEKC-CE separation of BSA digest.[18]

One strategy to increase the orthogonality of reversed-phase LC-CE separations is to alter the properties of the peptides after the first dimension analysis is completed. This approach was taken by Hooker *et al.* by using an acidic LC mobile phase (pH ~2)

followed by a basic CE BGE (pH 10.5).[3] In our microchip device it was easier to perform the electrokinetic injections using solutions with a similar pH in both dimensions.

3.3.5 TRITC Labeled Peptides

Theoretically, a complete tryptic digest of BSA is expected to produce approximately 74 peptide fragments. The additional components observed in Figure 3-9 may be caused by multiple factors including: impurity of the labeling reagent, incomplete protein digestion, auto-digestion of trypsin, and amine containments. In an attempt to identify the source of these "extra" peaks, the following three solutions were labeled with TRITC: 1) digestion buffer; 2) digestion buffer and trypsin; 3) digestion buffer, trypsin and cytochrome c. The three solutions were prepared in parallel using the same digestion and labeling procedure as the BSA digest. The only modification was that all three solutions were filtered through a 10,000 MW regenerated cellulose cut-off filter (Micron YM-10, Millipore Corp., Bedford, MA) after labeling. These three solutions were analyzed by LC-LIF without moving any component of the LIF detection setup so the relative fluorescence intensities can be compared among these three chromatograms. The chromatogram for the labeled digestion buffer is shown in Figure 3-11A. There are several intense peaks observed but it is difficult to reach any conclusions from this separation alone. The analysis of the labeled digestion buffer and trypsin solution is shown in Figure 3-11B. This chromatogram is very similar to the labeled digestion buffer which suggests the "extra" peaks are not from the auto-digestion of trypsin or contaminates in the trypsin reagent. The analysis of the digestion buffer, trypsin, and cyctochrome c digest is shown in Figure 3-11C. All of the intense peaks

from the previous two samples are greatly reduced and numerous smaller peaks now appear. One can speculate that the large peaks are multiple forms of the TRITC which are consumed in the labeling reaction. This would also suggest that other amine contaminates in the solvents or buffers do not significantly contribute to these extra peaks. Interestingly, few extra peaks were observed when single peptides were labeled with the same reagent and analyzed by CEC-LIF as shown in Chapter 2.

3.4 Conclusion

In conclusion, novel instrumentation for performing 2D LC-CE separations has been presented. The custom capillary-to-microchip fittings enabled small volume LC peaks to be transferred onto the microchip without excessive band broadening. This is the first report of an electrokinetically-controlled gated injection scheme used for performing CE injections in a LC-CE system. This injection strategy significantly reduced the complexity of the instrumentation and enabled faster CE separations to be achieved. The polyE-323 surface coating enabled reproducible CE migration times and peak areas to be obtained. The LIF detection system provided high sensitivity at an acquisition rate that was able to fully characterize the very narrow CE peaks. The separation power of this system was illustrated by highly efficient separations of peptides.

Future work should address the skew in the overall peptide map shown in the 2D LC-CE plot to maximize the practical peak capacity for peptide separations. In addition, it may be possible concentrate the material injected into the CE dimension by selecting a BGE to optimize electrokinetic sample stacking. The procedure for labeling peptides with fluorescent molecules should be reviewed further to identify sources that add to the

sample complexity. It is likely that other forms of LC, such as size exclusion chromatography or hydrophilic interaction liquid chromatography, may also be utilized in this LC-CE system with minor modifications. In addition, the integration of MS detection would allow confident identification of the separated components and is address in the next chapter.

3.5 Figures

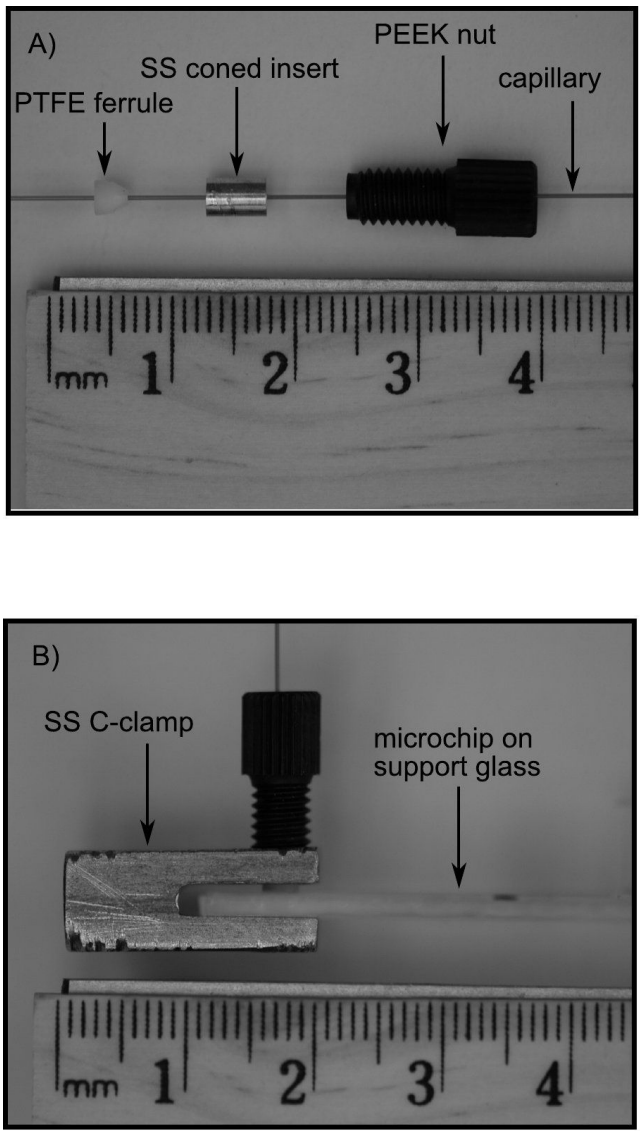

Figure 3-1. Photographs of the capillary-to-microchip fittings: A) disassembled fittings, B) side view of the assembled fitting in use.

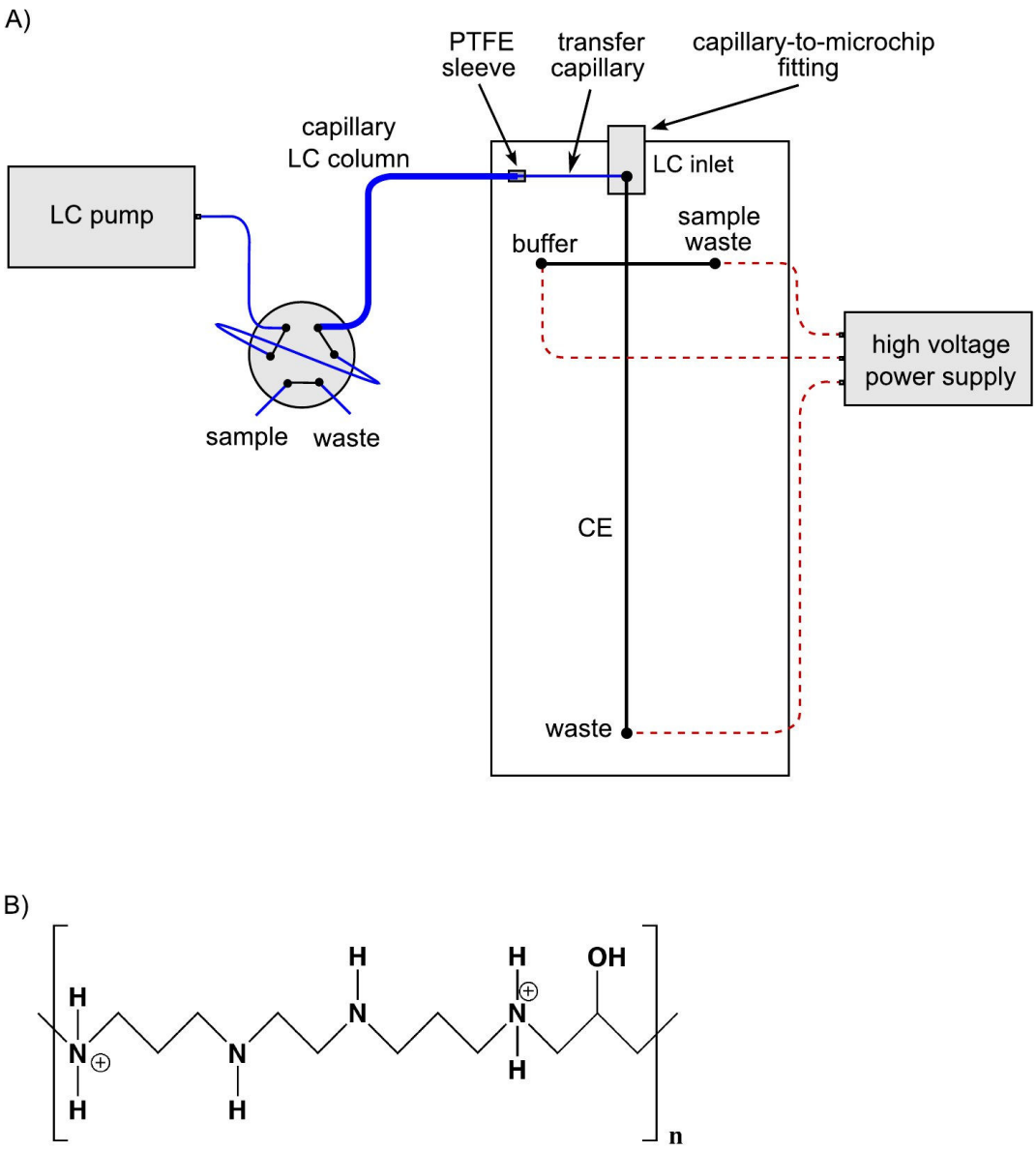

Figure 3-2. A) Schematic for the hybrid 2D LC-CE-LIF separation system, B) chemical structure for the PolyE-323 channel surface coating.

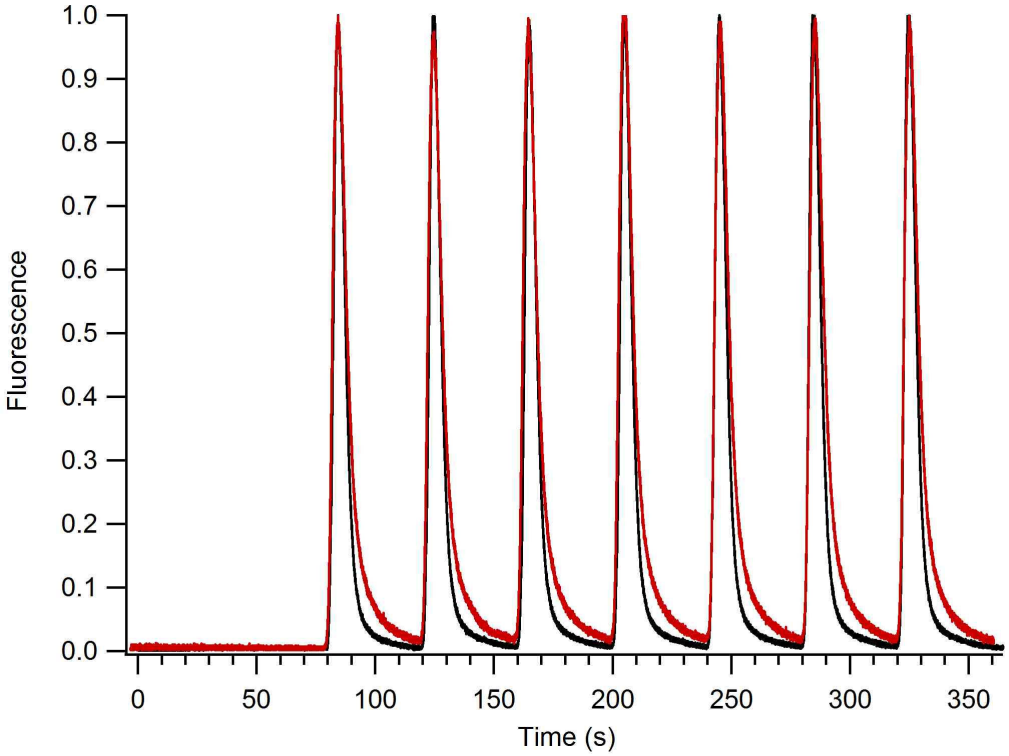

Figure 3-3. LIF detection of rhodamine B peaks at the transfer capillary (black) and in the LC inlet channel on the microchip (red).

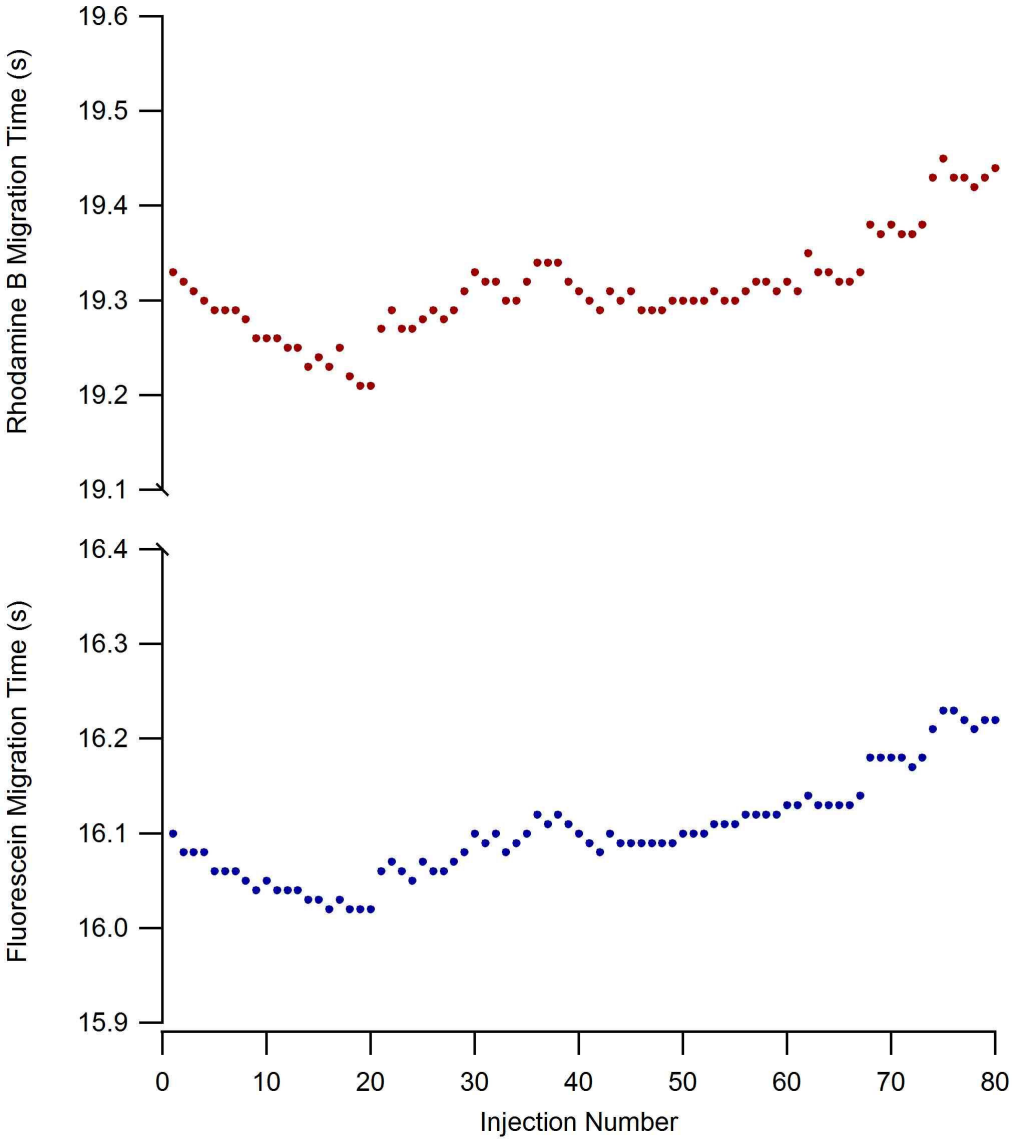

Figure 3-4. Migration times for 80 consecutive CE injections of the same fluorescein and rhodamine B sample. Analysis performed on a microfluidic device with a 10 cm CE separation channel. BGE: 0.1% formic acid, 25% acetonitrile, pH 2.5, E = 1 kV/cm, L = 95 mm.

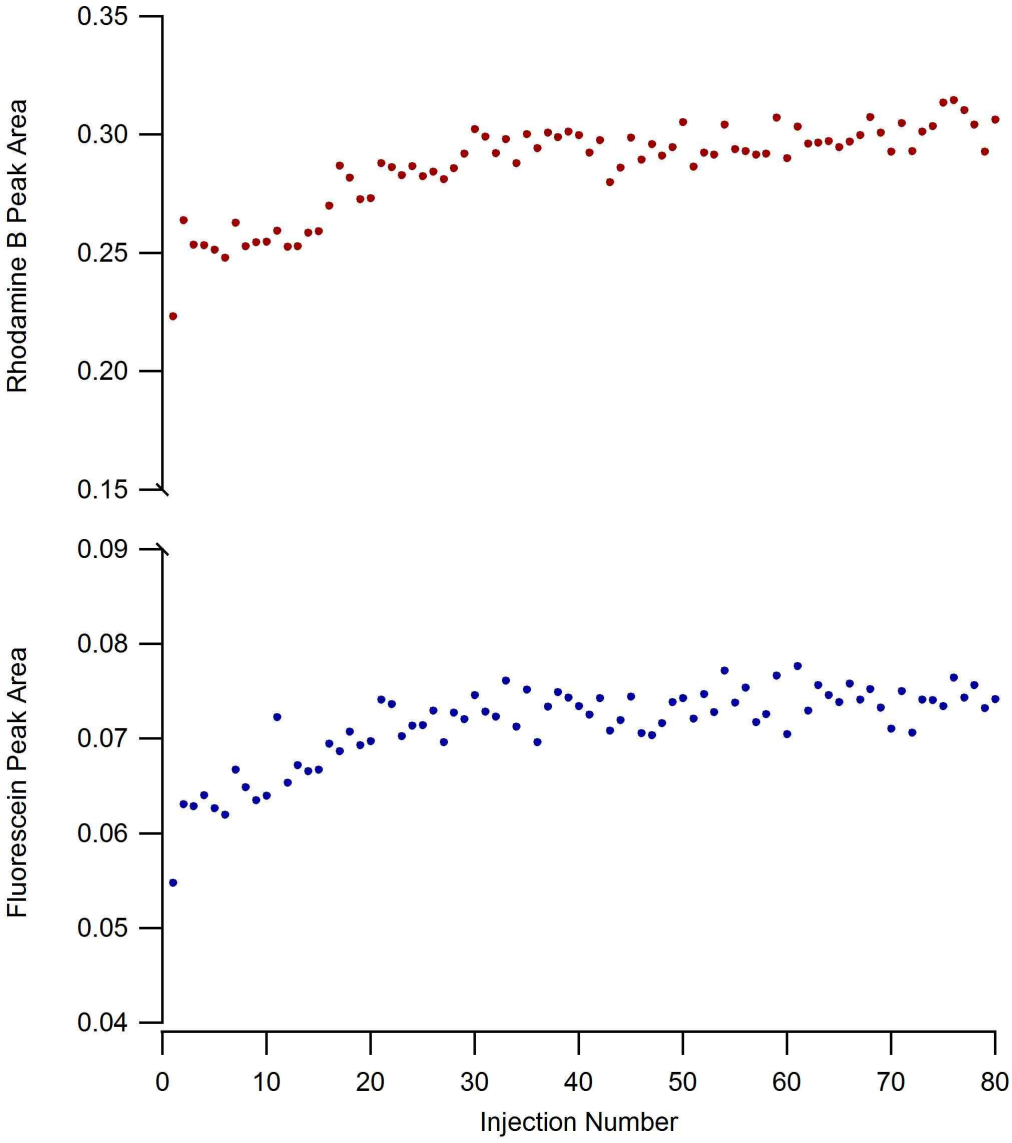

Figure 3-5. Peak area for 80 consecutive CE injections of the same fluorescein and rhodamine B sample. Analysis performed on a microfluidic with a 10 cm CE separation channel. BGE: 0.1% formic acid, 25% acetonitrile, pH 2.5, E = 1 kV/cm, L = 95 mm.

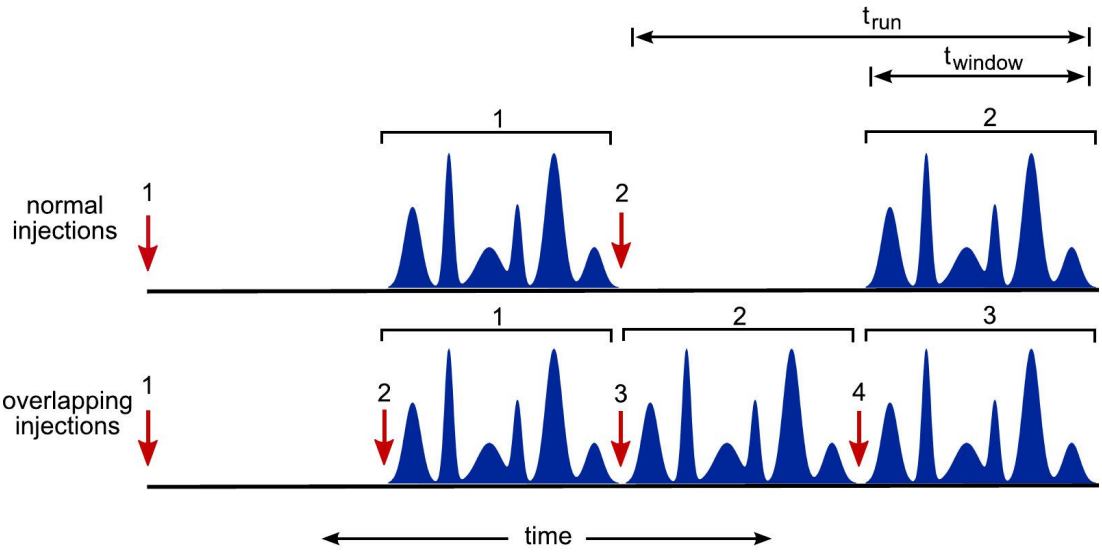

Figure 3-6. Diagram of injection sequences for maximizing the number of separations per unit time using normal and "overlapping" injections. See text for a detailed explanation.

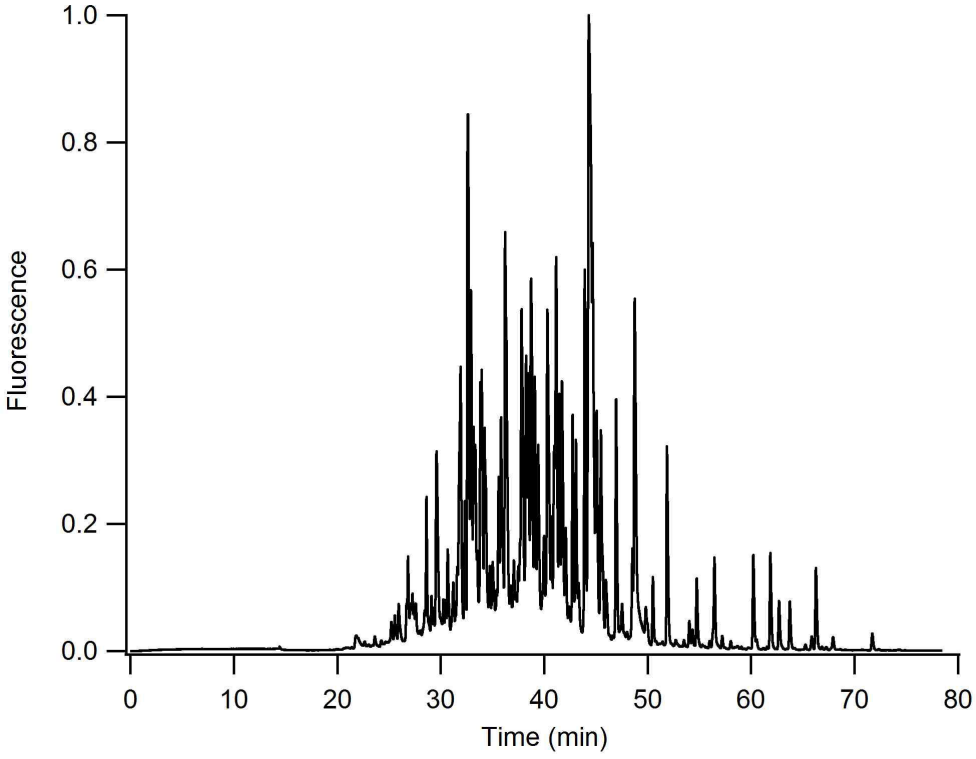

Figure 3-7. LC-LIF separation of a BSA tryptic digest. Flow rate: 150 nL/min. Gradient: 15-50% B in 60 min (MPA: 0.1% formic acid in water, MPB: 0.1% formic acid in acetonitrile.)

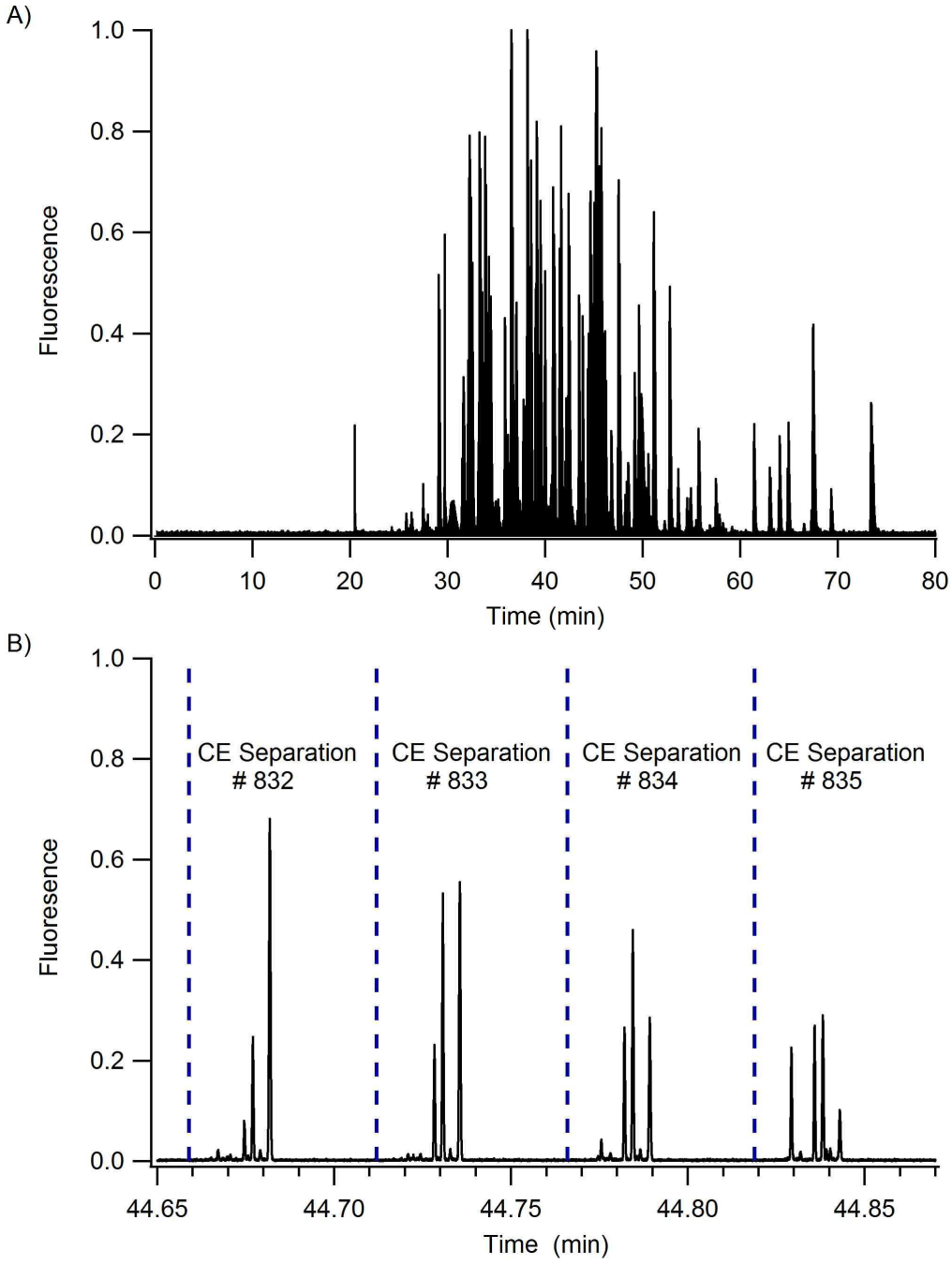

Figure 3-8. LC-CE-LIF separation of a BSA tryptic digest. Flow rate: 150 nL/min. Gradient: 15-50% B in 60 min (MPA: 0.1% formic acid in water, MPB: 0.1% formic acid in acetonitrile.) CE BGE: 1% formic acid, 25 % acetonitrile; L: 23.5 mm, E: 1.5 kV/cm.

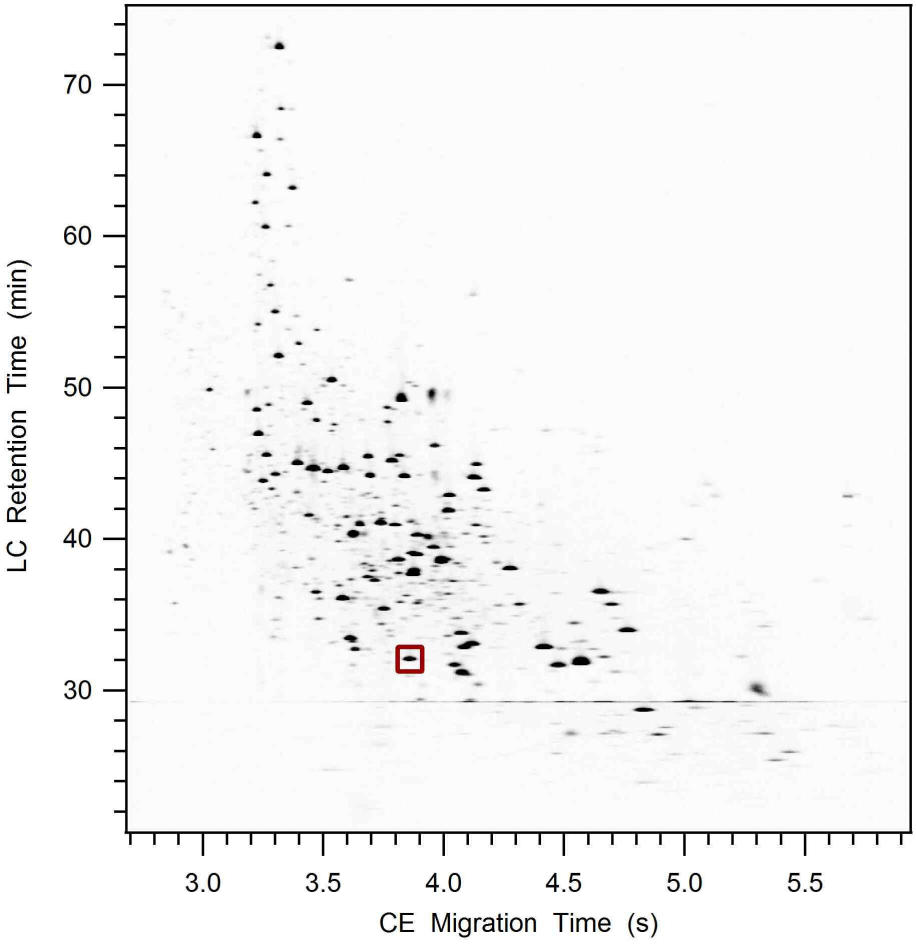

Figure 3-9. A 2D plot of the LC-CE-LIF data shown in Figure 3-7. The red box indicates the region that is enlarged and shown in Figure 3-10.

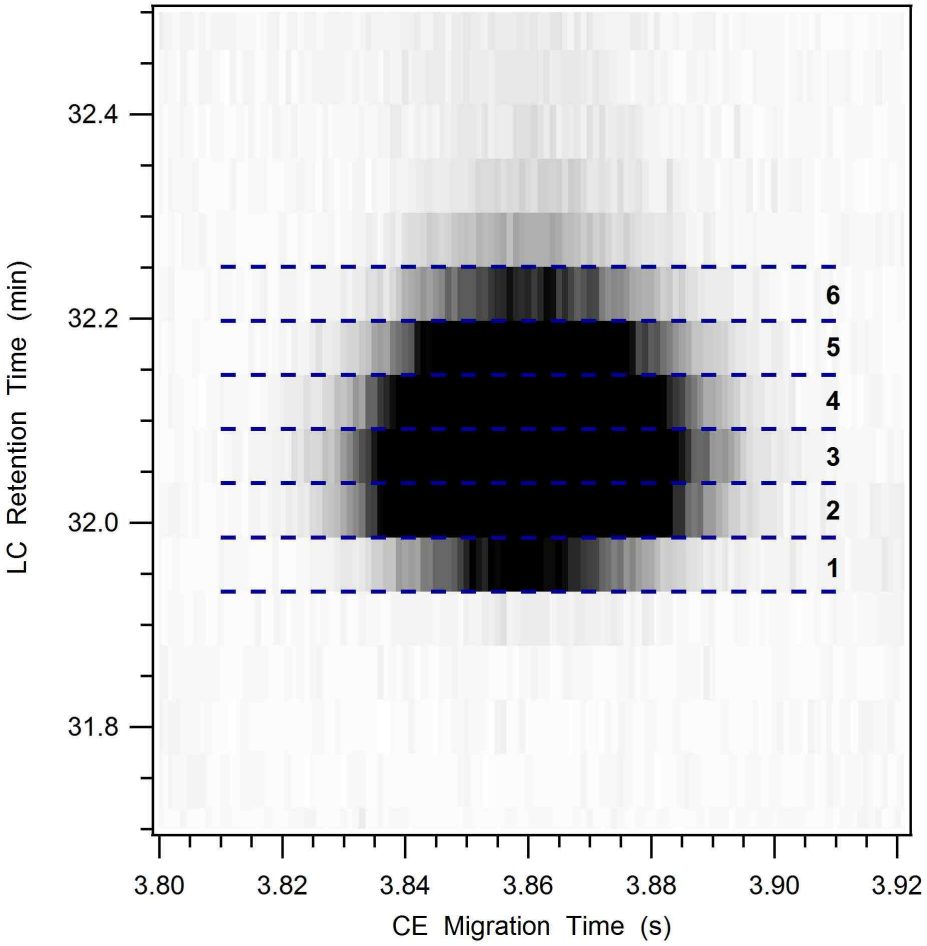

Figure 3-10. Enlarged spot from the 2D LC-CE-LIF data in Figure 3-9.

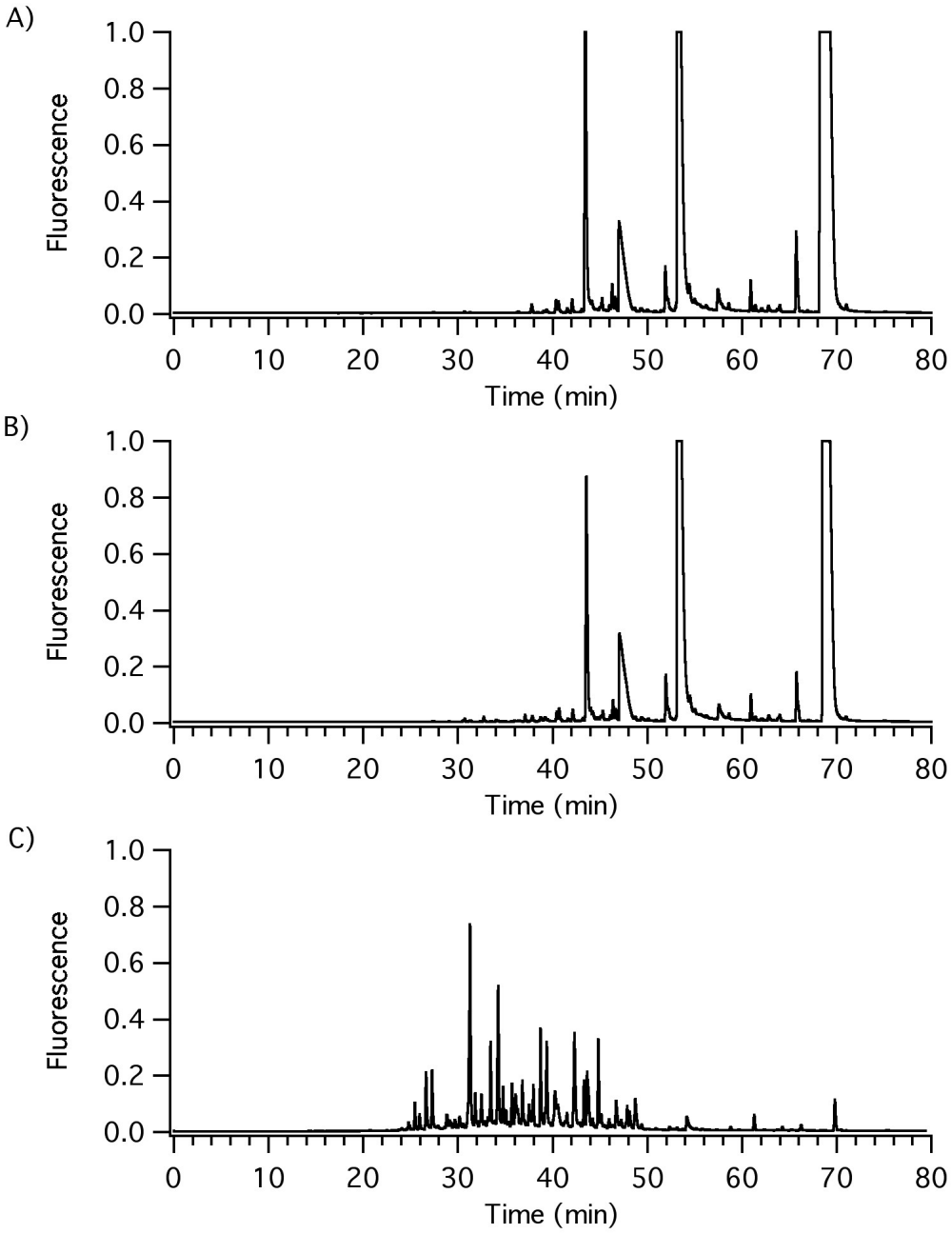

Figure 3-11. LC-LIF analysis of A) digestion buffer, B) digestion buffer and trypsin, and C) digestion buffer, trypsin and cytochrome c. Flow rate: 150 nL/min. Gradient: 15-50% B in 60 min (MPA: 0.1% formic acid in water, MPB: 0.1% formic acid in acetonitrile.)

3.6 References

1. Bushey, M. M.; Jorgenson, J. W. Automated instrumentation for comprehensive 2-dimensional high-preformance liquid-chromatography capillary zone electrophoresis. *Anal. Chem.* **1990**, *62*, 978.

2. Lemmo, A. V.; Jorgenson, J. W. Transverse flow gating interface for the coupling of microcolumn-LC with CZE in a comprehensive 2-dimensional system. *Anal. Chem.* **1993**, *65*, 1576.

3. Hooker, T. F.; Jorgenson, J. W. A transparent flow gating interface for the coupling of microcolumn LC with CZE in a comprehensive two-dimensional system. *Anal. Chem.* **1997**, *69*, 4134.

4. Bergstrom, S. K.; Samskog, J.; Markides, K. E. Development of a poly(dimethylsiloxane) interface for on-line capillary column liquid chromatography-capillary electrophoresis coupled to sheathless electrospray ionization time-of-flight mass spectrometry. *Anal. Chem.* **2003**, *75*, 5461.

5. Bergstrom, S. K.; Dahlin, A. P.; Ramstrom, M.; Andersson, M.; Markides, K. E.; Bergquist, J. A simplified multidimensional approach for analysis of complex biological samples: on-line LC-CE-MS. *Analyst* **2006**, *131*, 791.

6. Petersen, N. J.; Nikolajsen, R. P. H.; Mogensen, K. B.; Kutter, J. P. Effect of Joule heating on efficiency and performance for microchip-based and capillary-based electrophoretic separation systems: A closer look. *Electrophoresis* **2004**, *25*, 253.

7. Jacobson, S. C.; Hergenroder, R.; Koutny, L. B.; Ramsey, J. M. High-speed separations on a microchip *Anal. Chem.* **1994**, *66*, 1114.

8. Yang, X. H.; Zhang, X. M.; Li, A. Z.; Zhu, S. Y.; Huang, Y. P. Comprehensive two-dimensional separations based on capillary high-performance liquid chromatography and microchip electrophoresis. *Electrophoresis* **2003**, *24*, 1451.

9. Jacobson, S. C.; Hergenroder, R.; Koutny, L. B.; Warmack, R. J.; Ramsey, J. M. Effects of injection schemes and column geometry on the performance of microchip electrophoresis devcies. *Anal. Chem.* **1994**, *66*, 1107.

10. Hardenborg, E.; Zuberovic, A.; Ullsten, S.; Soderberg, L.; Heldin, E.; Markides, K. E. Novel polyamine coating providing non-covalent deactivation and reversed electroosmotic flow of fused-silica capillaries for capillary electrophoresis. *J. Chromatogr. A* **2003**, *1003*, 217.

11. Maiolica, A.; Borsotti, D.; Rappsilber, J. Self-made frits for nanoscale columns in proteomics. *Proteomics* **2005**, *5*, 3847.

12. MacNair, J. E.; Lewis, K. C.; Jorgenson, J. W. Ultrahigh pressure reversed-phase liquid chromatography in packed capillary columns. *Anal. Chem.* **1997**, *69*, 983.

13. Patel, K. D.; Jerkovich, A. D.; Link, J. C.; Jorgenson, J. W. In-depth characterization of slurry packed capillary columns with 1.0-um nonporous particles using reversed-phase isocratic ultrahigh-pressure liquid chromatography. *Anal. Chem.* **2004**, *76*, 5777.

14. Mellors, J. S.; Gorbounov, V.; Ramsey, R. S.; Ramsey, J. M. Fully integrated glass microfluidic device for performing high-efficiency capillary electrophoresis and electrospray ionization mass spectrometry. *Anal. Chem.* **2008**, *80*, 6881.

15. Ullsten, S.; Zuberovic, A.; Wetterhall, M.; Hardenborg, E.; Markides, K. E.; Bergquist, J. A polyamine coating for enhanced capillary electrophoresis-electrospray ionization-mass spectrometry of proteins and peptides. *Electrophoresis* **2004**, *25*, 2090.

16. Jacobson, S. C.; Koutny, L. B.; Hergenroder, R.; Moore, A. W.; Ramsey, J. M. Microchip capillary electrophoresis with an integrated postcolumn reactor. *Anal. Chem.* **1994**, *66*, 3472.

17. Rocklin, R. D.; Ramsey, R. S.; Ramsey, J. M. A microfabricated fluidic device for performing two-dimensional liquid-phase separations. *Anal. Chem.* **2000**, *72*, 5244.

18. Ramsey, J. D.; Jacobson, S. C.; Culbertson, C. T.; Ramsey, J. M. High-efficiency, two-dimensional separations of protein digests on microfluidic devices. *Anal. Chem.* **2003**, *75*, 3758.

19. Gottschlich, N.; Jacobson, S. C.; Culbertson, C. T.; Ramsey, J. M. Two-dimensional electrochromatography/capillary electrophoresis on a microchip. *Anal. Chem.* **2001**, *73*, 2669.

20. Giddings, J. C. Two-dimensional separations - concept and promise. *Anal. Chem.* **1984**, *56*, 1258A.

CHAPTER 4: Hybrid 2D Liquid Chromatography-Capillary Electrophoresis with Mass Spectrometry Detection for the Analysis of Monoclonal Antibodies

4.1 Introduction

The hybrid 2D LC-CE separation system described in Chapter 3 will now be extended to incorporate mass spectrometry detection. This work utilizes a fully integrated microchip ESI interface that was previously used for CE-MS.[1-2] In this chapter the operation of a hybrid 2D LC-CE-MS system will be described in detail and compared with conventional 1D LC-MS analysis. This 2D system will also be evaluated for peptide mapping applications focusing on the determination of both monoclonal antibody (mAb) identity and modification.

4.2 Experimental

4.2.1 Reagents

Water used in this experiment was deionized and filtered (Nanopure Diamond, Barnstead International, Dubuque, IA). The following materials were purchased from Fisher Chemicals (Fairlawn, NJ): 2-propanol (HPLC grade), acetonitrile (optima grade), glacial acetic acid (sequencing grade), hydrochloric acid (ACS certified plus), hydrogen peroxide (30%, ACS certified), sodium acetate (enzyme grade), sodium chloride (ACS certified) and sodium hydroxide. The following materials were obtained from Sigma Chemical Co. (St. Louis, MO): 1,2-bis(3-aminopropylamino)ethane, epichlorohydrin, formic acid (Acros Organics, 99%), trichloro(1H,1H,2H,2H-perfluorooctyl)silane and

Trizma Pre-Set Crystals (pH 8.0 and pH 8.5). The trypsin (sequencing grade modified) was from Promega (Madison, WI) and the lysyl endopeptidase (lys-C) (sequencing grade) was from Wako (Richmond, VA). Leucine enkephalin was purchased from American Peptide Co., Inc. (Sunnyvale, CA). The PolyE-323 polymer was synthesized as previously described, adjusted to pH 7 with acetic acid and diluted with water to 15% (by mass) polymer.[3]

4.2.2 Sample Preparation

The monoclonal antibody (mAb) material was provided by the sponsor of this research who wishes to remain unnamed. This mAb is proprietary and therefore neither the amino acid sequence nor mass measurements with precision beyond nominal mass values will be reported. A solution containing the mAb at a concentration of 11.8 mg/mL was received without any further details regarding the solution composition. The protein digestion procedures were adapted from protocols provided with the mAb material.

The tryptic digestion of the mAb was performed as follows. The stock mAb solution was diluted to 4 mg/mL with an aqueous solution of 20 mM sodium acetate and 140 mM sodium chloride. An aliquot of 100 mL of this solution was combined with 50 µL of acetonitrile. The trypsin digestion buffer was prepared from 3.28 g of Trizma Pre-Set Crystals (pH 8.5) in 50 mL of water. A volume of 10 µL of this digestion buffer was added to the mAb mixture. One vial containing 20 µg of lyophilized trypsin was reconstituted by adding 20 µL of Trypsin Resuspension Buffer (provided with the product) and incubated at 30 °C for 15 min. The entire mAb mixture was then transferred into the activated trypsin vial and incubated at 37 °C for 24 hours. This

digestion was quenched by adding 10 μL of 1 M hydrochloric acid. The mixture was diluted to 1.5 μM with water and frozen at -20 °C until use.

The lys-C digestion of the mAb was performed as follows. The stock mAb solution was diluted to 2 mg/mL with an aqueous solution of 20 mM sodium acetate and 140 mM soldium chloride. A volume of 500 μL of this solution was combined with 25 μL of acetonitrile. The lys-C digestion buffer was prepared by dissolving 1.4 g of Trizma Pre-set Crystals (pH 8.0) in 100 mL of water. A volume of 455 μL of this digestion buffer was added to the mAb mixture. Lys-C was diluted to 1.0 mg/mL with water and 20 μL of this solution was added to the mAb mixture. The digestion was allowed to procede for 24 hours at 37 °C before quenching with 50 μL of 1 M hydrochloric acid. The lys-C digest was diluted to 1.0 μM with water and frozen at -20 °C until required.

The 10% oxidized control for the lys-C digestion was prepared by forced oxidation of a fraction of this digest. A volume of 38 μL of lys-C digest was combined with 2 μL of 30% hydrogen peroxide and allowed to react for 1 hour. The 10% spike oxidized control was then created by adding 360 μL of the original lys-C digest to this oxidized sample.

4.2.3 Microchip Fabrication

Microchips were fabricated from 150-μm-thick glass substrates (Corning 0211 borosilicate, Erie Scientific Co., Portsmouth, NH) using standard photolithography, wet-chemical etching, and bonding procedures.[1] The microchip layout is shown in Figure 4-1A. The channel lengths were as follows: LC inlet, 7 mm; waste A, 8 mm; waste B, 8 mm; buffer, 8 mm; waste C, 8 mm; segment between crosses, 4 mm; CE,

100 mm; and electroosmotic (EO) pump, 20 mm. All channels had a depth of 10 μm and a full width of 75 μm except waste A and buffer channels which had a full width of 330 μm. The electrospray tip was machined by cutting the bonded microchip with a precision dicing saw (Dicing Technology, San Jose, CA) so that the CE channel terminated at a 90° corner of the microchip.

The surface of all channels, except the EO pump channel, were coated with PolyE-323 to reverse the EOF and prevent peptide adsorption as previously described in Chapter 3. The exterior of the integrated electrospray tip was coated with trichloro(1H,1H,2H,2H-perfluorooctyl)silane to make the surface hydrophobic as previously reported.[2] The use of this coating on the electrospray tip prevents wetting and droplet formation improving electrospray stability over a wide range of conditions without raising the background in the MS signal.

4.2.4 Capillary LC

The LC pump (nanoAcquity, Waters Corp., Milford, MA) delivered the mobile phase at 500 nL/min. Mobile phase A was 0.1% formic acid in water and mobile phase B was 0.1% formic acid in acetonitrile. The LC injection volume was 200 nL for the tryptic digests and 400 nL for the lys-C digests. The profile of the mobile phase gradient was as follows: 3-10% B step, 10-40% B in 15 min. The capillary LC column used in all experiments was 0.1 mm x 150 mm and packed with 1.7 μm BEH C4 bonded particles with a 300 Å pore size (Waters Corp.) The column was held at 30 °C. These chromatography conditions were chosen for analysis of the larger peptide fragments resulting from the lys-C digest. Largely due to convenience, these same conditions were also employed to analyze the tryptic digests.

4.2.5 Microchip CE

The capillary LC column was connected to the microchip CE-ESI device using a custom low dead-volume fitting described in Chapter 3. The effluent from the LC column was split at the first cross channel intersection (waste A and waste B) to reduce the flow rate to 100 nL/min. Electrokinetic CE injections were performed at the second cross using the modified gated injection scheme described in Chapter 3. High voltages were generated by an in-house built power supply that was computer-controlled via LabVIEW software (National Instruments, Austin TX). During CE separations, the voltages applied to the buffer, waste C and EO pump reservoirs were -6.0 kV, -3.0 kV and +5.0 kV, respectively. For each CE injection these voltages were adjusted to -5.8 kV, -5.8 kV and +5.0 kV. Both voltage profiles resulted in a CE field strength of 0.8 kV/cm. The background electrolyte (BGE) for the CE separations was an aqueous solution that contained 0.1% formic acid and 5% 2-propanol by volume.

4.2.6 Microchip ESI Interface

The operation of the integrated ESI interface relies on a reversed electroosmotic pumping strategy, which will be described briefly.[1] The PolyE-323 coated CE channel had anodic (reversed) EOF while the uncoated EO pump channel had cathodic (normal) EOF. When the voltages described above were applied, the direction of the EOF in both the CE and EO pump channels was toward the electrospray tip. This created a positive pressure at the intersection which pumped fluid out of the microchip through the short channel segment leading to the electrospray orifice. The voltage at the intersection of the CE and EO pump channels provided the ESI potential. Given the relative channel lengths, the voltage at the ESI tip was calculated to be +3.3 kV. The ESI tip was

positioned approximately 5 mm from the inlet of the mass spectrometer. A voltage of 0.5-1.0 kV was applied to an external copper plate near the ESI tip to shield the electrospray region from the high voltages applied to the fluid reservoirs. A photograph of the microchip positioned in front of the inlet of the mass spectrometer is shown in Figure 4-1B. The electrospray plume was illuminated using a 3-mW green diode laser and imaged with a zoom lens (VZM 450, Edmund Optics Inc., Barrington, NJ) and a CCD camera (Sony SSC-DC83). Alternatively, LC-MS analysis was performed by connecting the capillary LC column to a capillary ESI emitter (10-μm i.d. PicoTip, New Objective, Woburn, MA).

4.2.7 Mass Spectrometry

All MS data was acquired on a time-of-flight instrument (LCT-Premier, Waters Corp.) using MassLynx software (v4.1, Waters Corp.). No sheath gas or curtain gas was used and the sample cone voltage was set to 100 V. The desolvation temperature on the mass spectrometer was set to 170 °C. The mass analyzer was operated in V mode and MS data over a range of 300-1600 mass-to-charge (m/z) was acquired at 10 Hz unless otherwise noted.

4.2.8 Data Analysis

All LC chromatograms were smoothed twice by the Savitzky-Golay method (3 scans) using software within Masslynx. The time axis for all chromatograms shown in the figures is given in minutes. The 2D chromato-electropherograms were background subtracted using software within Masslynx. Peak capacity values for the LC separations were calculated with software described in Chapter 2. The creation of 2D image plots was done as follows: the "chromatogram list" was copied from MassLynx and pasted into

a spreadsheet program used to segment the 2D data according to the individual CE separation windows. This data was then loaded into imaging software (Image J, available at http://rsb.info.nih.gov/ij; developed by Wayne Rasband, National Institutes of Health, Bethesda, MD) using an available plug-in (XYZ2DEM importer). Images were then imported into a second imaging program (Igor Pro, WaveMetrics, Lake Oswego, OR) for additional graphing options.

4.3 Results and Discussion

4.3.1 LC-CE-MS System Characterization

The mAb tryptic digest was first analyzed by LC-MS and LC-CE-MS to evaluate the basic operation of the 2D system shown in Figure 4-1A. Figure 4-2A shows the base peak index (BPI) chromatogram for the LC-MS analysis of 300 fmol of the mAb tryptic digest. Figure 4-2B shows a separate LC-CE-MS analysis of the same sample in which the LC effluent was transferred to the microchip and CE injections were performed every 10 s. Identical LC and MS conditions were employed for both analyses. The ion count for the most intense m/z value in each chromatogram is displayed in the upper right corner. The median LC peak width (4σ) was 10.1 s as measured from the LC-MS analysis. With a 10 s interval between CE injections, each component eluting from the LC dimension was only injected once on average during the 2D experiment. Therefore it is unlikely that each LC peak was sampled at its maximum peak amplitude and this may largely explain the reduced signal intensity for the LC-CE-MS analysis.

Figure 4-3 shows the data from Figure 4-2 where the regions between 6.0 min to 7.5 min have been expanded. The dashed lines indicate the individual CE separation windows in the LC-CE-MS analysis. Components are observed to elute several seconds

later in the 2D experiment due to the additional time required to perform the CE separation. The CE peaks were roughly 0.45 s wide (4σ) and therefore an average of 4.5 MS data points were recorded for each peak. The components corresponding to the 654 m/z and 506 m/z ions coeluted in the LC dimension, but were baseline resolved in the CE dimension. A similar result can be seen for the components that correspond to the 644 m/z and 933 m/z ions. Sequential CE separation windows were stacked to create the 2D plot shown in Figure 4-4A. Several components from Figure 4-3 are correlated and identified in the 2D plot by their m/z values. Analytes are well distributed across both dimensions of the 2D plot and there are a relatively large number of fully resolved spots for this 15 min analysis. For reasons unknown, the skew observed in the 2D LC-CE-LIF analysis in Figure 3-9 is not observed here.

To improve the sampling of the first dimension, "overlapping injections" were employed as discussed in Chapter 3.[4-5] This CE injection strategy enabled multiple CE separations to occur simultaneously as long as the time interval between injections was sufficient to prevent peaks in adjacent CE separations from overlapping before arrival at the ESI emitter. Figure 4-4B shows a 2D plot for the LC-CE-MS analysis of the same sample using a 5 s CE injection interval. Several peptide fragments of interest are labeled in this 2D plot and will be discussed in the next section of this chapter. The use of overlapping injections doubled the number of CE injections performed for each component eluting from the LC column. The component with a CE migration time of ~10 s was observed to wrap around to the other side of the 2D plot because the CE injection interval was slightly shorter than the CE separation window. The interval

between consecutive CE injections should have been at least 5.25 s to prevent this from occurring.

For the LC-CE-MS analysis in Figure 4-5B, the estimated peak capacities for the LC and CE dimensions were 55 and 11, respectively. Theoretically this system could produce an overall peak capacity of 605 (the product of the individual peak capacities).[6-7] However, the actual peak capacity is slightly lower because the peaks eluting from the LC dimension were only sampled twice on average. In theory, 3-4 CE injections per LC peak are required to retain the resolution obtained in the first dimension.[8] Two different approaches could to be taken to achieve optimal sampling between dimensions to maintain the same separation power in each dimension. The LC peak widths could be doubled by increasing the duration of the LC mobile phase gradient, but this would double the overall analysis time. Alternatively, the time required to perform the second dimension can be reduced. For example, the LC-CE-LIF system described in Chapter 3 generated a peak capacity of 58 in the CE dimension every 3.25 s. If this rate of peak generation could be duplicated by this LC-CE-MS device, then a peak capacity of 11 could be achieved every 0.6 s. The challenge would be obtaining a mass spectrometer with an acquisition rate fast enough to adequately sample CE peaks that are only tens of ms wide. Therefore the first approach is more feasible until considerable increases in MS data acquisition rates are realized.

To evaluate the run-to-run reproducibility of the 2D LC-CE-MS system, three replicate analyses of mAb tryptic digest were performed. The 10 most intense components (spots) were selected to compare their LC retention time and CE migration time among the three 2D plots shown in Figure 4-5. The average RSD for the LC

retention times and CE migrations times was 0.33% and 3.3%, respectively. These low RSD values compare favorably with those typically reported in the literature for LC and CE separations of peptides.

4.3.2 Antibody Tryptic Peptide Mapping

The sponsor of this research identified the amino acid sequence of 7 peptides that they commonly use for identifying this particular mAb. Reconstructed ion chromatograms for 5 of these peptides identified in the mAb digest by LC-MS are shown in Figure 4-6. Only peptide 4 is baseline resolved in the BPI chromatogram shown in the lower trace. Peptides 1 and 2 were not observed. It is likely that these peptides are not sufficiently retained on the C4 stationary phase. Peptides that are unretained are not concentrated on the column during the sample injection resulting in reduced sensitivity. In addition, these peptides likely elute with the high concentration buffers used in the protein digest, and therefore suffer reduced ionization efficiency in the ESI-MS process. For the tryptic digest, a stationary phase with a longer alkyl chain, such as C12 or C18, would have been more appropriate for retaining these smaller peptides. In addition, the step at the beginning of the LC mobile phase gradient could be replaced with a linear ramp. A 2D plot of the mAb tryptic digest is shown in Figure 4-4B. All 5 peptides observed in the LC-MS analysis were also located in this LC-CE-MS analysis and are labeled in this 2D plot.

In addition to manually identifying these peptides of interest, attempts were made to identify all peptides in the sample using the ProteinLynx Global Server (PLGS) software published by Waters Corp. Figure 4-7 shows the masses observed in the LC-MS (Figure 4-2A) and LC-CE-MS (Figure 4-2B) analyses. Only masses in the range

of 1,500-2,000 Da are shown for simplicity. The numerical labels indicate the peak elution time (LC retention time with additional CE migration time if applicable) in minutes. As mentioned earlier, the analysis time for the same component in the LC-CE-MS analysis is slightly longer due to the time required to perform the CE separation. The masses highlighted in blue were identified as masses of peptides from the mAb tryptic digest. There are several masses in the LC-CE-MS analysis that have the same analysis time as an identified peptide but are 22 Da larger in mass. For example, the first two labeled masses in Figure 4-7B have an analysis time of 9.44 min. The larger mass in each pair is likely a sodium adduct of the corresponding peptide. Sodium hydroxide was occasionally used to flush the EO pump channel after microchip storage. As long as the device was rinsed well with water after the sodium hydroxide flush, these sodium adducts were not normally observed.

A total of 25 peptides were identified by LC-MS analysis generating a sequence coverage of 55% for the light mAb chain and 35% for the heavy mAb chain. Only 18 peptides were identified in the LC-CE-MS analysis resulting in a sequence coverage of 50% for the light mAb chain and 22% for the heavy mAb chain. There are two main reasons why there were fewer identifications observed in the 2D experiment. First, the formation of sodium adducts reduced the abundance of native peptide ions. Secondly, LC peaks were undersampled by the CE dimension reducing the sensitivity of the 2D system as discussed earlier.

4.3.3 Foreign Contaminate Identification

To simulate the introduction of a foreign contaminate, leucine enkephalin was spiked into the mAb tryptic digest at a 1:1 molar ratio. Figure 4-8 shows expanded BPI

chromatograms from the LC-MS analysis of the original and spiked samples over a two minute window that includes the leucine enkephalin retention time. It is difficult to determine the presence of the leucine enkephalin peak ($[M+H]^+$, 556 m/z) from the chromatogram alone because it coelutes with other components at 9.17 min. The mass spectra at this retention time for the original and spiked samples are shown in Figure 4-9 to reveal the other ions that are present. The three most intense ions in the spectrum from the original sample were identified as tryptic peptides from the mAb digest. The 556 m/z ion (leucine enkephalin) is the base peak in the spectrum of the spiked sample. Figure 4-10 shows the 2D plots of the LC-CE-MS analysis of original and spiked samples. Although the leucine enkephalin spot is not completely resolved, it is readily visible as a new component without using the mass spectral information.

4.3.4 Determination of Methionine Oxidation

The LC-MS analysis of 400 fmol of the original mAb lys-C digest and the corresponding 10% spiked oxidized control are shown in Figure 4-11. When comparing the chromatograms, three peaks in the 10% spiked oxidized control are shifted to earlier LC retention times and gained a mass of 16 amu. This may suggest methionine oxidation of a peptide fragment. The isotope patterns for suggested native and oxidized pairs are similar which helps to confirm the relation of these components. The masses of these components correspond to peptides resulting from a lys-C digest of the mAb material that have a methionine amino acid residue. The blue numbers in Figure 4-11 indicate peaks that contain native peptides and the red numbers indicate peaks that contain corresponding oxidized peptides. Some of these indicated peaks contain multiple components; therefore, the m/z labels in the figure do not necessarily correspond to the

native or oxidized peptides. This data was also processed by PLGS and the observed masses for these peptides are shown in Figure 4-12. The native peptide masses are highlighted in blue and the oxidized peptide masses are highlighted in red. In all three cases, no native peptides are observed in the 10% spiked oxidized control and therefore it is likely that these peptides are completely oxidized. It is suspected that the excess hydrogen peroxide in the oxidized material was sufficient to cause complete oxidation of components in the 10% spiked oxidized control.

The LC-CE-MS analyses of these samples are shown in Figure 4-13. The horizontal streaking is a result of a slight malfunction of the CE injection interface that allowed a small amount of LC effluent to be continuously injected into the CE channel. The blue numbers identify native peptides and the red numbers identify oxidized peptides. These numbers also correspond with the labeled peptides in the LC-MS analysis in Figures 4-11 and 4-12. A very small amount of the oxidized form of peptide 3 can be observed in the 2D plot of the original sample. As expected, the oxidized peptides elute slightly earlier than their parent peptides in the LC dimension. Very little change was observed in the CE migration times for the native and oxidized peptides, but the CE dimension helped to resolve these peptides from other analytes. Figure 14 is an overlay of the LC-CE-MS results for the original sample and the 10% oxidized control to show the subtle change in spot position more clearly. The analysis of this data by PLGS revealed similar masses as in the LC-MS analysis in Figure 4-12 with the exception that the oxidized form of peptide 1 was not observed in the LC-CE-MS analysis of the original sample. This mass was present at relatively low abundance in the LC-MS

analysis and it is likely that this LC peak was not sampled near its maximum in the LC-CE-MS experiment.

4.4 Conclusion

In conclusion, a novel 2D LC-CE-MS system proved useful in the rapid analysis of mAb digests. This 2D system was shown to increase the peak capacity compared to LC-MS analysis. The increased resolving power of the LC-CE-MS system allowed the presence of contaminate peaks to be observed in the 2D plot without relying on mass spectral information. This work focused on high-speed analysis (≤15 min); however, the analysis time could be lengthened to generate higher peak capacities if required. The 2D separation system presented here is compatible with LIF, using methods described in Chapter 3, and MS detection. Ultimately, MS detection could identify the components in the peptide map and LIF could be utilized for routine quantitative analysis.

4.5 Figures

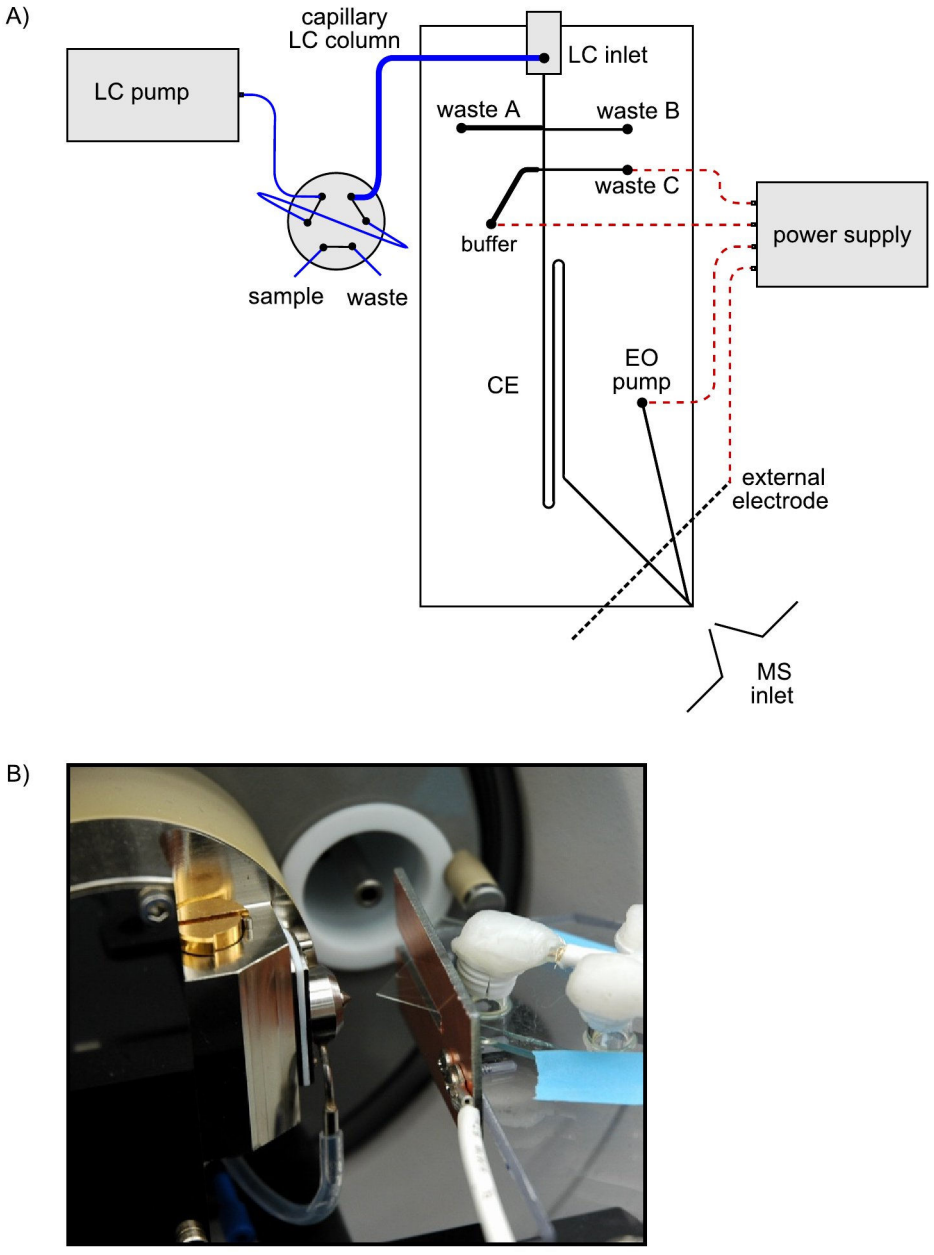

Figure 4-1. A) Schematic for the hybrid 2D LC-CE-MS system. ESI was performed from the lower right corner of the glass microchip device. B) Photograph of the microchip device mounted in front of the inlet of a mass spectrometer.

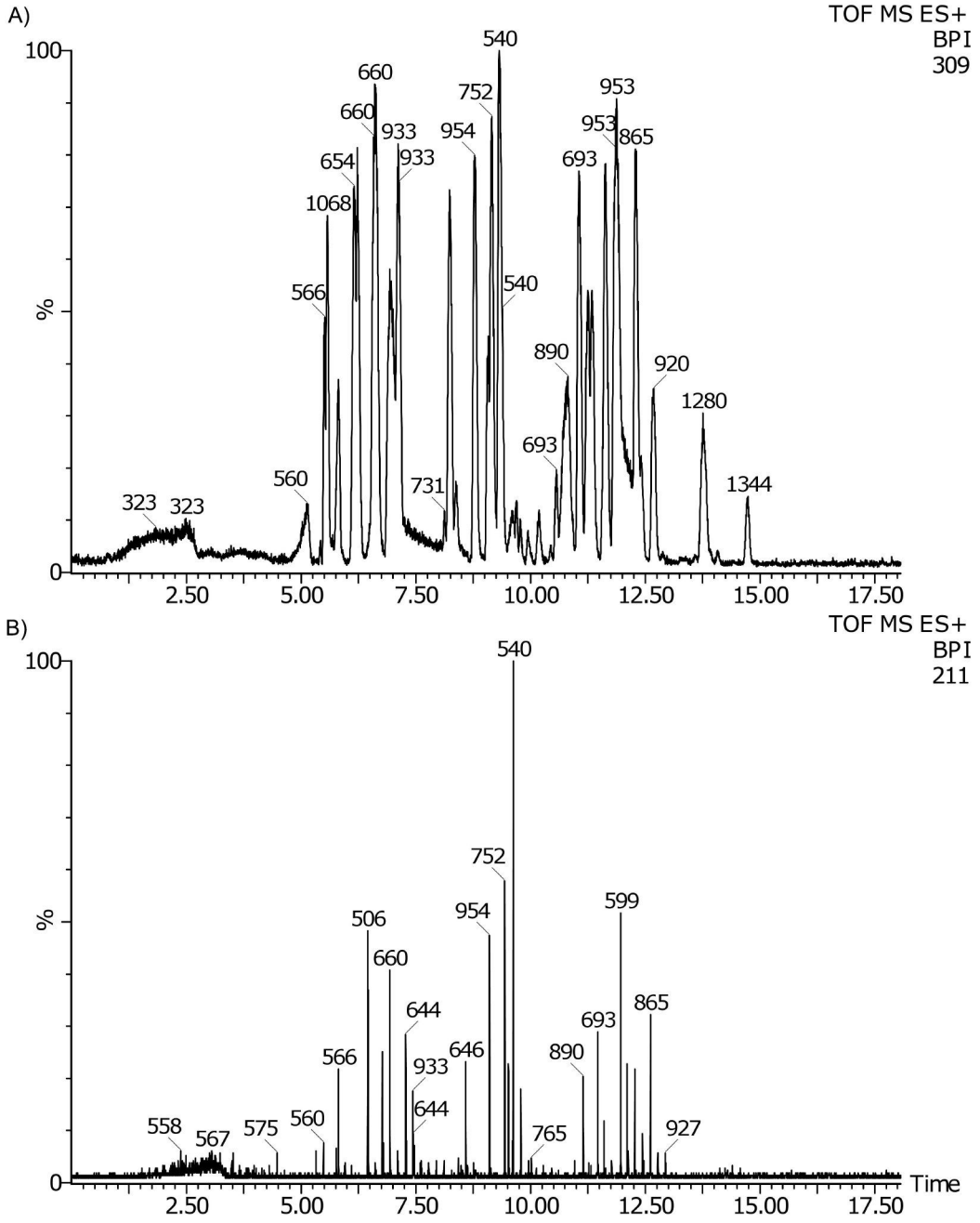

Figure 4-2. Analysis of the mAb tryptic digest by 1D and 2D methods. A) LC-MS BPI chromatogram, B) LC-CE-MS BPI chromato-electropherogram.

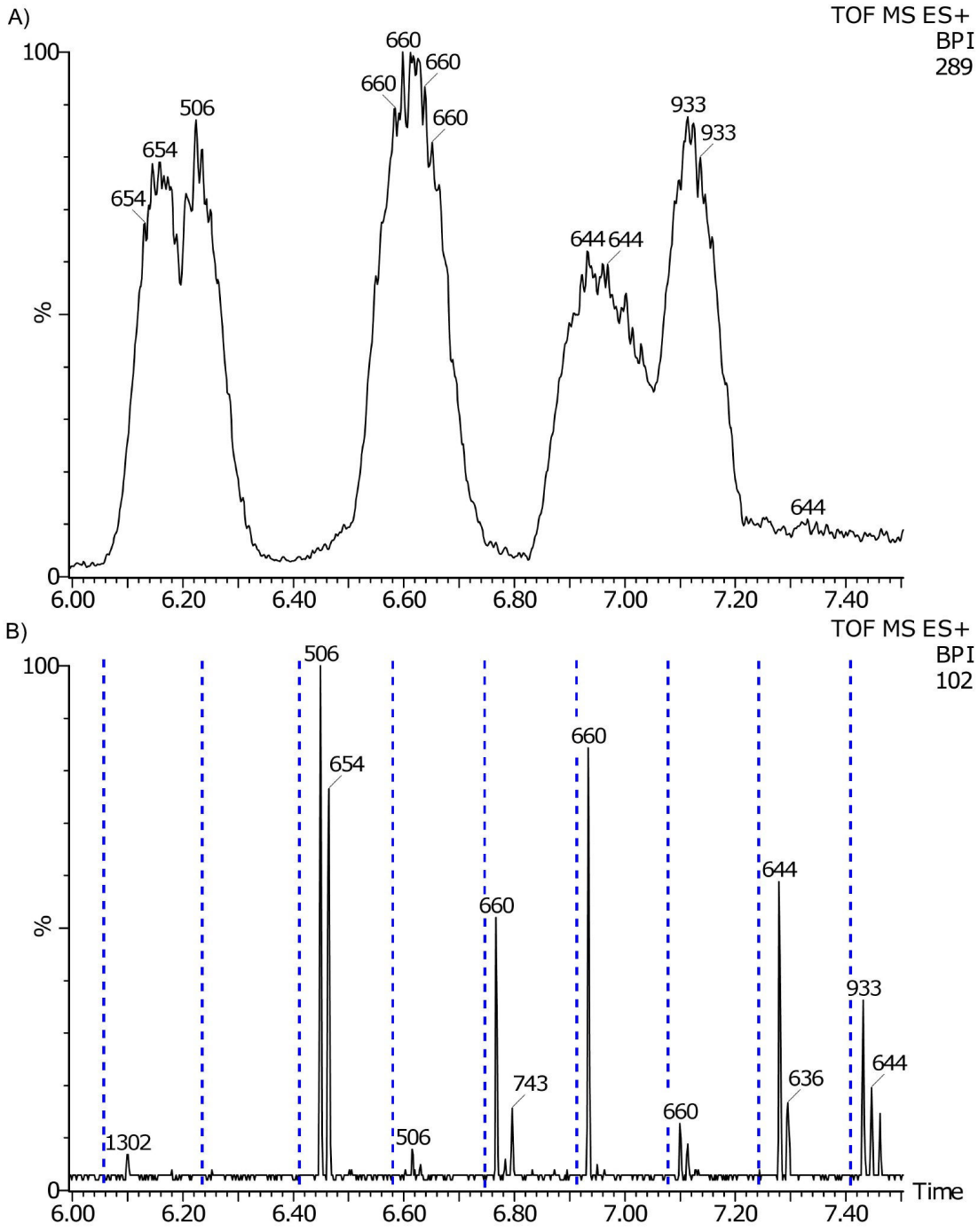

Figure 4-3. An enlarged time axis of the mAb tryptic digest analyses shown in Figure 4-2. A) LC-MS, B) LC-CE-MS. The dashed lines represent the individual CE separation windows.

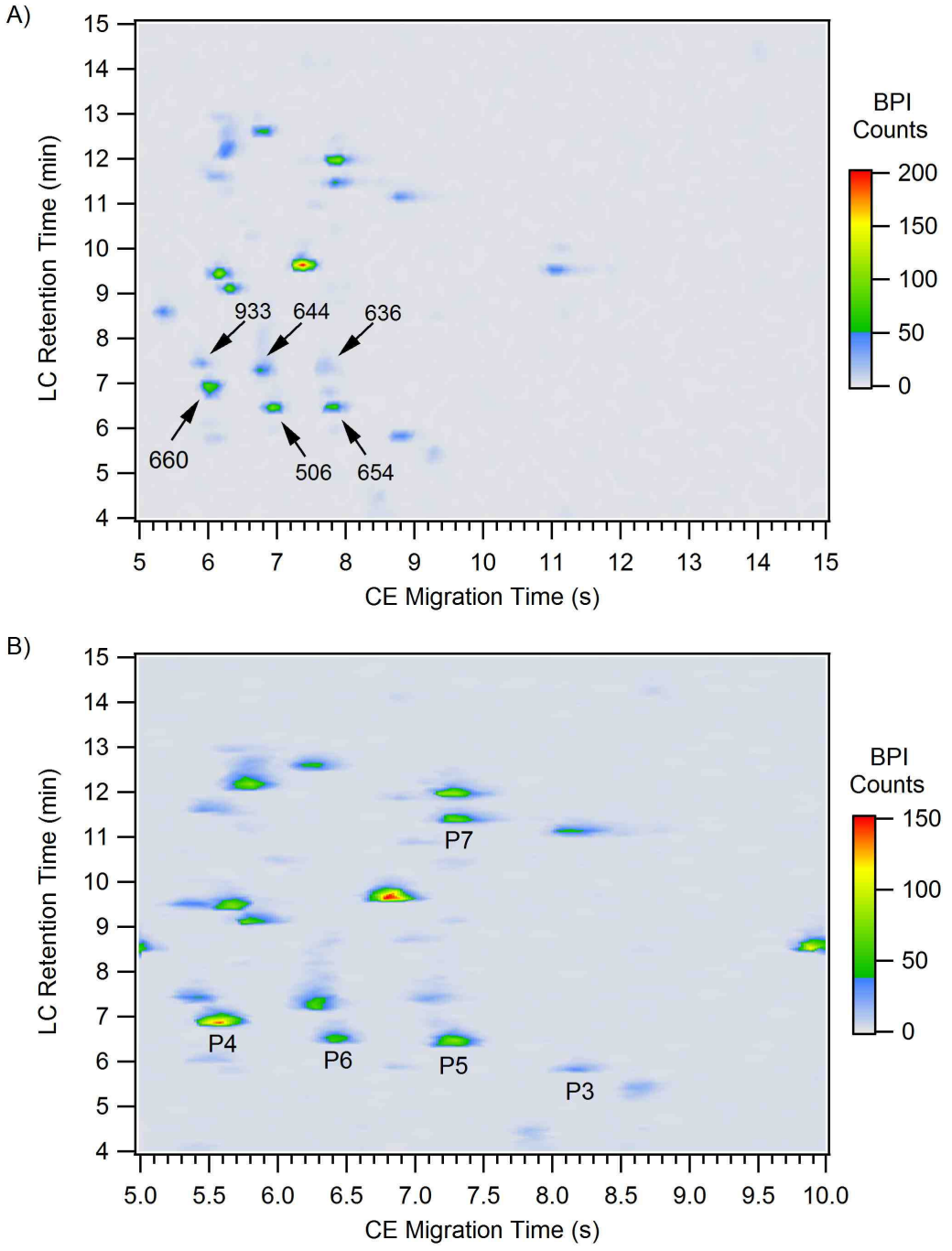

Figure 4-4. Two-dimensional LC-CE-MS analysis of the mAb tryptic digest. A) CE injections were performed every10 s. The m/z values for several components are labeled. B) CE injections every 5 s. Five peptides of interest are labeled P3-P7.

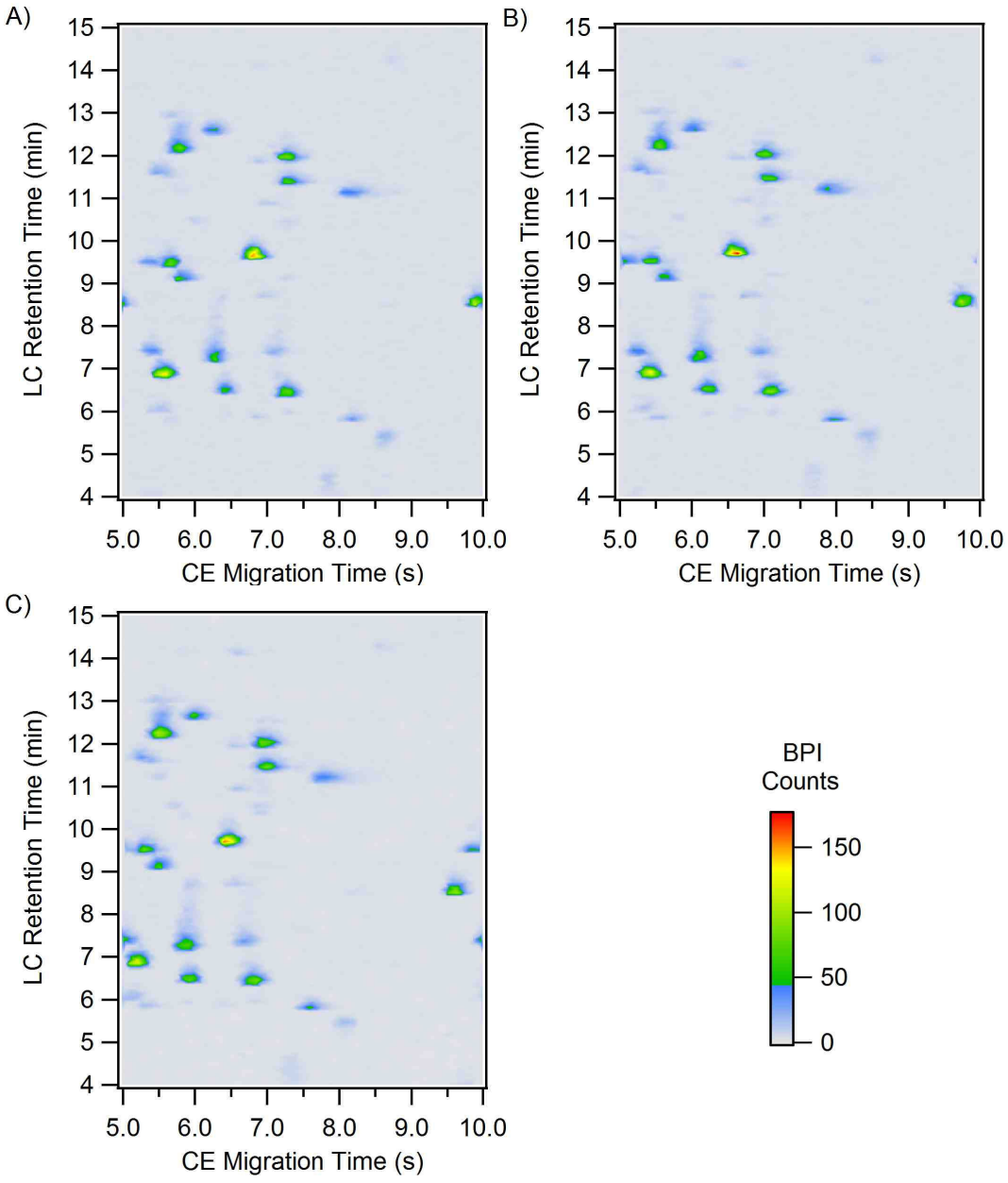

Figure 4-5. Three replicate LC-CE-MS analyses of the mAb tryptic digest.

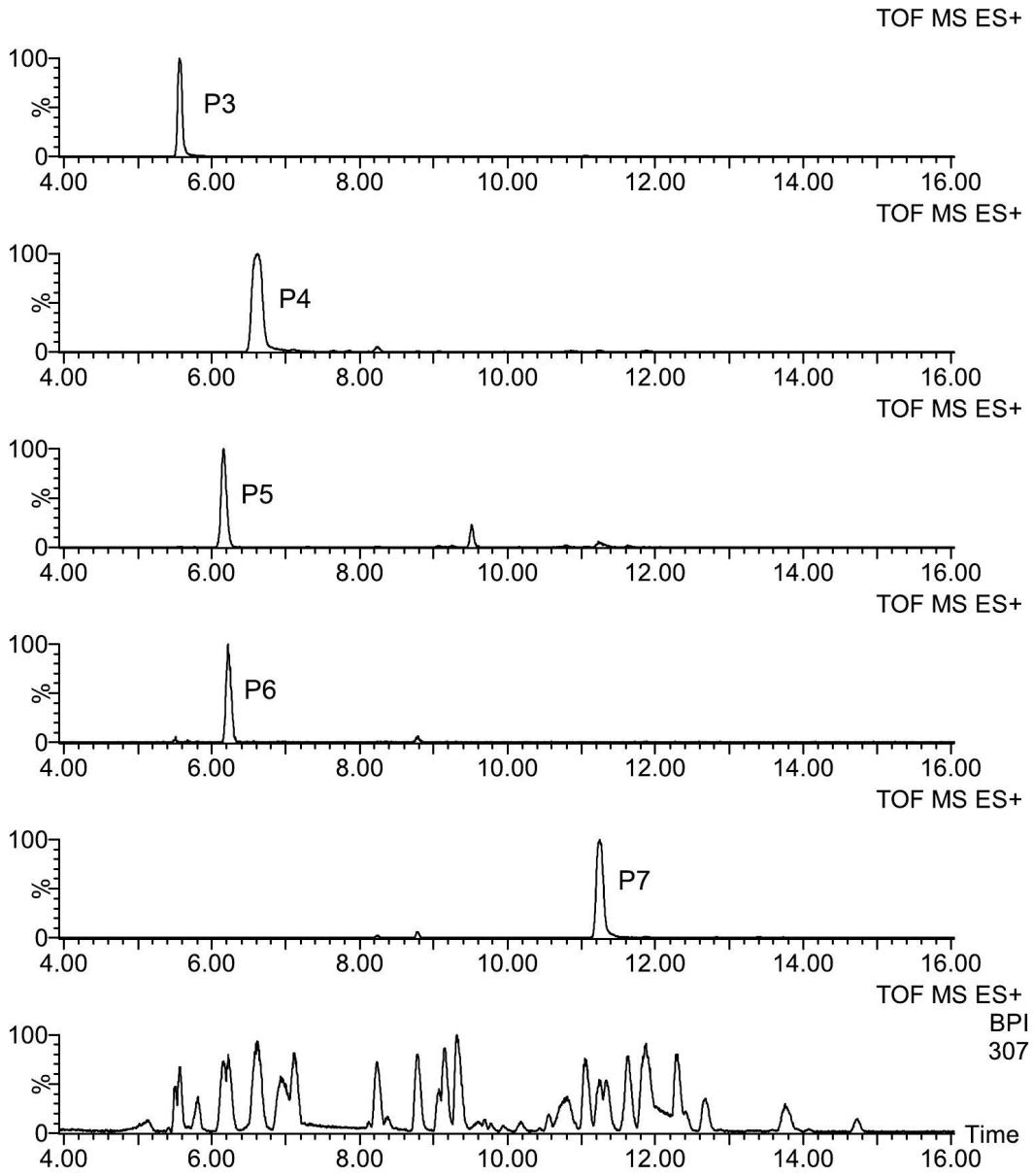

Figure 4-6. LC-MS of the mAb tryptic digest. Reconstructed ion chromatograms for 5 common tryptic peptides labeled P3-P7 and the BPI chromatogram (bottom trace).

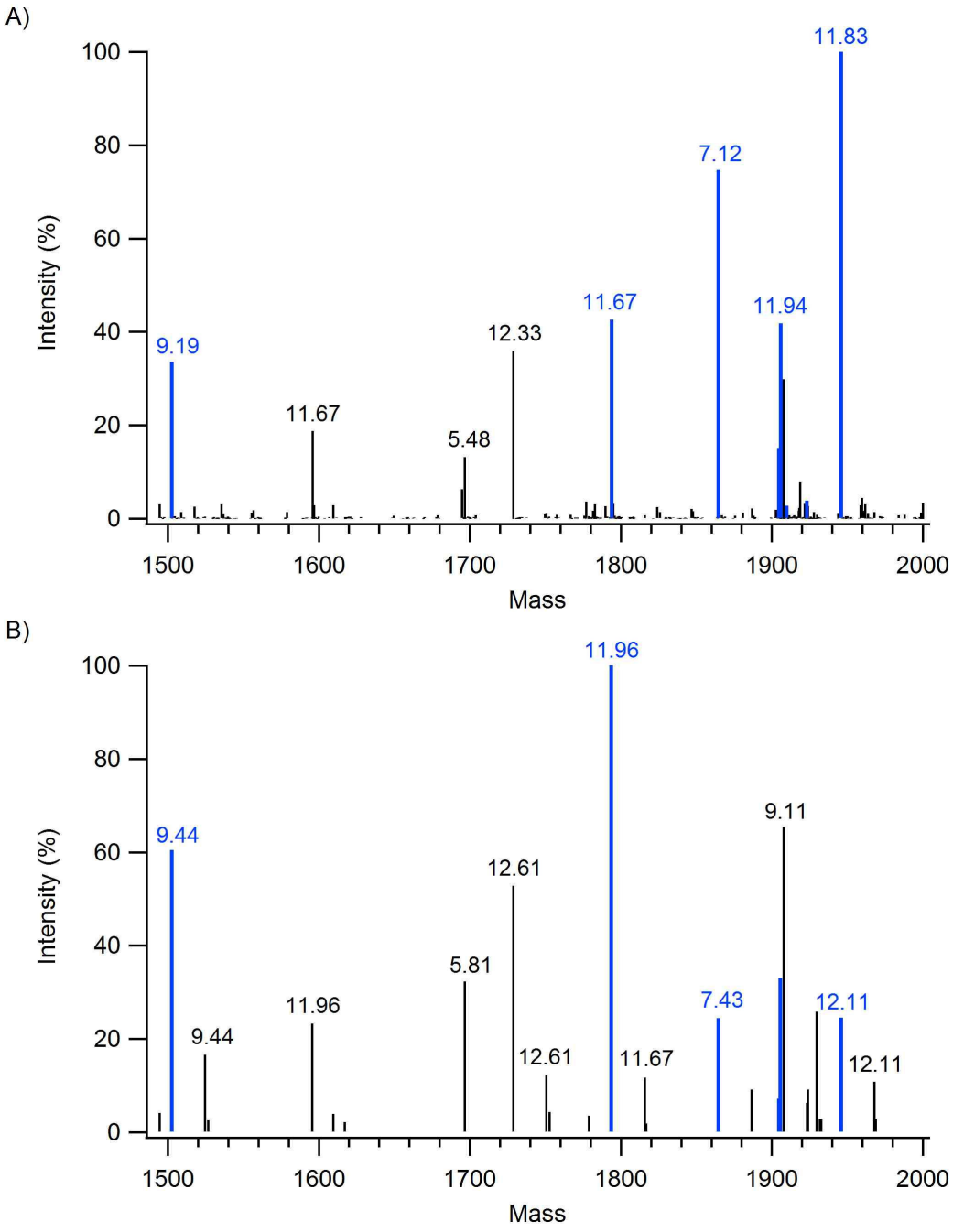

Figure 4-7. Observed ions in the 1,500-2,000 Da range from the mAb tryptic digest. A) LC-MS and B) LC-CE-MS. The numerical labels indicate the peak elution times for the detected masses in minutes. The masses highlighted in blue were identified as peptides from the mAb tryptic digest.

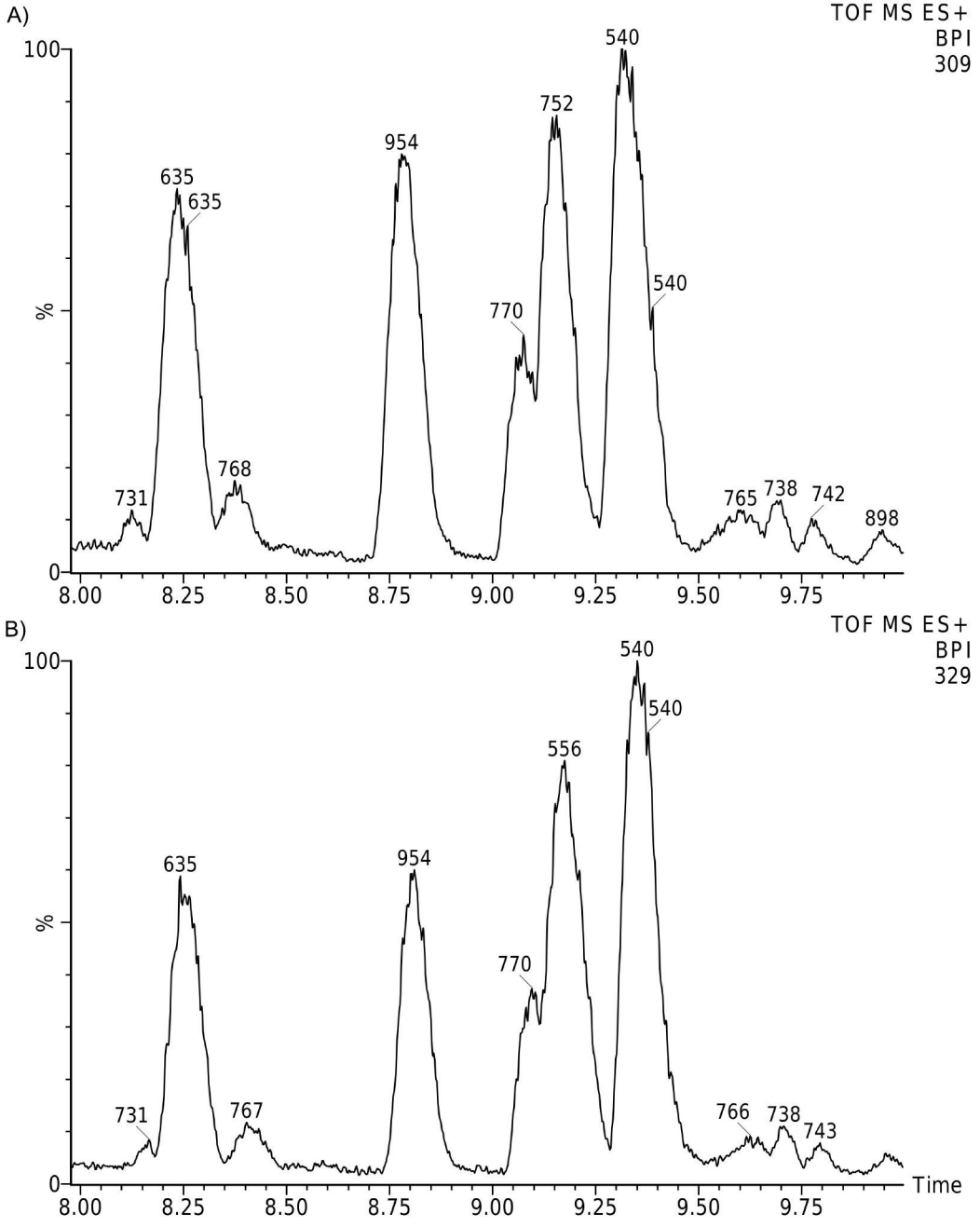

Figure 4-8. BPI chromatograms for the LC-MS analysis of the mAb tryptic digest. A) original sample, B) sample material spiked with leucine enkephalin (556 m/z).

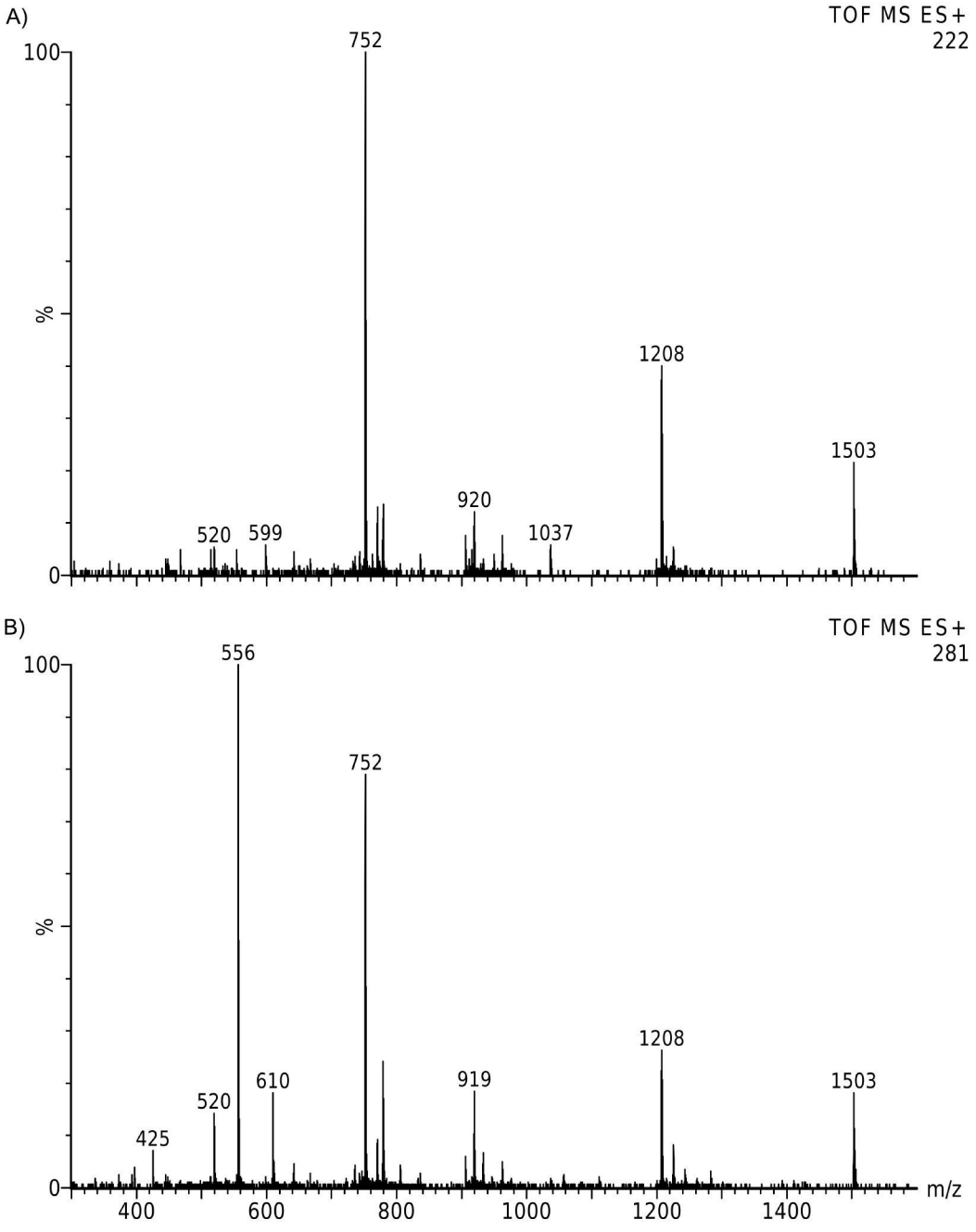

Figure 4-9. Mass spectra from the LC-MS analysis shown in Figure 4-8 at the retention time of leucine enkephalin. A) original sample, B) sample material spiked with leucine enkephlain (556 m/z).

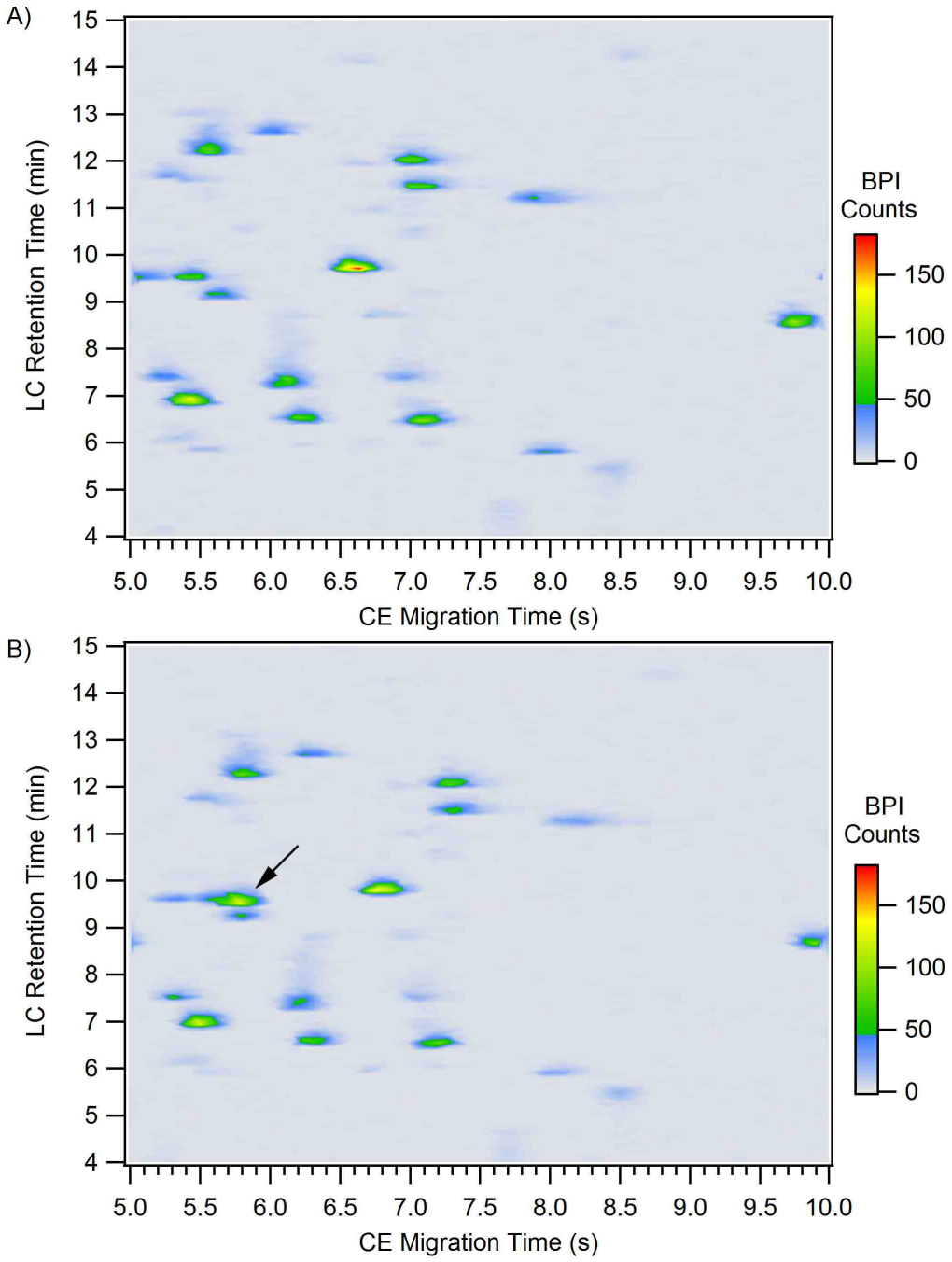

Figure 4-10. Two-dimensional LC-CE-MS analysis of the mAb tryptic digest. A) original sample, B) sample material spiked with leucine enkephalin. The arrow indicates the location of the leucine enkephalin.

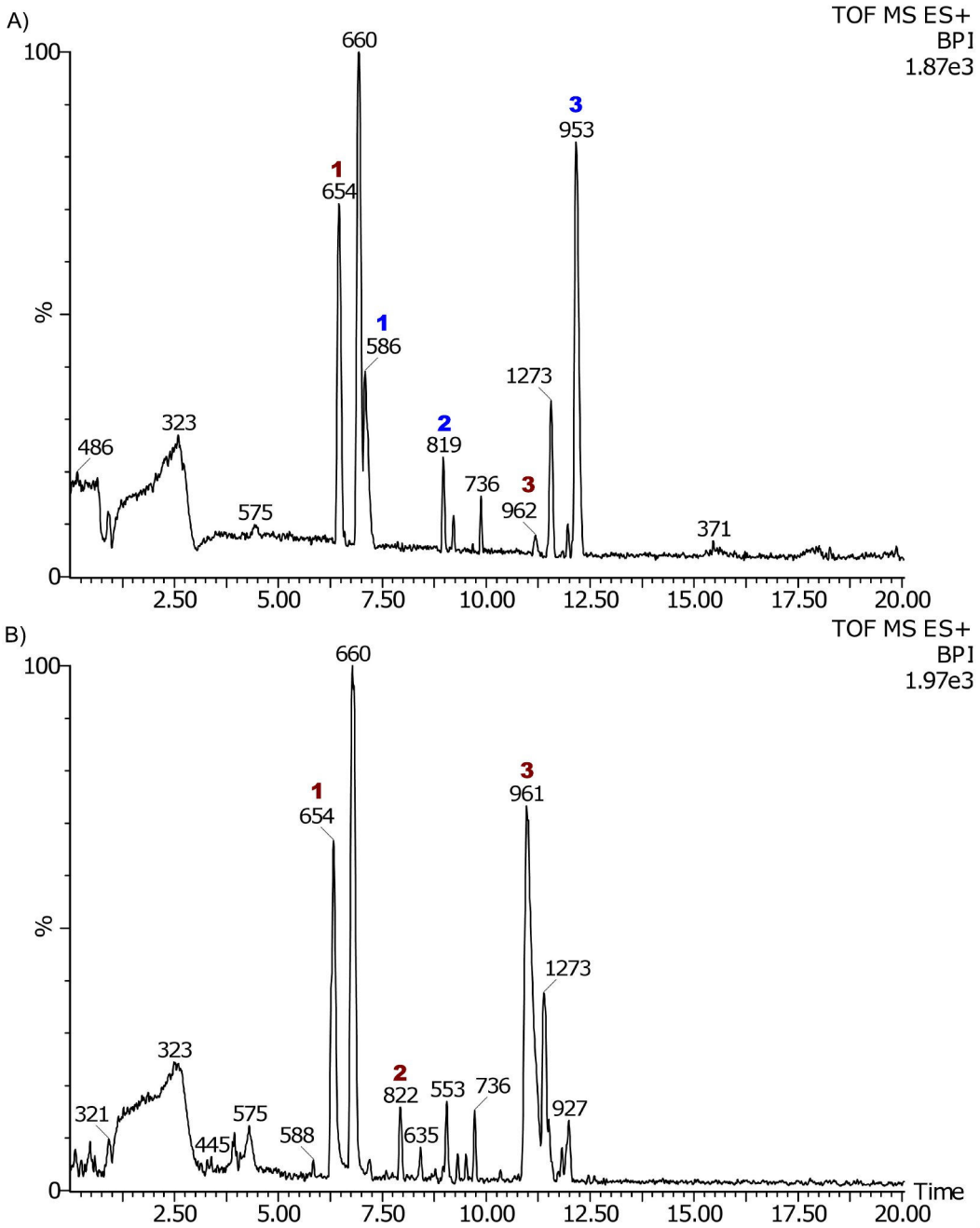

Figure 4-11. BPI chromatograms for LC-MS of the mAb lys-C digests.
A) original sample, B) 10% spiked oxidized control. The blue numbers indicate native peptides and red numbers indicate oxidized peptides. Data was acquired at 2 Hz.

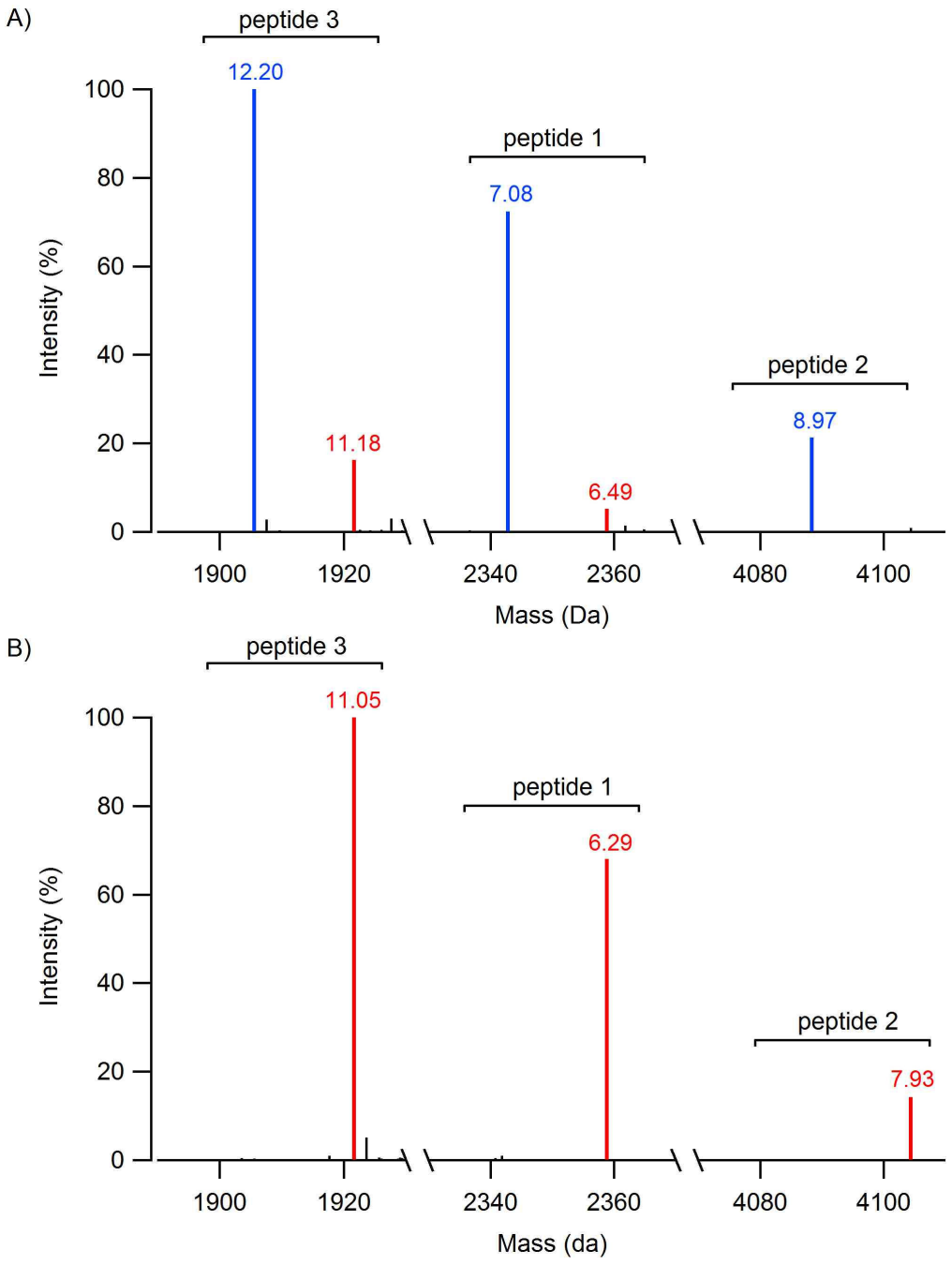

Figure 4-12. Masses observed in the LC-MS analysis of A) the original sample and B) 10% spiked control for peptides 1-3. Native peptides (blue), oxidized peptides (red). The numerical labels indicate the peak elution time in minutes for the detected masses.

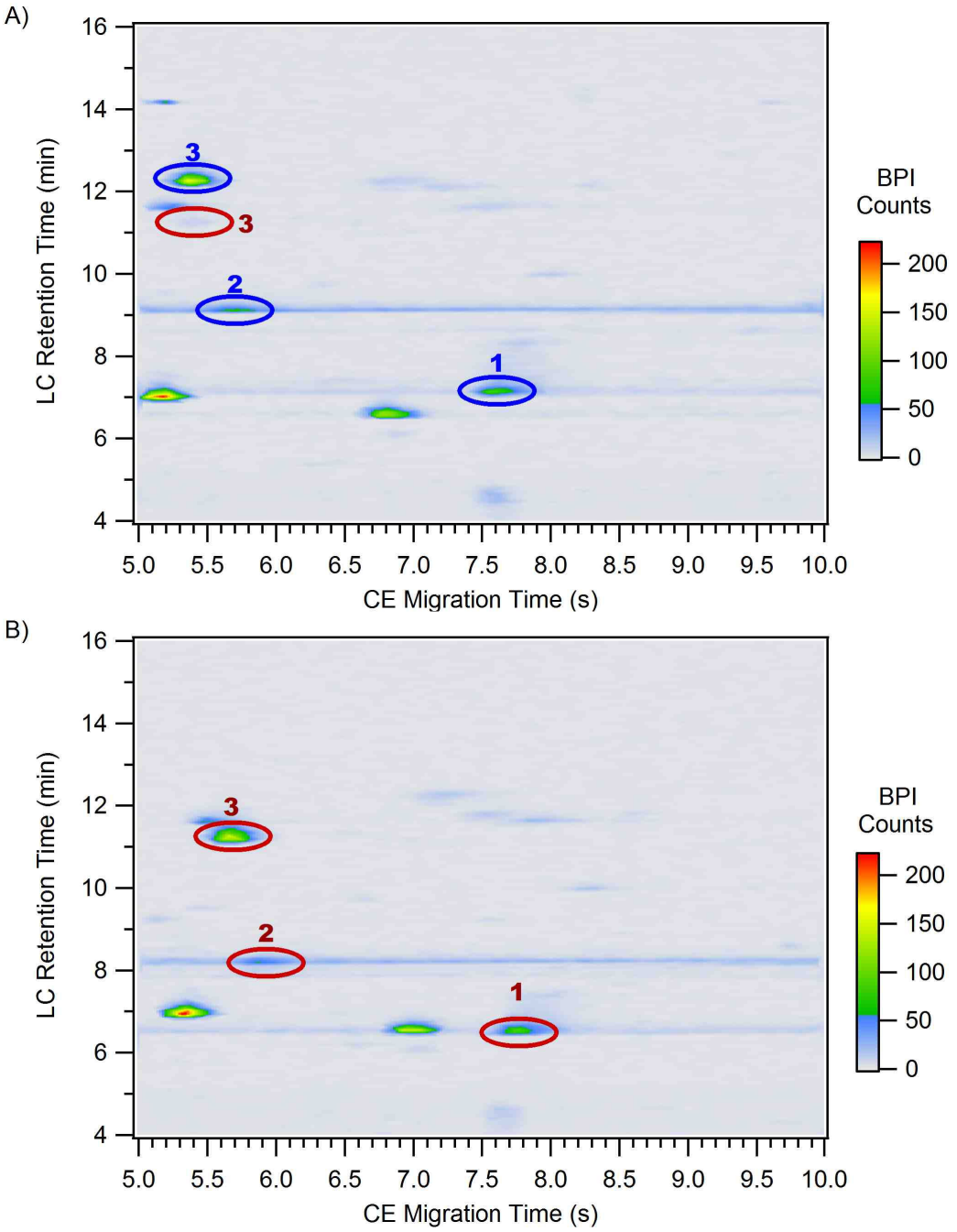

Figure 4-13. Two-dimensional LC-CE-MS analysis of the mAb Lys-C digests. A) original sample, B) 10% spiked oxidized control. The blue numbers indicate native peptides and red numbers indicate oxidized peptides.

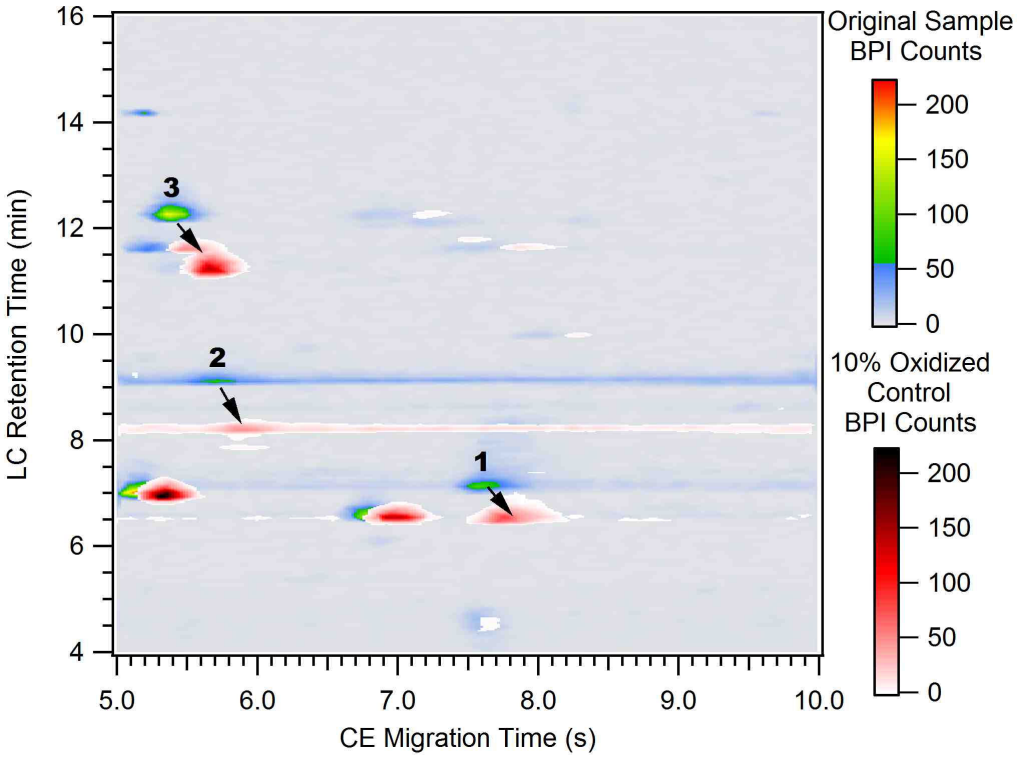

Figure 4-14. Two-dimensional LC-CE-MS analyses showing with the original sample and the 10% spiked oxidized sample control overlaid in the red color scheme.

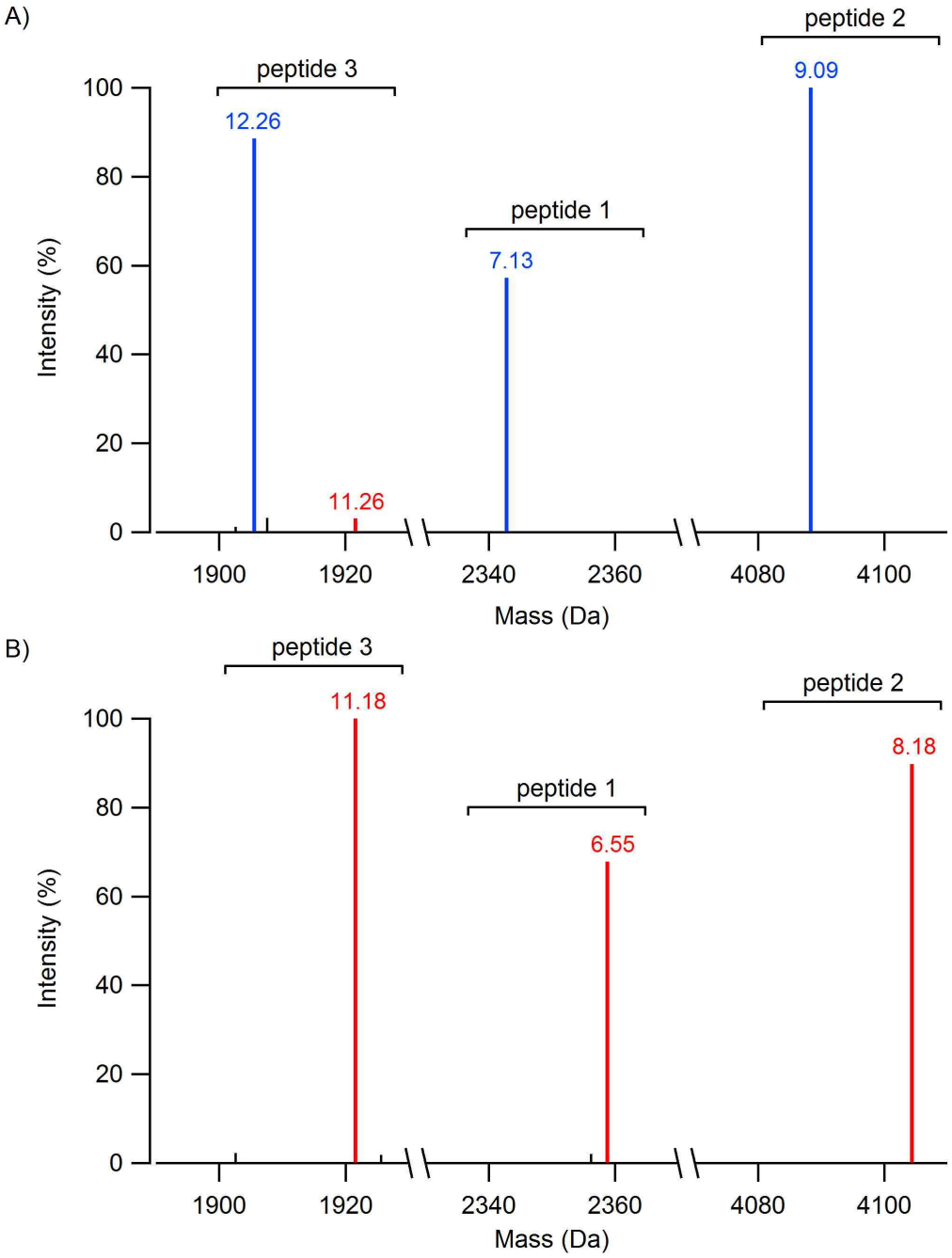

Figure 4-15. Masses observed in the LC-CE-MS analysis of A) the original sample and B) 10% spiked control for peptides 1-3. Native peptides (blue), oxidized peptides (red). The numerical labels indicate the peak elution time in minutes for the detected masses.

4.6 References

1. Mellors, J. S.; Gorbounov, V.; Ramsey, R. S.; Ramsey, J. M. Fully integrated glass microfluidic device for performing high-efficiency capillary electrophoresis and electrospray ionization mass spectrometry. *Anal. Chem.* **2008**, *80*, 6881.

2. Mellors, J. S.; Jorabchi, K.; Smith, L. M.; Ramsey, J. D. Integrated microfluidic device for automated single cell analysis using electrophoretic separation and electrospray ionization mass spectrometry. *Anal. Chem.* **2010**, *82*, 967.

3. Hardenborg, E.; Zuberovic, A.; Ullsten, S.; Soderberg, L.; Heldin, E.; Markides, K. E. Novel polyamine coating providing non-covalent deactivation and reversed electroosmotic flow of fused-silica capillaries for capillary electrophoresis. *J. Chromatogr. A* **2003**, *1003*, 217.

4. Larmann, J. P.; Lemmo, A. V.; Moore, A. W.; Jorgenson, J. W. 2-Dimensional separations of peptides and proteins by comprehensive liquid-chromatography capillary-electrophoresis. *Electrophoresis* **1993**, *14*, 439.

5. Moore, A. W.; Jorgenson, J. W. Rapid comprehensive 2-dimensional separations of peptides via RPLC optically gated capillary zone electrophoresis. *Anal. Chem.* **1995**, *67*, 3448.

6. Giddings, J. C. Two-Dimensional Separations - Concept and Promise. *Anal. Chem.* **1984**, *56*, 1258.

7. Giddings, J. C. Concepts and Comparisons in Multidimensional Separation. *J. High Resolut. Chromatogr.* **1987**, *10*, 319.

8. Gottschlich, N.; Jacobson, S. C.; Culbertson, C. T.; Ramsey, J. M. Two-dimensional electrochromatography/capillary electrophoresis on a microchip. *Anal. Chem.* **2001**, *73*, 2669.

CHAPTER 5: Monolithic 2D Liquid Chromatography-Capillary Electrophoresis with Mass Spectrometry Detection

5.1 Introduction

Chapters 3 and 4 presented hybrid 2D LC-CE systems that coupled capillary-based LC and microchip-based CE. One drawback to this approach was the band broadening of LC peaks within the capillary-to-microchip connection. This Chapter will discuss the integration of the first dimension on the microchip. This new device incorporates a sample-trapping region and LC channel packed with commercial porous particles. This system is capable of performing LC-ESI and LC-CE-ESI without modifying the instrumental setup. To evaluate the system, LC-MS and LC-CE-MS analysis of standard protein digests were performed and compared.

5.2 Experimental

5.2.1 Reagents and Materials

Deionized water was obtained from a Nanopure water purifier fitted with a 0.2-μm filter (Barnstead International, Dubuque, IA). Acetone, acetonitrile, methanol, and ammonium acetate were all HPLC grade from Fisher Chemical (Fairlawn, NJ). The PolyE-323 polymer was synthesized as previously described from 1,2-bis(3-aminopropylamino)ethane and epichlorohydrin both obtained from Sigma Chemical Co. (St. Louis, MO).[1] The PolyE-323 solution was adjusted to pH 7 with acetic acid (Fisher) and diluted with water to 15% (by mass) polymer. The trichloro(1H,1H,2H,2H-

perfluorooctyl)silane and rhodamine B were also acquired from Sigma Chemical Co. Tryptic digests of bovine serum albumin (BSA), yeast enolase, and Escherichia coli (MassPREP, Waters Corp., Milford, MA) were reconstituted in 0.1% (v/v) formic acid (99%, Fisher) in water prior to use.

5.2.2 Microchip Fabrication

Microchips were fabricated from 150-μm-thick glass substrates (Corning 0211 borosilicate, Erie Scientific Co., Portsmouth, NH) using standard photolithography and wet-chemical etching methods as previously described.[2] A schematic for the microchip is shown in Figure 5-1. A simple multi-step etching process was used to create channels with different depths. First, all channels were etched to the desired depth for the shallowest feature. After the substrate was rinsed and dried, photoresist (Microposit S1813, Microchem Corp., Newton, MA) was manually applied and cured at the location of the shallowest feature to prevent further etching. The remaining uncoated channels were then etched to the second depth and the process was repeated until all three selective depths were achieved. Access ports with a 400-μm internal diameter were created in the etched substrates by powder blasting (Microblaster, Comco, Inc., Burbank, CA). Channel depths and widths were measured with a profilometer (P15, KLA-Tencor Corp., San Jose, CA). The electrospray tip was machined by cutting the bonded microchip with a precision dicing saw (Dicing Technology, San Jose, CA) so that the CE channel terminated at a 90° corner of the microchip. The microchip was attached to 0.9-mm-thick glass with transparent UV epoxy (68, Norland Products Inc., Cranbury, NJ) to protect the device from mechanical damage. Glass cylinders with a volume of 200 μL were attached to the buffer, waste and electroosmotic (EO) pump channel access ports using chemically

resistant epoxy (Hysol E-120HP; Henkle Corp., Morrisville, NC) and used as fluid reservoirs. The channel lengths were as follows: LC inlet, 10 mm; vent, 22 mm; LC, 100 mm; buffer, 11 mm; waste, 3 mm; CE, 50 mm; and EO pump, 30 mm. The inlet, vent and LC channels were 25-μm deep and 120-μm at full width. The buffer, waste, CE and EO pump channels were 8-μm deep and 50 μm at full width. Both weirs were etched to a depth of 6 μm.

5.2.3 Particle Packing

The sample-trapping region and LC channel were packed with C18-bonded, 3.5-μm porous particles (X-Bridge, Waters Corp.). The particles were suspended in acetone at 5 mg/mL by vortexing and brief sonication. This slurry was then placed in a vial within a stainless steel vessel and helium gas pressure (70 bar) was used to force the slurry through a 50 μm i.d. capillary (Polymicro Technologies, Phoenix, AZ). The capillary was connected to the LC inlet channel on the microchip using the capillary-to microchip fitting described in Chapter 3. The vent channel was connected to a capillary leading to a union LC fitting. During packing the vent could be opened or closed by the use of a plug in the union. The vent was initially closed during the packing procedure to direct the particles towards the LC channel. Even though the weirs in the channels were 6-μm deep, they successfully retained the 3.5 μm particles. It is suspected that the particles were partially trapped by the "keystone effect," where particle aggregation at a taper is sufficient for retention of a packed bed.[3-4] Packing of the device was monitored using an optical microscope. When the packing reached the vent channel junction, the gas cylinder was shut off and the system was slowly depressurized to avoid decompression of the bed. As long as the device was not rapidly depressurized to

atmospheric pressure there was no need to frit the inlet of the packed channel. The vent was then opened and low pressure was used to pack the particles in the vent channel against the weir. Packing was continued until the bed extended 3 mm into the LC inlet, beyond the intersection of the vent channel. This 3 mm segment of packed particles functioned as the sample-trapping region. The microchip was then connected to the LC pump (nanoAcquity Binary Solvent Manager, Waters Corp.) and the packed LC channel was flushed overnight using a linear gradient from acetonitrile to water. Using a light microscope, no voids or other defects were visible in the packed LC channel. Figure 5-2 shows SEM images of a cross-section of a channel with similar dimensions packed with the same 3.5-μm particles.

5.2.4 Surface Modifications

The surface of the CE buffer, waste, and CE channels was coated with PolyE-323 to reverse the EOF and prevent peptide absorption as described in Chapter 3. The exterior of the integrated electrospray tip was coated with trichloro(1H,1H,2H,2H-perfluorooctyl)silane to make the surface hydrophobic as described in Chapter 4.

5.2.5 Microchip Operation

The experimental setup is shown in Figure 5-1. All of the fluidic connections outside of the microchip were made with 20 μm i.d. fused silica capillary tubing. The capillaries were attached to the microchip with in-house designed fittings described in Chapter 3. These fittings were capable of routinely holding over 100 bar pressure. The LC pump (nanoAcquity Binary Solvent Manager, Waters Corp.) delivered the LC mobile phase at 700 nL/min. Mobile phase A was 0.1% formic acid in water and mobile phase B was 0.1% formic acid in acetonitrile. The LC injections were performed with a 6-port

valve (C72, Valco Instruments Co. Inc., Houston, TX) with a 1 μL sample loop (labeled as V1 in Figure 5-1). After the injector, a low dead volume tee (MT.5XCS6, Valco) was used as a splitter to reduce the flow rate delivered to the inlet of the microchip device. A flow sensor (μ-Flow, Bronkhurst, Bethlehem, PA) was connected to the waste line to measure the split flow rate and to monitor flow stability. The capillary connected to the vent channel on the microchip was connected to a second 6-port valve (labeled as V2 in Figure 5-1) to open or close the vent. The vent was open during the LC injection providing a low flow resistance path through the sample-trapping region on the microchip. This resulted in 80% of the flow (570 nL/min) being delivered to the microchip. After the sample was loaded the vent was closed, reducing the flow rate through the microchip to 65 nL/min. A linear mobile phase gradient from 5 to 50% B in 30 min was used for all separations.

The effluent from the LC channel was directed towards the CE or waste channel by controlling the EOF within the microchip. The electric potentials were applied by a custom power supply built using three (two negative and one positive) 10-kV power supply modules (UltraVolt Inc., Ronkonkoma, NY.) The power supply was computer-controlled using an analog output board (PCI-6713; National Instruments, Austin, TX) and an in-house written LabVIEW program (National Instruments). Electrical connections were made to the buffer, waste and EO pump channel reservoirs with platinum electrodes. The background electrolyte for the CE separations was an aqueous solution of 0.1% formic acid with 25% acetonitrile, pH 2.5. CE injections were accomplished using a modified "gated" injection scheme as described in Chapter 3. Typical voltages applied to the CE buffer, waste and EO pump reservoirs were -0.8 kV,

-0.8 kV, and +8.0 kV for injections and -4.0 kV, 0.0 kV, and +8 kV for separations, respectively. Due to the electrical resistance of the channels in the device, both sets of applied voltages resulted in a potential of -0.6 kV at the injection cross and +5.0 kV at the electrospray tip. This relatively low potential at the injection cross minimized the electric field dropped across the LC channel to the valves and flow sensor, which were all held at ground. Furthermore, because the potentials at the beginning and the end of the CE channel did not change during injections, the separation field strength of 1.1 kV/cm was held constant. This provided stable electrospray and allowed the use of "overlapping injections" as described in Chapter 3. For the protein digests studied here, the CE separation window was 9 s while the run time was 18 s. Therefore, the CE injections were spaced 10 s apart to increase the sampling of peaks eluting from the first dimension while ensuring that peaks from adjacent CE runs would not overlap before arrival at the ESI emitter. When LC-MS analysis was performed, the CE injection interface was left in the "injection" voltage profile for the duration of the LC run.

Details regarding the operation of the integrated ESI interface are provided in Chapter 4. The microchip was positioned with the electrospray tip approximately 5 mm from the inlet of the mass spectrometer (Micromass QTof Micro, Waters Corp.) For optimal ESI, a voltage of approximately +5 kV was required at the electrospray tip with the inlet of the MS held at ground. The electrospray plume was visualized using a 3-mW green diode laser and a CCD camera. For all experiments, the mass spectrometer was set to scan a range of 300-1000 m/z with 0.24 s per summed scan and 0.1 s interscan delay to maximize the data acquisition rate.

5.2.6 Data Processing.

Peak capacities for the LC-MS runs were calculated using software described in Chapter 2. Chromatograms were produced by importing data from Masslynx (Waters Corp.) into Igor Pro (WaveMetrics, Lake Oswego, OR) for additional graphing options. LC-CE-MS data were processed into 2D image plots using the procedures outlined in Chapter 4.

5.3 Results and Discussion

5.3.1 ESI-MS

The integrated ESI interface was previously characterized and found to provide sensitivity and stability comparable to a commercial fused-silica nanospray emitter.[2] Initial stability tests were performed over 5 min intervals, which was adequate for the rapid CE-MS separations demonstrated on the device. In the current work the electrospray stability was measured for longer periods of time to ensure stable operation throughout the LC-CE-MS analysis. For this experiment rhodamine B (10 μM) was added to the background electrolyte in the buffer reservoir and it was continuously infused using the "separation" voltage profile of the CE injection interface. The ESI-MS signal from the rhodamine B protonated molecular ion was monitored for 60 min. The relative standard deviation (RSD) was 4.3% which agrees well with previous ESI stability tests.[2] Then the ESI flow rate was estimated by performing gated injections of rhodamine B-free buffer from the LC column and measuring the time until a decrease in the rhodamine B signal was observed. By this procedure, the rhodamine B-free buffer was essentially used as a dead time marker. Three injections of the rhodamine B-free

buffer were made and had a dead time of 12.2 s corresponding to a flow rate of 98 nL/min.

5.3.2 LC-MS

To test the chromatographic performance of the packed microchip channel, the device was utilized for reversed phase LC-MS. Figure 5-3A shows a BPI chromatogram for an LC-MS analysis of tryptic peptides from BSA and yeast enolase. The low flow resistance of the integrated sample-trapping region allowed for 800 nL of the dilute sample (0.25 μM) to be loaded onto the device in less than 2 min. In addition to preconcentration, the sample-trapping region may also be used to perform sample clean-up, such as desalting peptides, prior to the LC run. The peak capacity for this one-dimensional separation was 64. To illustrate the potential for analyzing more complicated samples, Figure 5-3B shows a separation of 800 ng of a tryptic digest of E. coli cell lysate. The peak capacity for this separation was 58. Both separations show that the device is capable of efficient LC separations in a relatively short analysis time. Tandem MS could be used to identify analytes in these microchip LC-MS experiments, but was not performed in this work.

5.3.3 LC-CE-MS

As mentioned in Chapter 4, one challenging aspect of performing online 2D separations with MS detection is ensuring adequate sampling between dimensions and between the second dimension and the mass spectrometer. With the gated injection scheme, a fraction of the LC effluent is injected into the CE dimension at regular intervals. For this method to be comprehensive, each component eluting from the LC channel must be injected into the CE dimension. To retain the resolution achieved in the

first dimension, a frequency of at least 3-4 injections per peak eluting from the first dimension to the second is required.[5] A limiting factor for obtaining this frequency is the time required to complete the second dimension separation and detection. Microchip CE is capable of extremely fast separations as demonstrated in Chapter 3 where a peak capacity of 58 was generated every 3.25 s. However, this requires a high bandwidth detection scheme, such as LIF, to adequately sample CE peaks that are only tens of milliseconds wide. Unfortunately, commercially available mass spectrometers have much slower sampling rates. As a result the CE peaks must be significantly wider to ensure adequate peak detection. In this work, we have purposely lengthened the CE injection time to produce wider peaks to improve detection with the relatively slow mass spectrometer.

A BPI chromato-electropherogram for the 2D analysis of tryptic peptides from BSA and enolase is shown in Figure 5-4A. The median base peak width for components eluting from the LC dimension was 15.7 s (as determined from the LC-MS separation) and the calculated peak volume was 17 nL. Since the time between successive CE injections was 10 s the components eluting from the LC channel were only sampled 1.6 times on average. Each 0.5 s CE injection corresponded to a volume of 0.8 nL. In Figure 5-4B an expanded time interval of the 2D analysis shows a few of the CE runs in greater detail, with dashed lines indicating individual CE separation windows. Due to the relatively slow data acquisition rate of the mass spectrometer (~3 Hz) these peaks were undersampled. An accurate measurement of CE peak widths was not possible as only 1-2 MS data points were obtained per component. It was estimated that the CE base peak widths were slightly greater than 0.5 s.

The sequential CE separation windows were stacked according to the corresponding LC retention to simulate the 2D plot shown in Figure 5-5. Analytes were fairly well distributed across both dimensions and there are a relatively large number of baseline resolved peaks (spots). The estimated peak capacities for the LC and CE dimensions are 64 and 10, respectively. If higher sampling rates could be achieved (4 CE injections per LC peak and 6-10 MS data points per CE peak), the theoretical peak capacity for this separation would be 640 for the 30 min analysis.

Three replicate 2D separations were performed using the same tryptic digest of BSA and enolase to evaluate the reproducibility of the system. The position of 15 components (spots) in the 2D plots in Figure 5-6 were used to compare the LC retention times and CE migration times. The average RSD for the LC retention times and CE migration times was 0.35% and 2.4%, respectively. The slow data acquisition rate (~3 Hz) likely contributed significantly to the observed variation in CE migration times.

To show the ability to separate more complex samples, a tryptic digest of E. coli cell lysate was analyzed by LC-CE-MS. The overall pattern of the 2D separation shown in Figure 5-7A matches well with the 1D separation of the same sample shown in Figure 5-3B. There are many components in this sample that fill the full CE separation windows shown in Figure 5-7B. The 2D plot for this separation is shown in Figure 5-8. Although many peaks were not baseline resolved due to the complexity of the sample, the 2D analysis clearly offered higher resolution as compared to the LC-MS analysis shown in Figure 5-3B. The increase in separation power is also illustrated by the reduction of the complexity in the mass spectra. Figure 5-9 shows single scan spectra containing the highest intensity for an abundant ion (552.2 m/z) from the LC-MS and LC-CE-MS

analyses. Fewer ions are present in the spectrum obtained from the 2D run. The intensity for the 552.2 m/z ion is also 23% higher in the 2D analysis. Although there are numerous variables that affect MS intensity, coeluting components may induce ionization suppression in the ESI process, which may account for the reduced intensity of the 552.2 m/z ion in the 1D analysis.

In the 2D LC-CE-MS analyses presented, the greatest limitation was the relatively slow scan rate of the mass spectrometer employed. While the maximum data acquisition rate for the instrument was ~3 Hz, commercially available time-of-flight instruments are capable of speeds in excess of 100 Hz. This faster acquisition rate would enable a 100 ms wide CE peak to be sampled 10 times providing a peak capacity of 30 in the CE dimension in only 3 s (assuming 6 s CE runs and "overlapping injections"). Therefore LC peaks would only have to be 12 s wide to obtain optimal sampling between separation dimensions (4 CE injections per LC peak). This system could potentially provide a 30-fold increase in total peak capacity compared to 1D separation methods with currently available MS technology.

5.4 Conclusion

A microchip device for performing 2D LC-CE-ESI is described for the analysis of protein digests for MS-based proteomic applications. Integrating all functional elements on the microfluidic platform enabled the use of low flow rates without incurring substantial band-broadening. Tryptic digests were separated to demonstrate the first report of microfluidic LC-CE separations directly coupled with MS detection. Faster data acquisition rate mass spectrometers (without loss of resolution or mass accuracy) will be required to take full advantage of the high-speed separation capabilities of the

device. In order to obtain tandem MS data, in particular, significant increases in data acquisition rates are needed. Future work should include modifying the LC-CE interface to incorporate sample preconcentration between the separation dimensions. In addition, enzymatic digestion and other processing steps may be integrated onto the device to further reduce the overall analysis time.

5.5 Figures

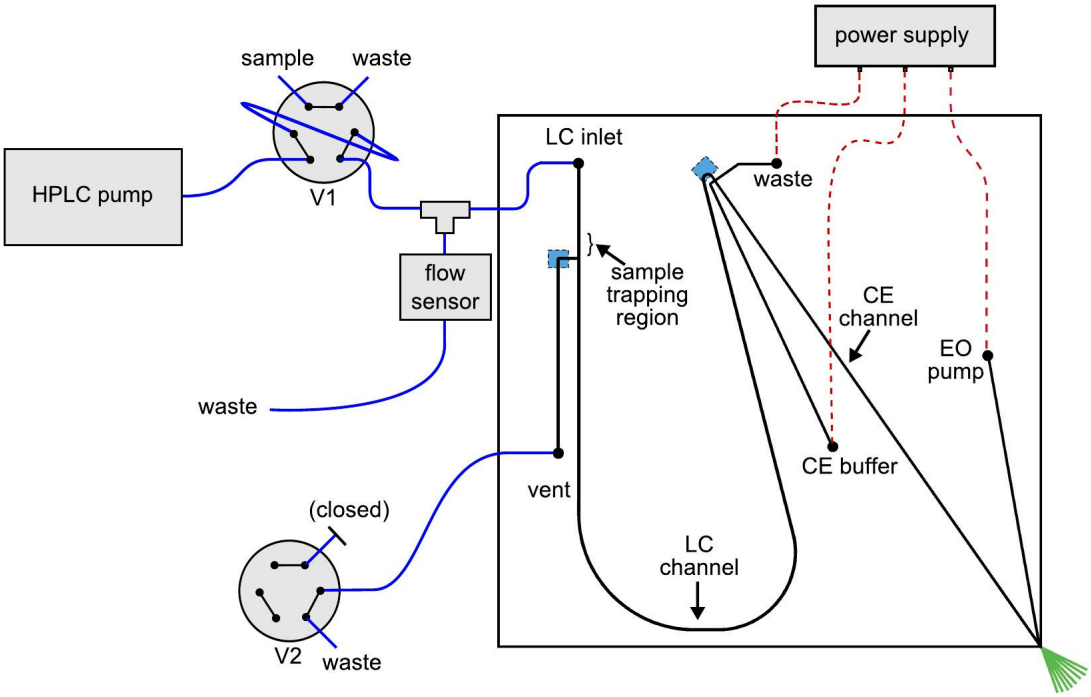

Figure 5-1. Schematic for the microchip-based LC-CE-MS system. The blue squares outlined in dashes on the microchip denote the location of the weirs that were used to retain the packed particles. Valve 1 (V1) was used to perform LC injections and valve 2 (V2) was used to open and close the vent line. Valves are shown in the "sample loading" configuration. Electrospray was performed from the lower right corner of the microchip.

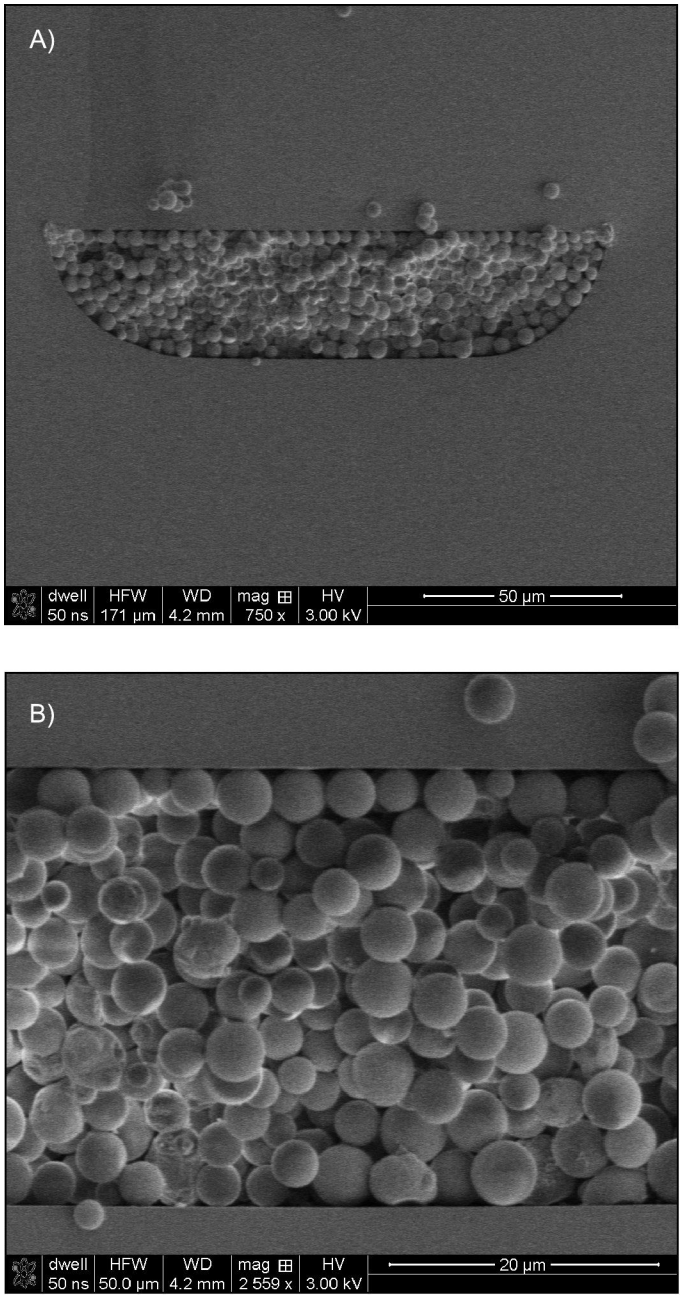

Figure 5-2. SEM images of the cross section of a microchip channel, 33 µm deep and 131 µm at full width, packed with 3.5 µm particles.

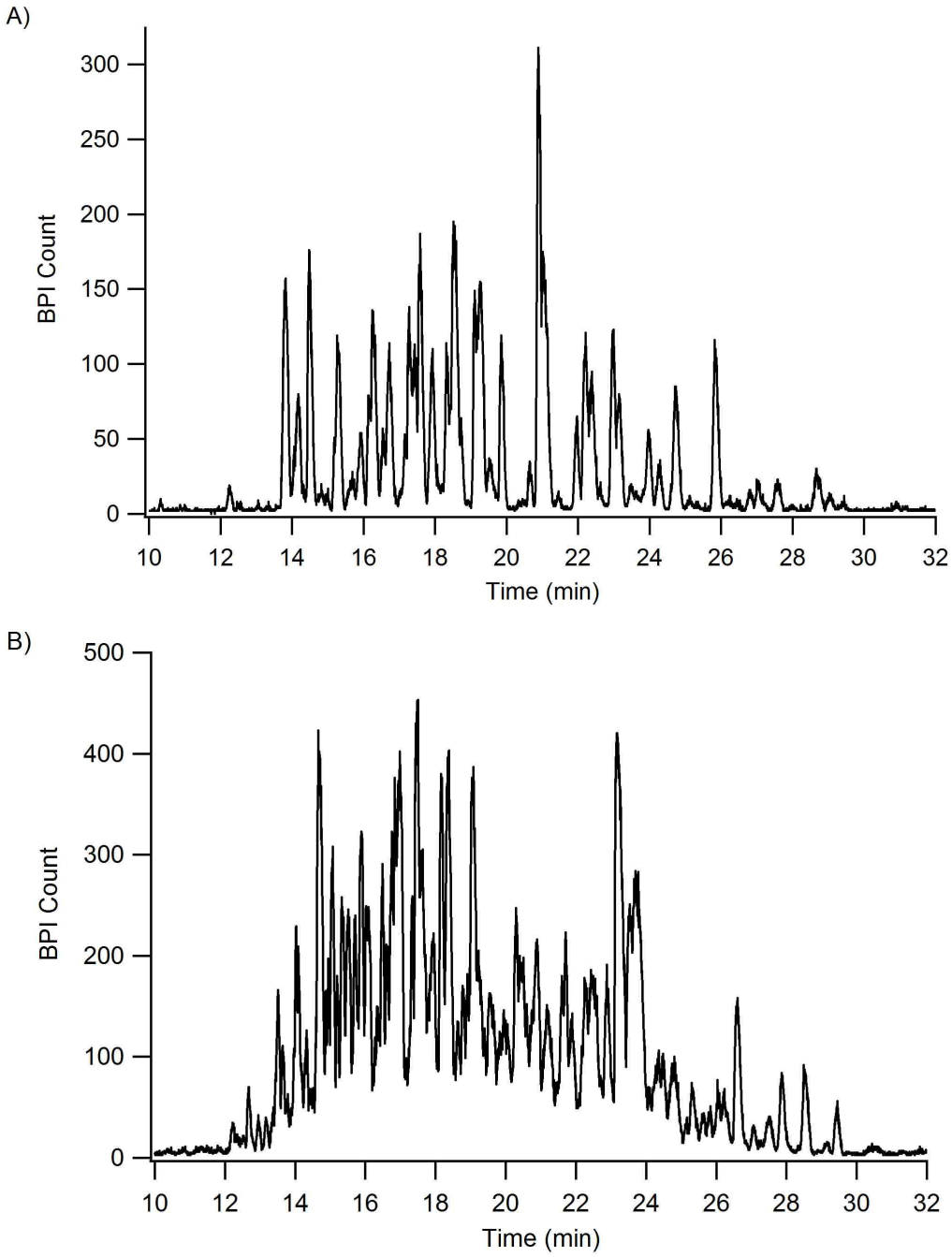

Figure 5-3. BPI chromatogram for the LC-MS analysis of A) 200 fmol of a tryptic digest of a bovine serum albumin and yeast enolase mixture B) 800 ng of E.coli lysate tryptic digets. MPA, 0.1% formic acid in water; MPB, 0.1% formic acid in acetonitrile; gradient 5 to 50% B in 30 min; flow rate 65 nL/min.

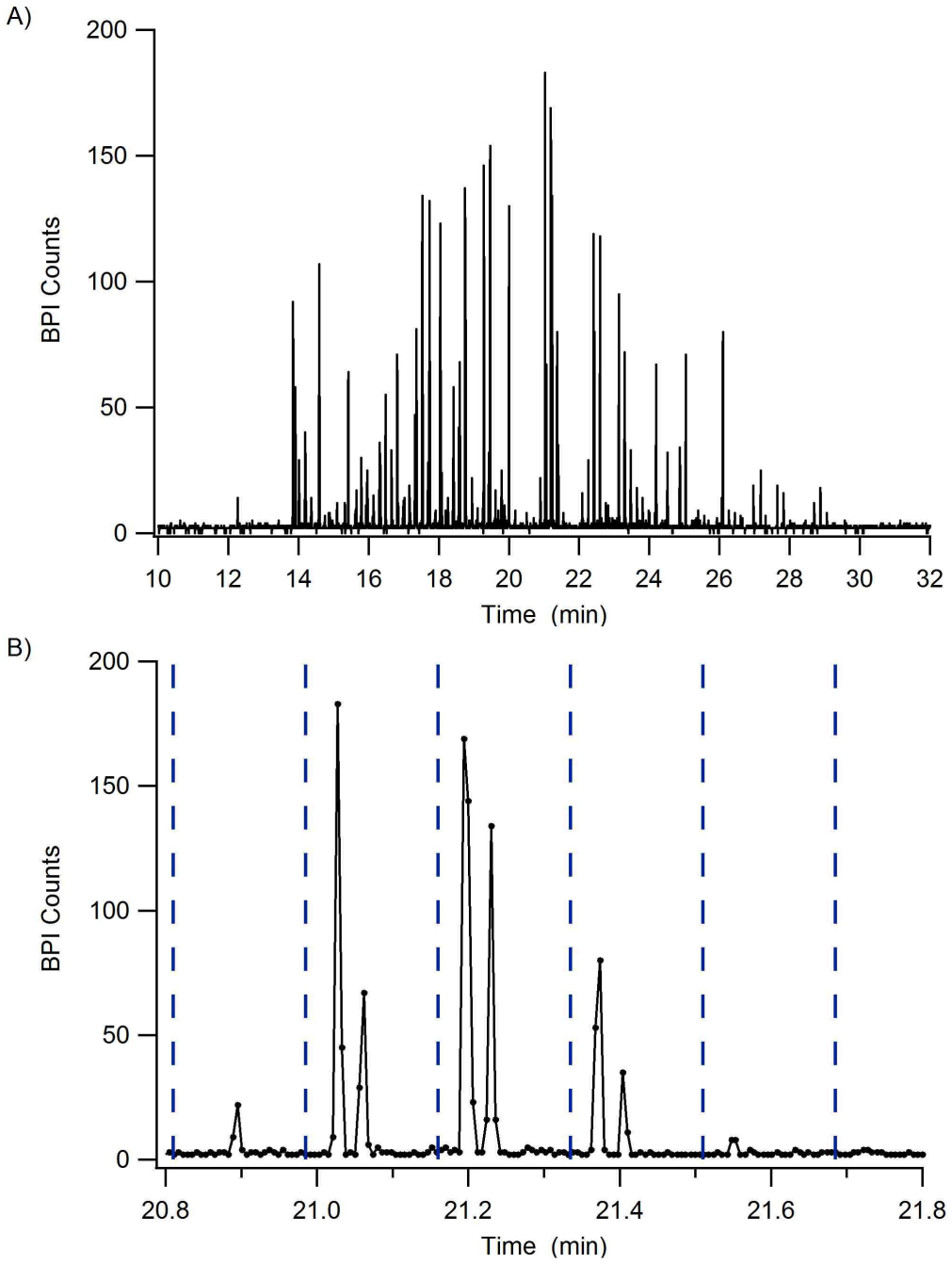

Figure 5-4. A) BPI chromato-electropherogram for the LC-CE-MS analysis of the same tryptic digest of BSA and enolase shown in Figure 5-3A. B) An expanded view of a 1 min interval in the separation above. Dashed lines indicate CE separation windows.

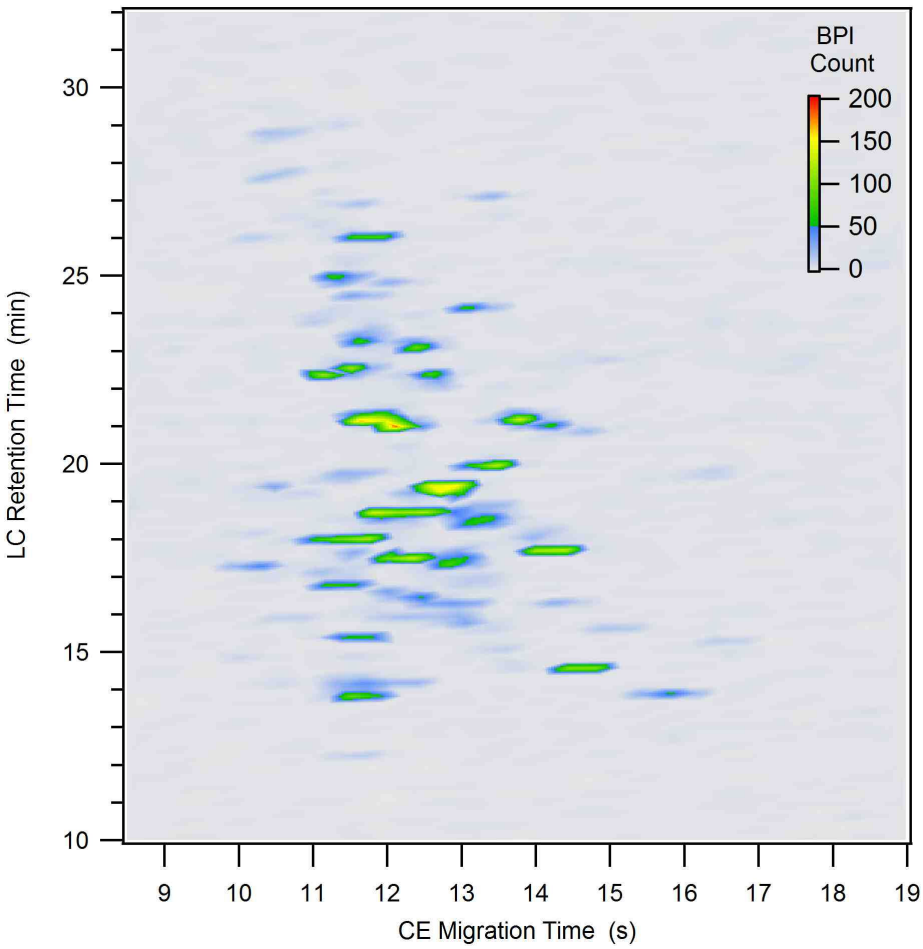

Figure 5-5. A two-dimensional plot for an LC-CE-MS analysis of 200 fmol of a tryptic digest of a bovine serum albumin and yeast enolase mixture.

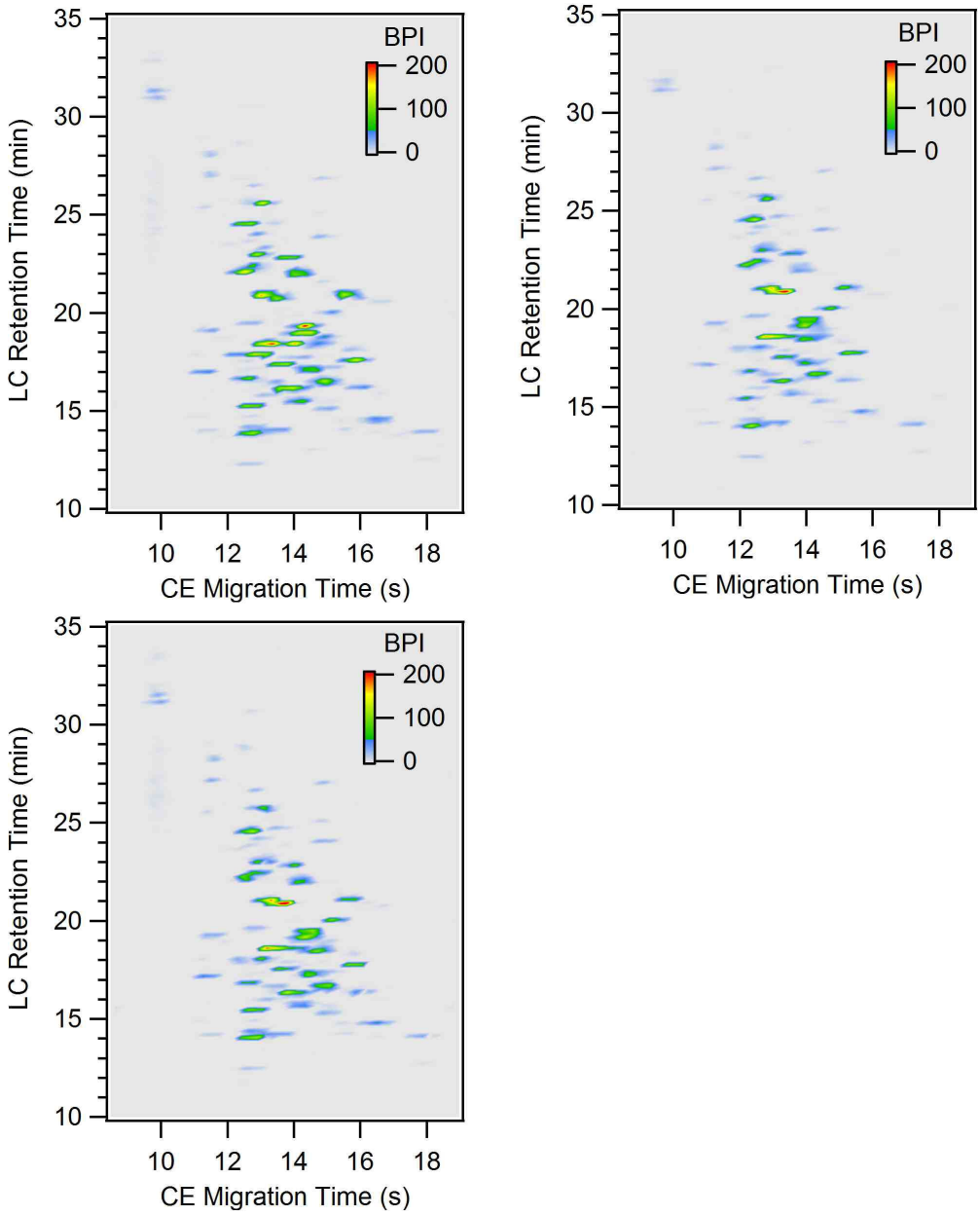

Figure 5-6. Three replicate LC-CE-MS analyses of 200 fmol of the BSA and enolase tryptic digest.

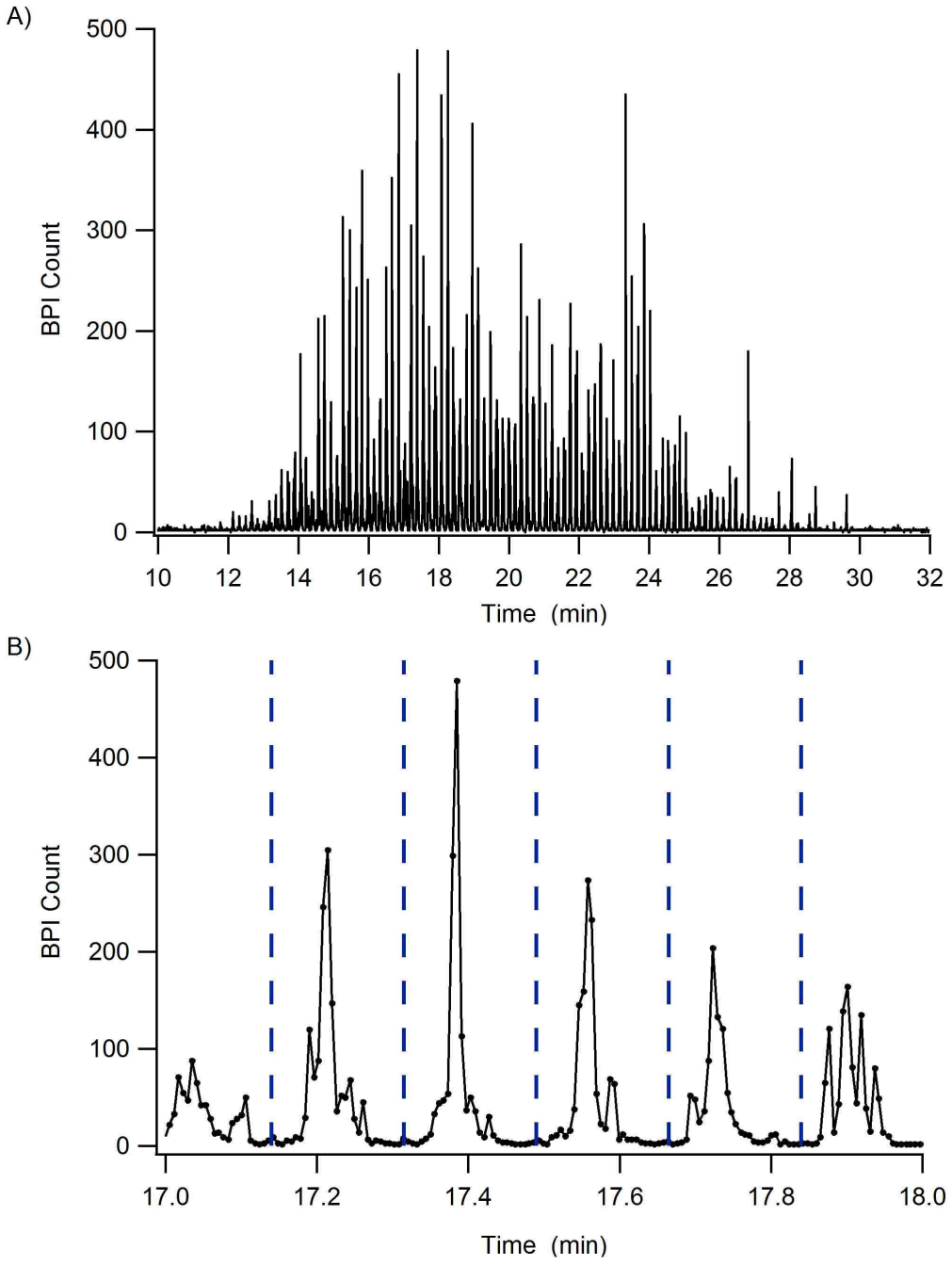

Figure 5-7. A) BPI chromato-electropherogram for the LC-CE-MS analysis of the same tryptic digest of E. coli lysate shown in Figure 5-3B. B) An expanded view of a 1 min interval in the separation above. Dashed lines indicate CE separation windows.

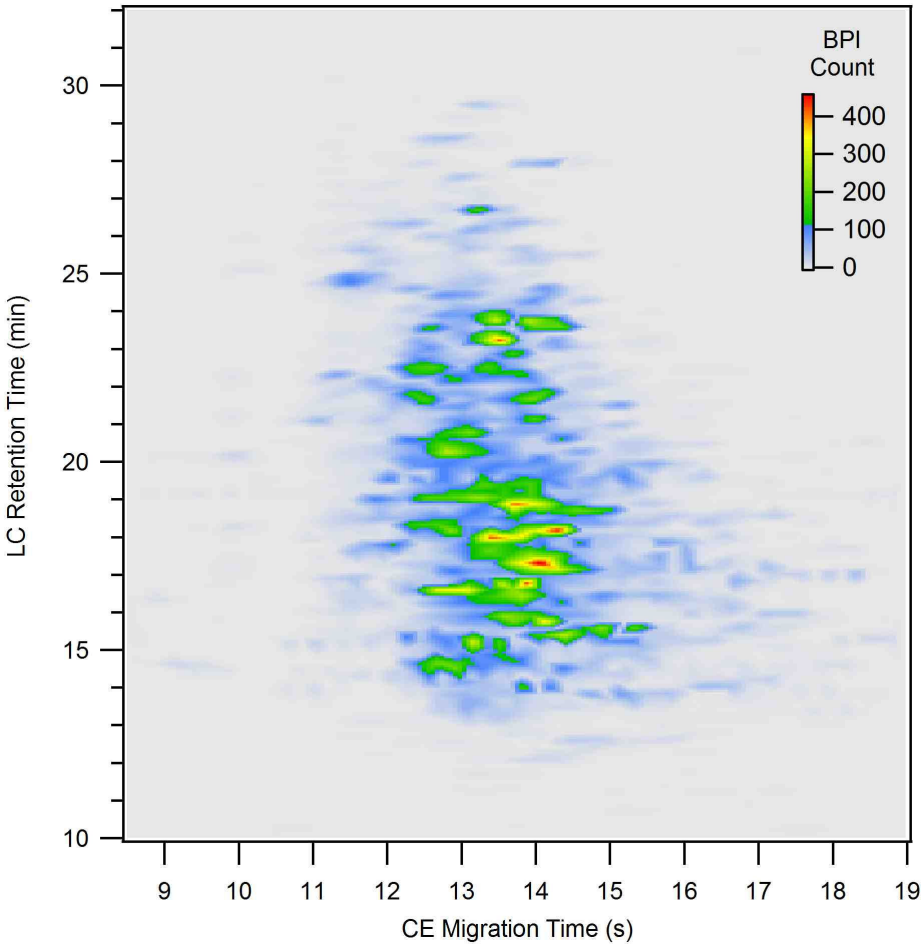

Figure 5-8. A two-dimensional plot of the LC-CE-MS analysis of 800 ng of an E. coli cell lysate tryptic digest.

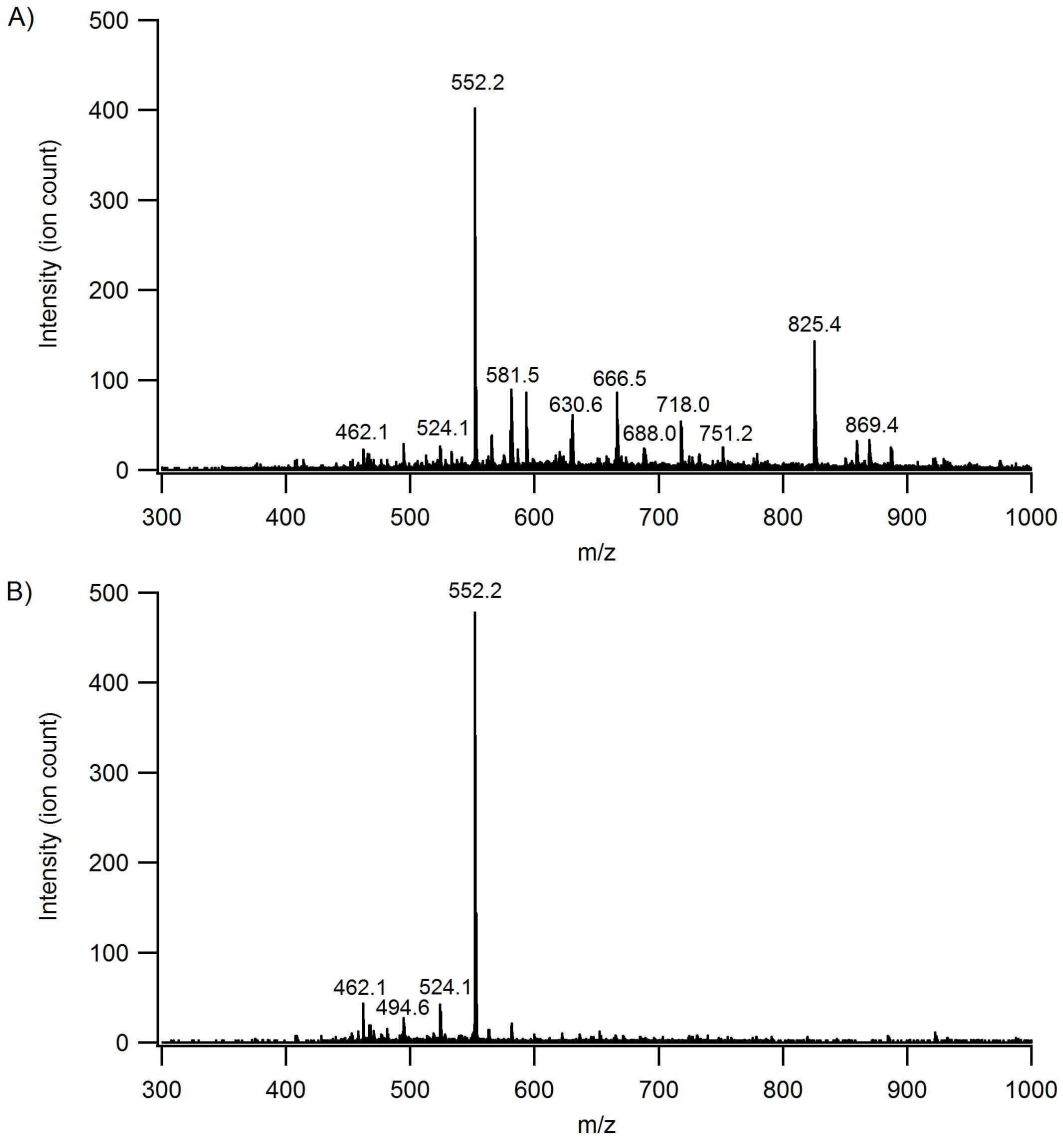

Figure 5-9. Mass spectra containing the highest abundance of the 552.2 m/z ion from an E. coli cell lysate tryptic digest analyzed by (A) LC-MS and (B) LC-CE-MS.

5.6 References

1. Hardenborg, E.; Zuberovic, A.; Ullsten, S.; Soderberg, L.; Heldin, E.; Markides, K. E. Novel polyamine coating providing non-covalent deactivation and reversed electroosmotic flow of fused-silica capillaries for capillary electrophoresis. *J. Chromatogr. A* **2003**, *1003*, 217.

2. Mellors, J. S.; Gorbounov, V.; Ramsey, R. S.; Ramsey, J. M. Fully integrated glass microfluidic device for performing high-efficiency capillary electrophoresis and electrospray ionization mass spectrometry. *Anal. Chem.* **2008**, *80*, 6881.

3. Lord, G. A.; Gordon, D. B.; Myers, P.; King, B. W. Tapers and restrictors for capillary electrochromatography and capillary electrochromatography mass spectrometry. *J. Chromatogr. A* **1997**, *768*, 9.

4. Ceriotti, L.; de Rooij, N. F.; Verpoorte, E. An integrated fritless column for on-chip capillary electrochromatography with conventional stationary phases. *Anal. Chem.* **2002**, *74*, 639.

5. Gottschlich, N.; Jacobson, S. C.; Culbertson, C. T.; Ramsey, J. M. Two-dimensional electrochromatography/capillary electrophoresis on a microchip. *Anal. Chem.* **2001**, *73*, 2669.

CHAPTER 6: Microfluidic Dual Electrospray Ionization Source for Accurate Mass Measurements

6.1 Introduction

Accurate mass measurements are crucial for providing elemental analysis of small molecules and improving peptide and protein identification.[1-2] Such measurements can be routinely obtained by ESI-MS using internal calibration. By this method, the signal from a reference compound corrects for drift in the mass spectrometer's calibration over the course of the experiment. The introduction of a reference compound was traditionally accomplished by mixing analyte and reference materials prior to ESI; however, this strategy has several critical limitations. The presence of both analyte and reference materials may lead to ionization suppression which lowers the sensitivity of the method.[3] When a column-based separation is performed, the solutions are commonly mixed at a post-separation "T" junction. This mixing introduces extra-column band broadening that is especially problematic when performing low flow rate separations, such as capillary LC or CE. A valve may be placed after the separation to sequentially introduce solutions, but this connection also introduces substantial extra-column band broadening.[4] Another alternative is the use of dual emitters that provide independent ionization without sacrificing the quality of the separation.[5-7] It is also advantageous to introduce the analyte and reference materials sequentially to avoid interference that arises if both have the same nominal m/z value. In this case, sampling of the reference material must be performed quickly to prevent undersampling of the analyte peaks. Numerous methods

have been reported for sequential introduction of analyte and reference solutions using two capillary ESI emitters including repositioning the ESI emitters,[8-12] mechanical baffles,[13-14] dynamic control of the ESI voltage,[15] and modification of external electric fields.[16-18] These methods typically allow the reference material to be sampled in less than 1 s.

There have been many reports of microfabricated devices which have multiple ESI emitters.[19] The majority of these devices simply contain duplicate channel structures that are not utilized in the same experiment. Here we are interested in multiple ESI emitters that can be operated on a rapid time scale. It is also important that the emitters are fabricated directly onto the device to facilitate zero dead-volume integration with microscale separations. Dayon and coworkers described a microfluidic device that meets some of these criteria. Their polyethylene terephthalate microchip device integrated six ESI emitters for potential use in high-throughput screening applications.[20] The gravity fed solutions were electrosprayed sequentially without moving the device by modulating the ESI voltage of each emitter at intervals as short as 6 s.

This chapter describes the development of a microfluidic dual ESI source for rapid analysis of two different solutions. Two different experimental setups were explored in developing a prototype device. Both strategies relied on two independent ESI emitters which can be turned on and off by the modulation of the applied voltage. First, a pressure-driven approach that utilized two separate microchip devices and off-microchip pumping is presented. This short study was conducted to test the feasibility of integrating dual ESI emitters in our experimental setups and proved useful in identifying parameters needed to design an integrated device. Secondly, an electrokinetically-driven strategy is

discussed in which all of the fluidic handling was performed on the microchip. After the initial characterization of this device, the ability to obtain accurate mass measurements is demonstrated.

6.2 Experimental

6.2.1 Pressure-Driven Strategy

The schematic for the pressure-driven dual ESI experiment is shown in Figure 6-1. Two identical glass microchips were fabricated from 150 μm thick glass substrates using the procedures described in Chapters 4 and 5. Each device had a straight channel that connected the fluid access port directly to an integrated ESI tip formed at a 90° corner. The channel cross-sections had a depth of 12 μm and a full width of 56 μm. The surface of the channels was not modified for these experiments. The exterior of the ESI tip was coated with trichloro(1H,1H,2H,2H-perfluorooctyl)silane (Sigma Chemical Co.) to reduce surface wetting as previously described.

The ESI solution consisted of 5 μM leucine enkephalin (American Peptide Co., Inc., Sunnyvale, CA) or 5 μM angiotensin II (American Peptide Co., Inc., Sunnyvale, CA) in an aqueous solution of 0.1% formic acid and 50% methanol. Fluid was delivered to each device using a syringe pump. The needle of each electrically floated syringe (1801, Hamilton Co., Reno, Nevada) was connected to 50 μm i.d. capillary with a PTFE sleeve. This capillary was connected to a stainless steel union to allow the ESI potential to be applied from an in-house built power supply controlled by LabVIEW (National Instruments, Austin, TX). From this union another 50 μm capillary was connected to the microchip devices using the capillary-to-chip connectors described in Chapter 3. Mass spectral data was collected with a QTof instrument (QTof Micro II, Waters Corp,

Milford, MA) using the maximum acquisition rate (~3 Hz). A photograph of both emitters positioned in front of the mass spectrometer inlet is shown in Figure 6-2.

6.2.2 Electrokinetically-Driven Strategy

The channel layout for the EK-driven microchip dual ESI device is shown in Figure 6-3. Microchannels were fabricated into 150-μm-thick glass substrates (Corning 0211 borosilicate, Erie Scientific Co., Portsmouth, NH) by standard photolithography, wet-chemical etching procedures as described in Chapters 4 and 5. The depth and full width of the channels were measured with a profilometer (P15, KLA-Tencor Corp., San Jose, CA) to be 8 μm and 60 μm, respectively. The lengths of the channels were as follows: analyte and reference 5 mm, buffer and waste 14 mm, transfer 42 mm, and U-shaped electroosomtic (EO) pump 12 mm. A nanojunction with dimensions 50 nm deep and 50 μm wide was created by focused ion beam milling (FEI Helios Nanolab 600, Hillsboro, OR) to connect the 75 μm gap between the U-shaped (EO) pump channel and the transfer channel. The electrospray tips were machined by dicing the bonded microchip with a precision dicing saw (Dicing Technology, San Jose, CA) so that the transfer channels terminated at ~50° edges. The distance between the electrospray emitters was 3.6 mm. All channels except the EO pump channel were coated with PolyE-323 as described in Chapter 3 to provide stable anodic EOF when using a neutral to acidic background electrolyte. In addition, the exterior of the electrospray tips were coated with trichloro(1H,1H,2H,2H-perfluorooctyl)silane (Sigma Chemical Co.) to prevent wetting as described in Chapter 4.

Infusion of analyte and reference materials was accomplished by applying electric potentials to select reservoirs to generate EOF within the device. Electric potentials were

applied using two independent power supplies (2866A; Bertan, Hicksville, NY) that had voltage rise and fall times of approximately 5 ms. The power supplies were computer-controlled using an analog output board (PCI-6713, National Instruments) and LabVIEW software (version 8.5, National Instruments). High voltage was applied to the U-shaped EO pump reservoir located closer to the ESI spray tip. Typical voltages applied to this reservoir during the "off" and "on" states were approximately 0 kV and +4.8 kV, respectively. The analyte and reference reservoirs were held at ground. No electrical connection was made to the buffer and waste channels as they were not utilized in these infusion experiments. The operation of the electroosmotically pumped electrospray interface has been described in Chapter 4. The nanojunction between the transfer channel and the U-shaped EO pump channel reduced the EOF in the EO pump channel by creating electrical double layer overlap.[21-22] Given the relative channel dimensions, the voltage at the ESI tip during the "on" state was calculated to be +2.4 kV. An x-y-z translational stage was used to position the microchip emitters approximately 5 mm from the plane of the mass spectrometer inlet orifice. Both ESI emitters were aligned an equal distance (1.8 mm) from the axis of the mass spectrometer inlet orifice unless otherwise stated and the device remained stationary during all experiments. MS data was acquired using a quadrupole time-of-flight (QTof) mass spectrometer (Micromass QTof Micro, Waters Corp., Milford, MA) except as indicated in the text where a Tof mass spectrometer (LCT-Premier, Waters Corp.) was utilized for its faster data acquisition rate. Data was acquired by the QTof using 1 s summed scans and an interscan delay of 0.1 s whereas the Tof acquired data using 0.05 s summed scans and an interscan delay of 0.01 s. Both MS instruments were configured to acquire spectra over a m/z range of 100-

1000. For accurate mass measurements, the switching of the electrospray signals was synchronized with the data acquisition on the QTof instrument. The instrument software (MassLynx version 4.1, Waters Corp.) was originally designed to control the baffle position in the commercial dual ESI source (NanoLockSpray, Waters Corp.) to select the analyte or reference electrospray signal.[13-14] Here, we used this trigger voltage from the mass spectrometer to switch the voltages applied to the microchip device.

6.3 Results and Discussion

6.3.1 Pressure-Driven Setup

The effects of modulating the ESI voltage were first investigated for a single microchip emitter positioned directly on axis with the inlet of the mass spectrometer. Using a flow rate of 100 nL/min and an emitter distance of 5 mm from the inlet, the optimal ESI voltage was +5.0 kV. If the ESI voltage was lowered to 0 kV, the ESI ceased and a relatively large fluid volume immediately pooled at the ESI emitter. This fluid at the tip prevented the ESI from restarting when the high voltage (+5.0 kV) was restored. Alternatively, the ion signal could be eliminated by reducing the voltage to +3.5 kV. At this attenuated voltage, droplets that formed on the ESI emitter were ejected due to the electric field before the fluid wet the entire ESI emitter. This allowed the electrospray to be readily restored on demand with the return to the optimal ESI voltage. Images of the ESI region of the microchip during the “active” (optimal ESI voltage) and “inactive” (attenuated ESI voltage) states are provided in Figure 6-4.

Next, two identical emitters were positioned in front of the inlet of the mass spectrometer as show in Figure 6-1 and Figure 6-2. The left emitter was supplied with 5 μM of leucine enkephalin while the right emitter was supplied with 5 μM of

angiotensin II. The emitter positions and ESI voltages were adjusted to obtain the highest signal intensity when one emitter was in the "active" state and the other in the "inactive" state. The most favorable emitter positions were approximately 3-4 mm apart and 5 mm from the plane of the inlet of the mass spectrometer. The optimal emitter voltages for the "active" and "inactive" states were approximately +5.0 kV and +1.5 kV, respectively. To demonstrate rapid switching between the two solutions, electrospray was alternated between the left emitter (leucine enkephalin) and the right emitter (angiotensin II) every 5 s. Figure 6-5 shows the reconstructed ion chromatograms for each peptide.

Although electrospray could be generated from both emitters simultaneously, signal was only observed from one emitter at a time despite attempts to optimize emitter positions and applied voltages. The coulombic repulsion between electrospray plumes likely prevented simultaneous detection.[23] It may be possible to achieve simultaneous detection by reorientation of the ESI emitters or the use of a mass spectrometer with multiple inlets.[5,16,24] However, sequential introduction of the analyte and reference materials was preferred in this work for reasons discussed above.

6.3.2 Electrokinetically-Driven Setup

In the electrokinetically-driven device, the voltage applied at the EO pump channels generated both the EOF and the ESI potential. When the voltage was turned off, the fluid flow stopped immediately, preventing droplet formation on the electrospray tip and minimizing the time required for the electrospray to be restarted. Similarly to the pressure-driven dual ESI setup, electrospray could be generated from both emitters but ions were observed only from one emitter at a time.

Previously, a single integrated ESI emitter was characterized and found to yield sensitivity and stability comparable to a commercial capillary emitter.[25] Here we compared the sensitivity of a single emitter in isolation to a single emitter in the sequentially operated, dual ESI configuration. For the single emitter in isolation configuration, the analyte emitter was aligned on axis with the mass spectrometer inlet orifice and the reference emitter was floated (no electrical contact was made to any channels connected to the reference emitter). For the sequentially operated, dual emitter configuration, both emitters were positioned an equal distance from the axis of the mass spectrometer inlet orifice as shown in Figure 6-6, and 0 kV was applied to the EO pump B channel. In both configurations, the voltage applied to the EO pump A channel was optimized for the highest signal from the analyte emitter. An infusion of leucine enkephalin revealed a similar composition of ions for both configurations; however, a 12% decrease in signal intensity was observed for the sequentially operated, dual emitter configuration.

To demonstrate the speed at which two solutions can be analyzed, reserpine (reference emitter) and leucine enkephalin (analyte emitter) were sequentially electrosprayed at 2 s intervals. Photographs of the laser light scatter from the electrospray plumes are shown in Figure 6-6. Reconstructed ion chromatograms for the $[M+H]^+$ ions of reserpine (609 m/z) and leucine enkephalin (556 m/z), as measured by the Tof instrument, are shown in Figure 6-7A,B. Each time the voltage was applied, the electrospray signal immediately recovered from the "off" state to its previous signal intensity. In this experiment, the ion intensities of the analyte and reference signals were approximately equal. A reconstructed ion chromatogram for both ions, shown in

Figure 6-7C, had an RSD of 7.2%. Even with the fast data acquisition rate (~15 Hz), large spikes or dips in the combined signal were not observed, demonstrating a seamless transition from one electrospray source to another. A portion of the time scale in Figure 6-7 is expanded in Figure 6-8 to reveal the switching speed between electrospray signals. At the time of 14.52 s the reference electrospray was turned off and the analyte electrospray was turned on. This data shows that the switch occurred in less than 70 ms (the time required for 1 summed scan and 2 interscan delays). Video imaging of the light scattered by the electrospray plume suggests that the switching time was <33 ms as only one video frame shows electrospray plumes from both emitters.

Next, the dual ESI device was synchronized with the QTof mass spectrometer and used for infusion ESI-MS with internal calibration. During these experiments a single reference scan was completed every 5 s. The software (MassLynx, Waters Corp.) automatically stored the reference and analyte data in separate files. Ideally there should be no analyte signal present in the reference data file and no reference signal in the analyte data file. To quantify the amount of crosstalk, 1 min of data from the reference and analyte data file was summed and is shown in Figure 6-9. No analyte signal was found in the reference data file and vice versa. The raw analyte data was stored and the "accurate mass measure" function in the software (MassLynx, Waters Corp.) was later used to apply a "continuous masslock correction" using the reserpine $[M+H]^+$ ion (609.2812 m/z). A comparison of the mass error between the raw and corrected analyte signal is shown in Figure 6-10A. Each data point represents 12 spectra from the analyte signal (leucine enkephalin, $[M+H]^+$) that were summed, smoothed (twice by Savitzky-Golay, 4 channels) and centroided (top 80% of peak). The mass error root mean squared

values for the raw and corrected analyte signal were 61.9 ppm and 1.4 ppm, respectively. All corrected measurements had a mass error less than 3 ppm as shown in Figure 6-10B, which is within the 5 ppm specification for the commercial dual ESI source on this instrument.

6.4 Conclusion

Simple microfluidic devices were used for sequential electrospray of two different solutions without the need for external pressure sources or any moving parts. In this demonstration, a single ion was used for internal calibration; however, multiple ions over the entire m/z range of interest may also be used to improve the mass accuracy. Future work should focus on integration of electrokinetically-driven separation mechanisms (e.g. CE, CEC, MEKC) on the microchip dual ESI device. In addition to internal calibration, this dual emitter technology may prove useful in monitoring multiple microfluidic separations with a single mass spectrometer.

6.5 Figures

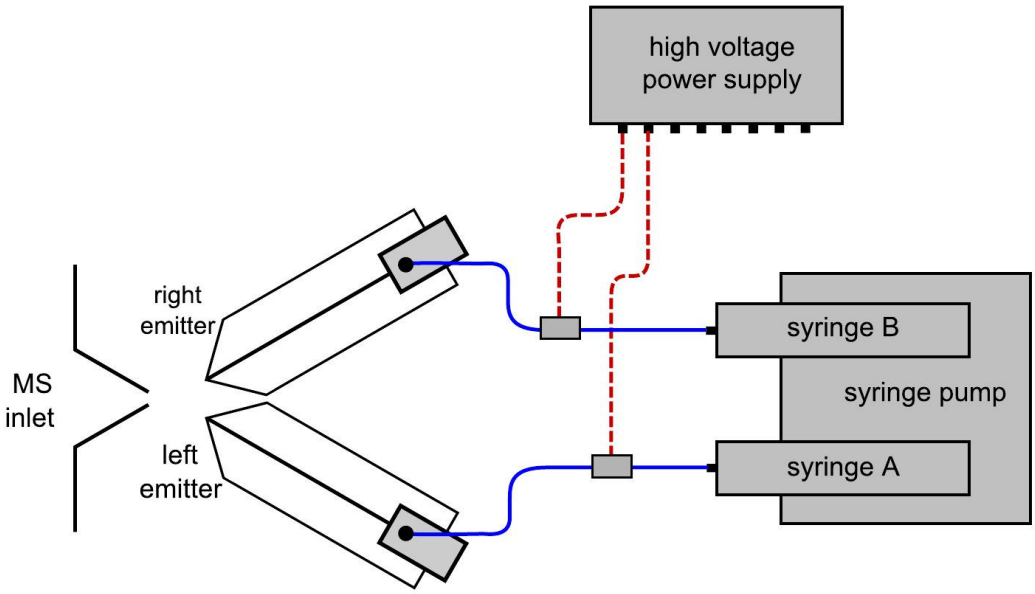

Figure 6-1. Schematic for the pressure-driven dual ESI setup.

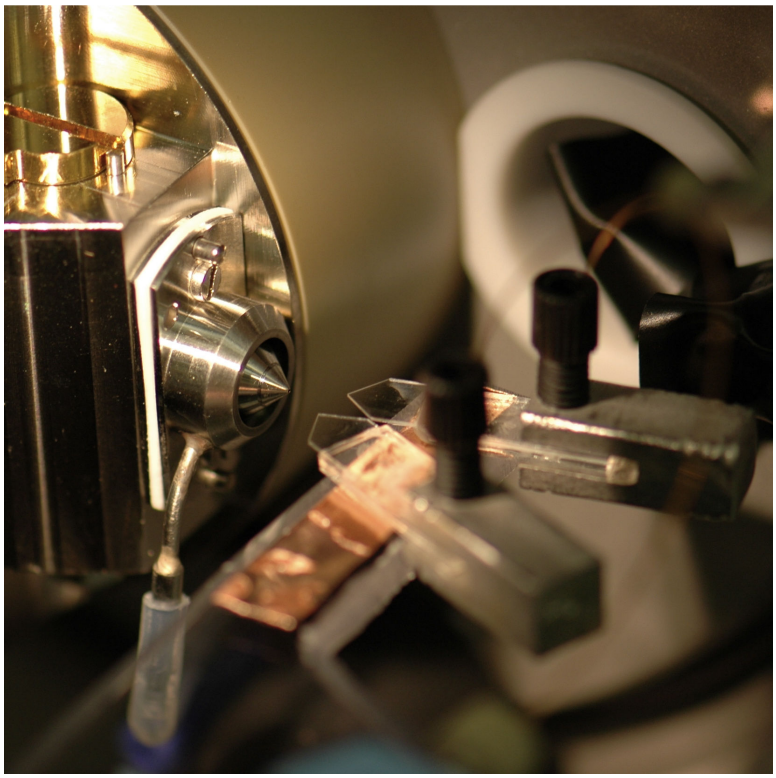

Figure 6-2. Photograph of the two pressure-driven microchip emitters positioned in front of the inlet of the mass spectrometer according to the schematic in Figure 6-1.

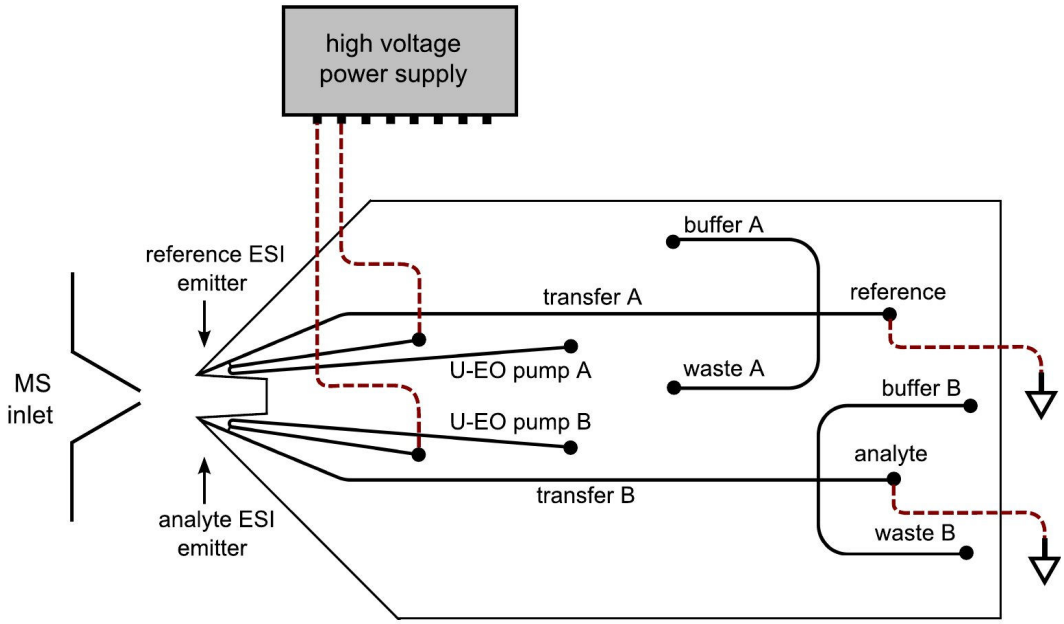

Figure 6-3. Schematic of the microchip dual ESI device. A nanojunction connects the transfer channels and the U-shaped EO pump channels.

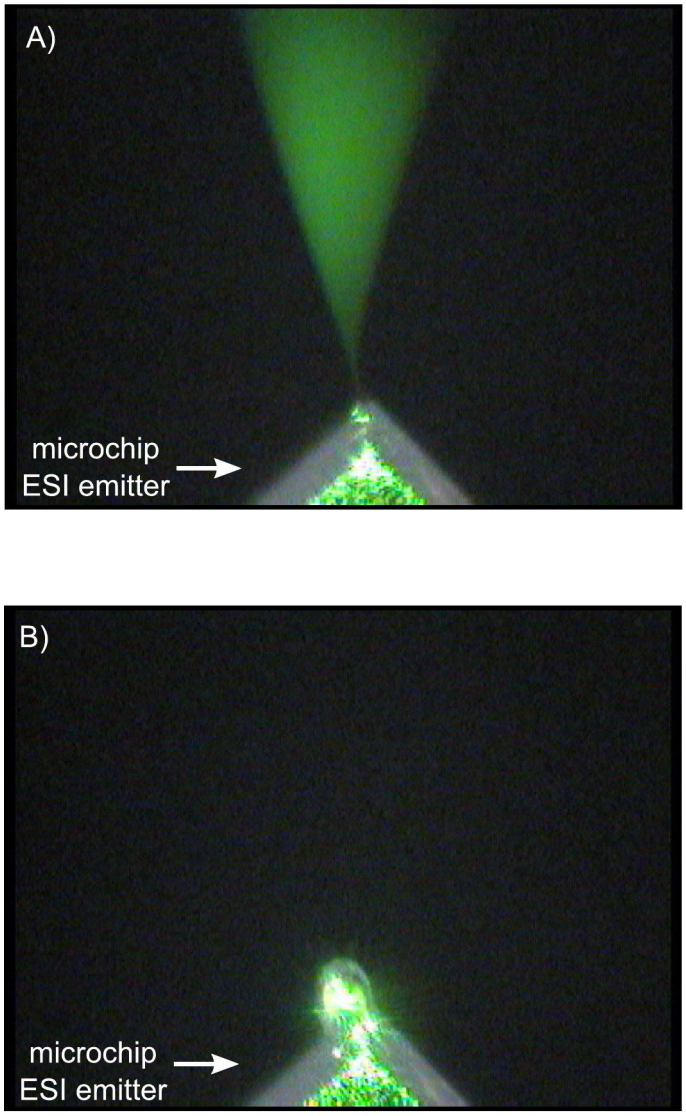

Figure 6-4. A single microchip emitter positioned on axis with the inlet of the mass spectrometer showing A) the electrospray plume at the optimal emitter voltage, B) droplet formation at an attenuated emitter voltage.

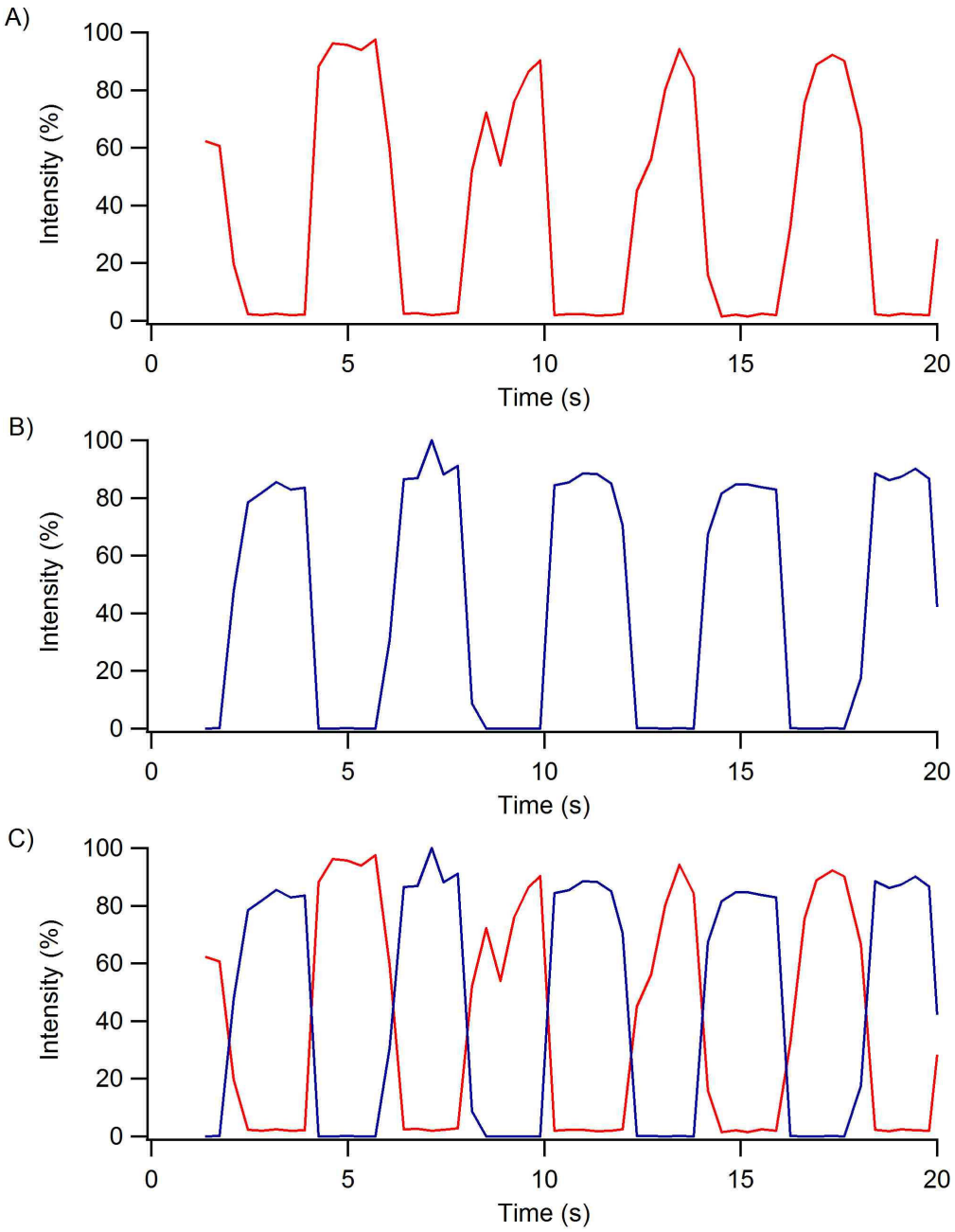

Figure 6-5. Sequential sampling of ions produced from the A) left emitter [leucine enkephalin], B) right emitter [angiotensin II], C) both emitters (overlaid)

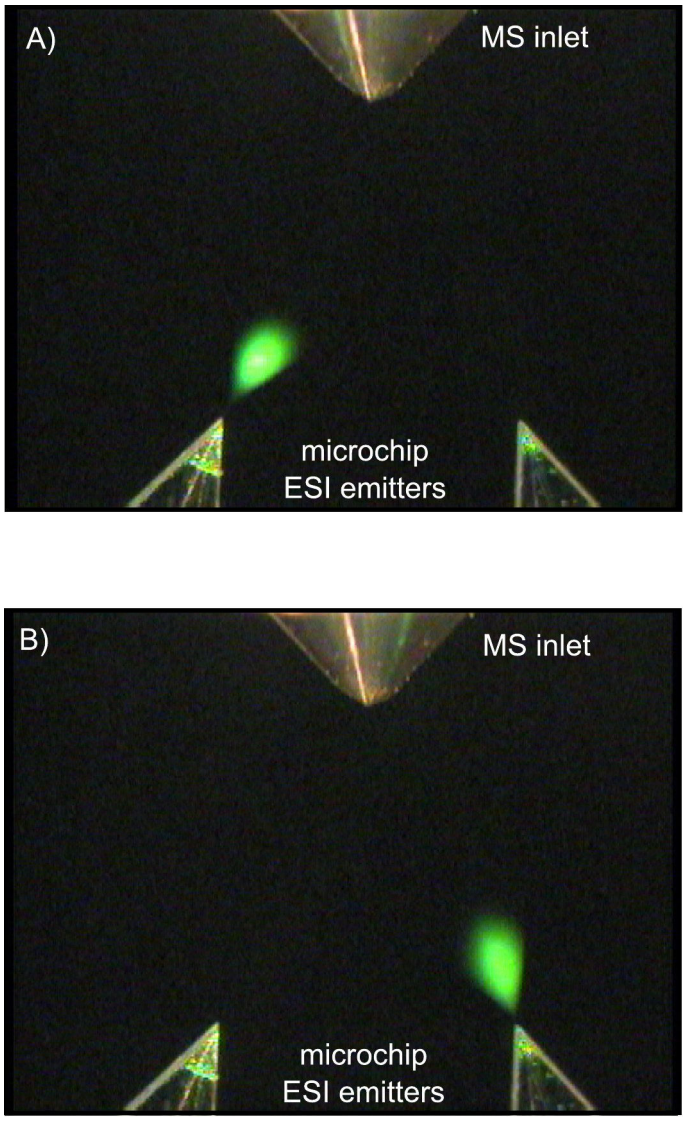

Figure 6-6. Microchip dual ESI device with A) analyte emitter active and B) reference emitter active. The electrospray plumes are illuminated with green diode lasers.

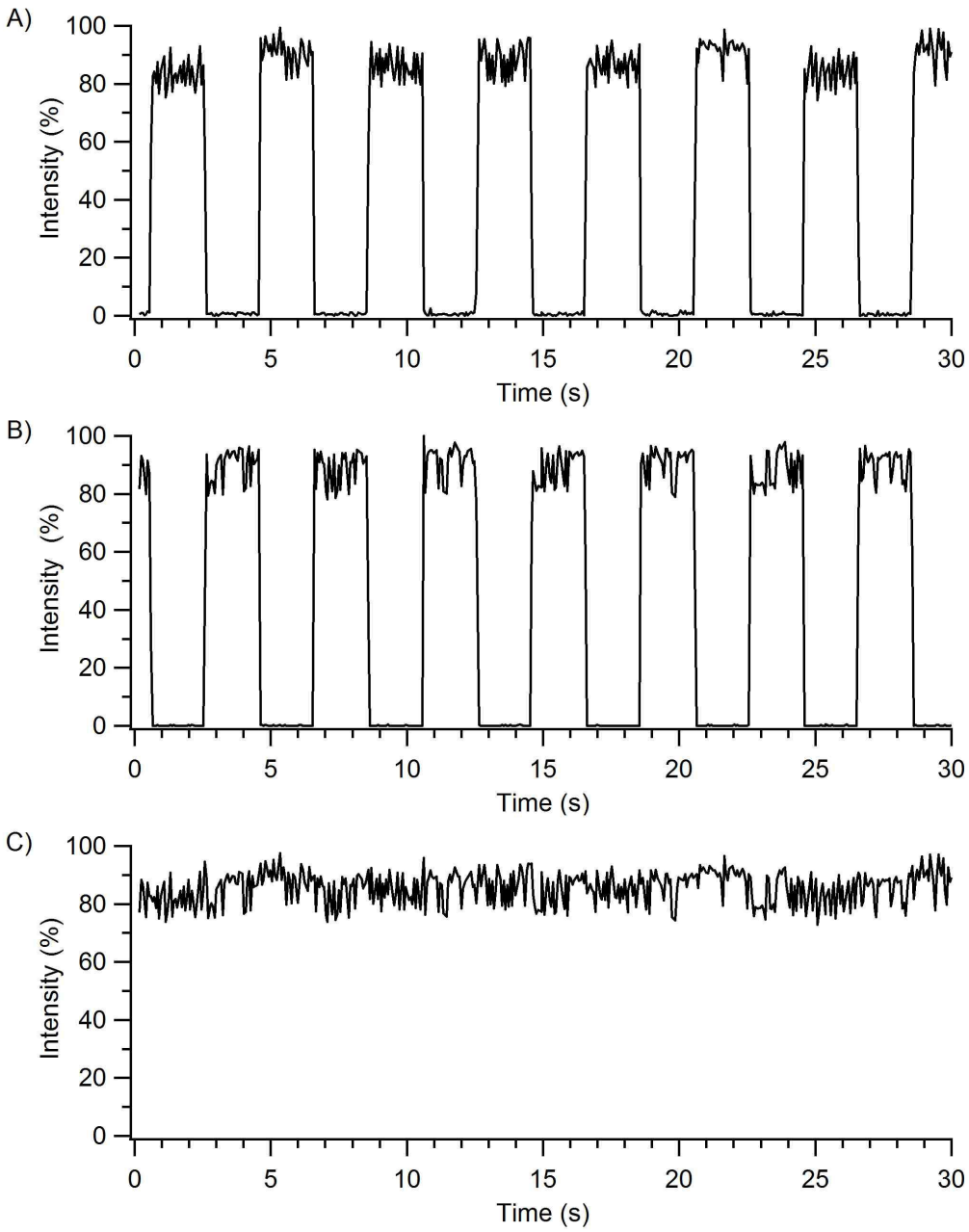

Figure 6-7. Sequential sampling of analyte and reference materials every 2 s. Reconstructed ion chromatograms are shown for A) reference signal [reserpine] B) analyte signal [leucine enkephalin] and C) the combined reference and analyte signal.

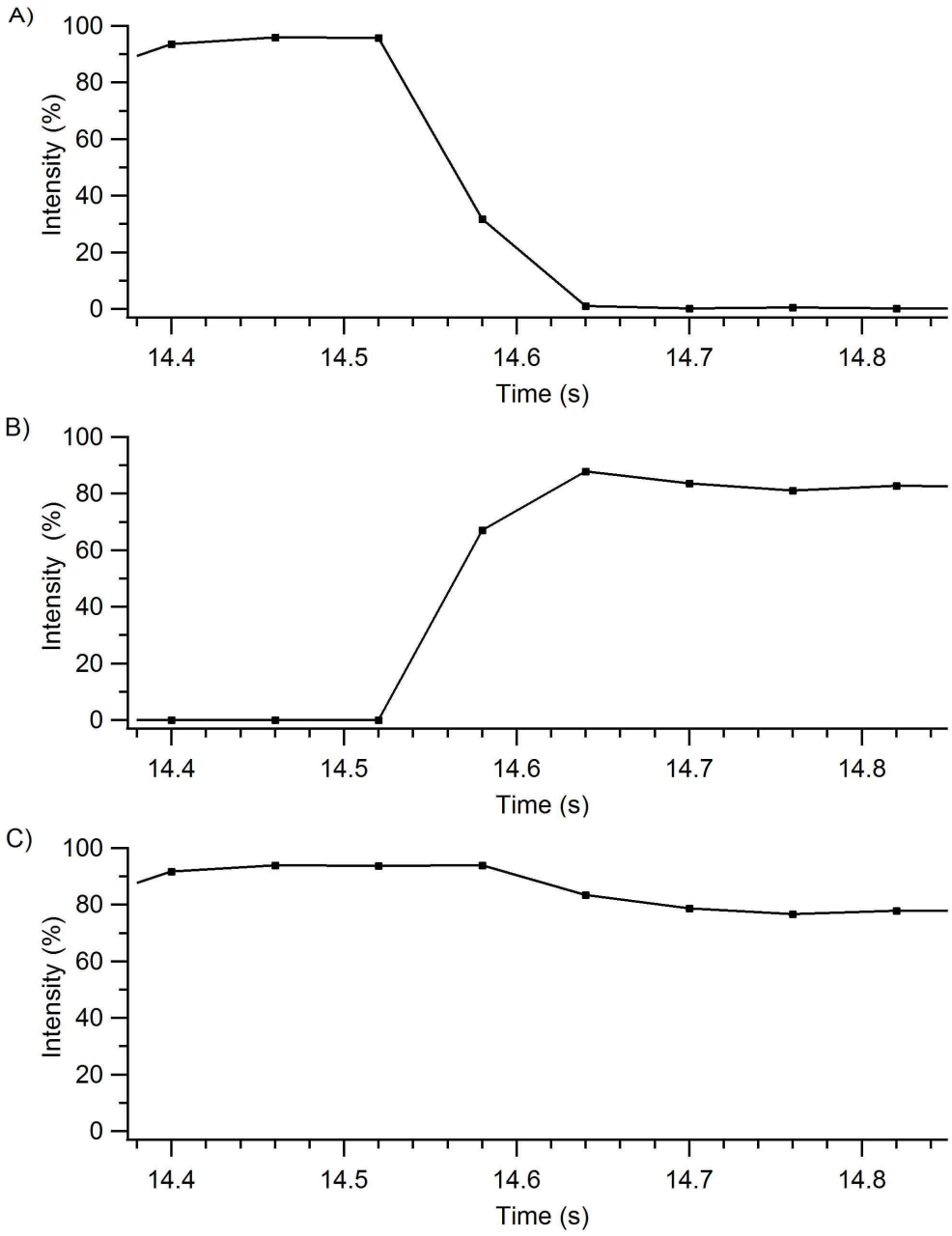

Figure 6-8. Enlarged section of the data in Figure 3. Reconstructed ion chromatograms are shown for A) reference signal [reserpine] B) analyte signal [leucine enkephalin] and C) the combined reference and analyte signal. At 14.52 s the reference electrospray is turned off and the analyte electrospray is turned on.

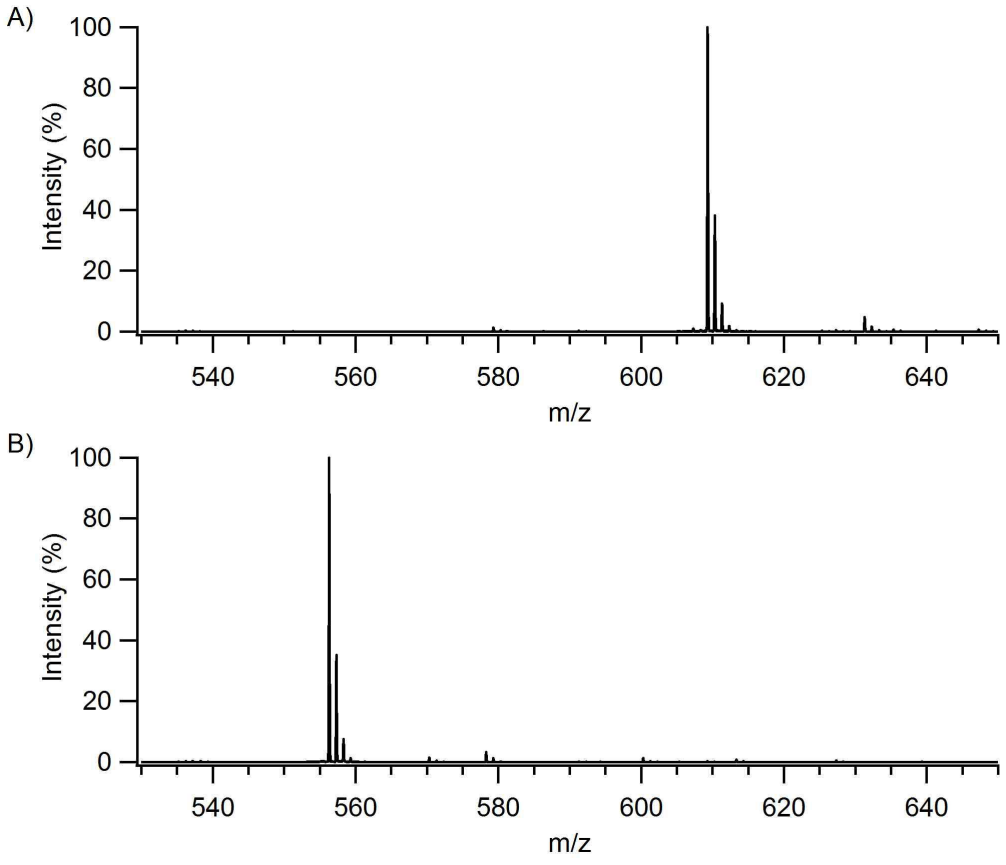

Figure 6-9. One minute of summed mass spectra from the A) reference [reserpine] and B) analyte [leucine enkephalin] data file.

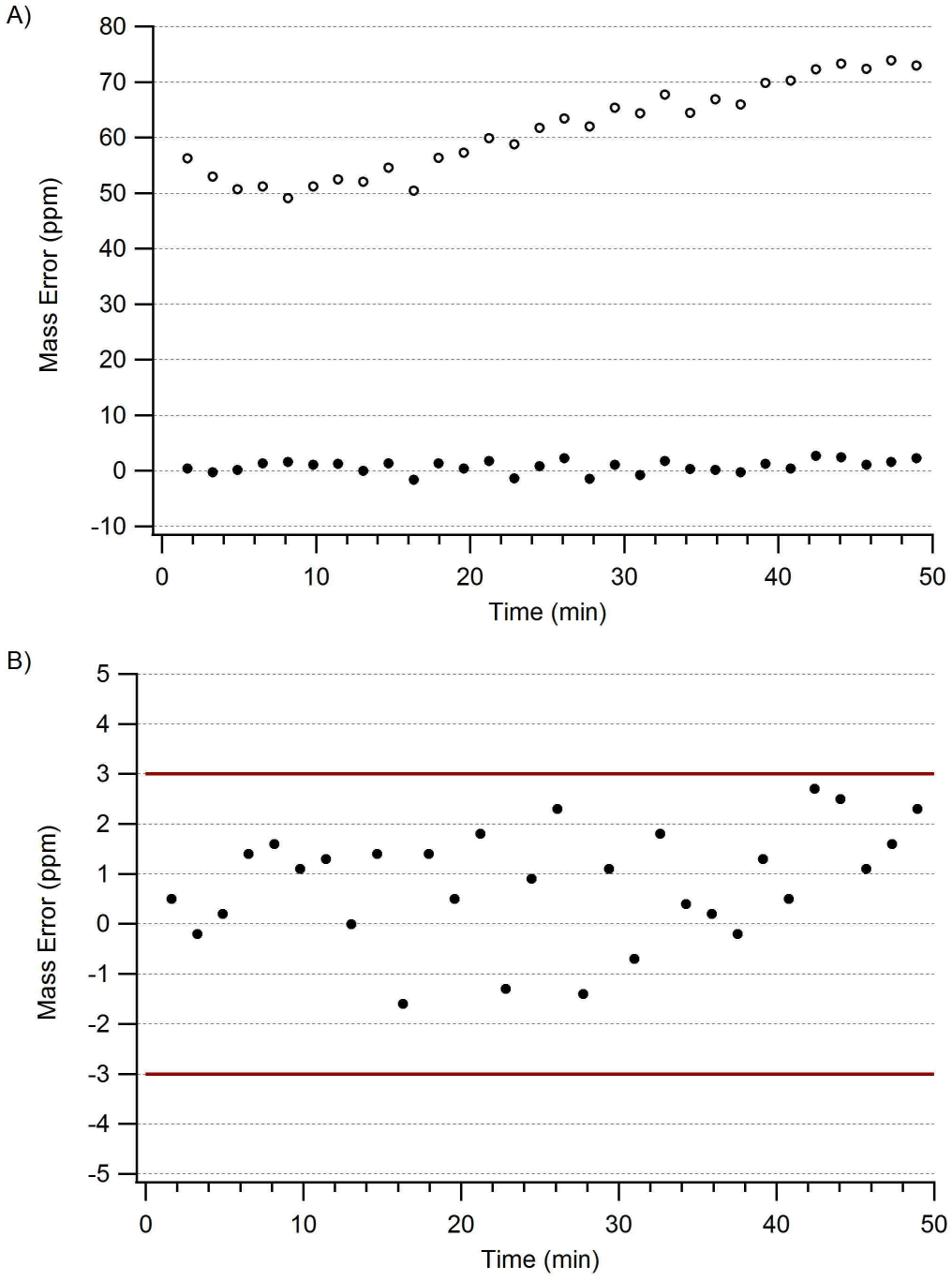

Figure 6-10. A) Mass measurement errors for infusion ESI-MS of leucine enkeplain. Raw data (open circles), corrected data (closed circles). B) Expansion of the mass error axis for the corrected data showing all measurements were within 3ppm.

6.6 References

1. Bristow, A. W. T. Accurate mass measurement for the determination of elemental formula - A tutorial. *Mass Spectrom. Rev.* **2006**, *25*, 99.

2. Liu, T.; Belov, M. E.; Jaitly, N.; Qian, W. J.; Smith, R. D. Accurate mass measurements in proteomics. *Chem. Rev.* **2007**, *107*, 3621.

3. Sojo, L. E.; Lum, G.; Chee, P. Internal standard signal suppression by co-eluting analyte in isotope dilution LC-ESI-MS. *Analyst* **2003**, *128*, 51.

4. Charles, L. Flow injection of the lock mass standard for accurate mass measurement in electrospray ionization time-of-flight mass spectrometry coupled with liquid chromatography. *Rapid Commun. Mass Spectrom.* **2003**, *17*, 1383.

5. Jiang, L. F.; Moini, M. Development of multi-ESI-sprayer, multi-atmospheric-pressure-inlet mass spectrometry and its application to accurate mass measurement using time-of-flight mass spectrometry. *Anal. Chem.* **2000**, *72*, 20.

6. Zhou, F.; Shui, W. Q.; Lu, Y.; Yang, P. Y.; Gu, Y. L. High accuracy mass measurement of peptides with internal calibration using a dual electrospray ionization sprayer system for protein identification. *Rapid Commun. Mass Spectrom.* **2002**, *16*, 505.

7. Glish, G. L.; Danell, R.M. (The University of North Carolina, Chapel Hill, NC, USA) Electrospray ionization device. U.S. Patent 6,703,611, March 9, 2004.

8. Takahashi, Y.; Fujimaki, S.; Kobayashi, T.; Morita, T.; Higuchi, T. Accurate mass determination by multiple sprayers nano-electrospray mass spectrometry on a magnetic sector instrument. *Rapid Commun. Mass Spectrom.* **2000**, *14*, 947.

9. Hannis, J. C.; Muddiman, D. C. A dual electrospray ionization source combined with hexapole accumulation to achieve high mass accuracy of biopolymers in fourier transform ion cyclotron resonance mass spectrometry. *J. Am. Soc. Mass Spectrom.* **2000**, *11*, 876.

10. Flora, J. W.; Hannis, J. C.; Muddiman, D. C. High-mass accuracy of product ions produced by SORI-CID using a dual electrospray ionization source coupled with FTICR mass spectrometry. *Anal. Chem.* **2001**, *73*, 1247.

11. Nepomuceno, A. I.; Muddiman, D. C.; Bergen, H. R.; Craighead, J. R.; Burke, M. J.; Caskey, P. E.; Allan, J. A. Dual electrospray ionization source for confident generation of accurate mass tags using liquid chromatography Fourier transform ion cyclotron resonance mass spectrometry. *Anal. Chem.* **2003**, *75*, 3411.

12. Williams, D. K.; McAlister, G. C.; Good, D. M.; Coon, J. J.; Muddiman, D. C. Dual electrospray ion source for electron-transfer dissociation on a hybrid linear ion trap-orbitrap mass spectrometer. *Anal. Chem.* **2007**, *79*, 7916.

13. Eckers, C.; Wolff, J. C.; Haskins, N. J.; Sage, A. B.; Giles, K.; Bateman, R. Accurate mass liquid chromatography/mass spectrometry on orthogonal acceleration time-of-flight mass analyzers using switching between separate sample and reference sprays. 1. Proof of concept. *Anal. Chem.* **2000**, *72*, 3683.

14. Wolff, J. C.; Eckers, C.; Sage, A. B.; Giles, K.; Bateman, R. Accurate mass liquid chromatography/mass spectrometry on quadrupole orthogonal acceleration time-of flight mass analyzers using switching between separate sample and reference sprays. 2. Applications using the dual-electrospray ion source. *Anal. Chem.* **2001**, *73*, 2605.

15. Satomi, Y.; Kudo, Y.; Sasaki, K.; Hase, T.; Takao, T. Accurate mass measurement in nano-electrospray ionization mass spectrometry by alternate switching of high voltage between sample and reference sprayers. *Rapid Commun. Mass Spectrom.* **2005**, *19*, 540.

16. Schneider, B. B.; Douglas, D. J.; Chen, D. D. Y. Multiple sprayer system for high-throughput electrospray ionization mass spectrometry. *Rapid Commun. Mass Spectrom.* **2002**, *16*, 1982.

17. Tang, K. Q.; Tolmachev, A. V.; Nikolaev, E.; Zhang, R.; Belov, M. E.; Udseth, H. R.; Smith, R. D. Independent control of ion transmission in a jet disrupter dual-channel ion funnel electrospray ionization MS interface. *Anal. Chem.* **2002**, *74*, 5431.

18. Belov, M. E.; Zhang, R.; Strittmatter, E. F.; Prior, D. C.; Tang, K.; Smith, R. D. Automated gain control and internal calibration with external ion accumulation capillary liquid chromatography-electrospray ionization-fourier transform ion cyclotron resonance. *Anal. Chem.* **2003**, *75*, 4195.

19. Foret, F.; Kusy, P. Microfluidics for multiplexed MS analysis. *Electrophoresis* **2006**, *27*, 4877.

20. Dayon, L.; Abonnenc, M.; Prudent, M.; Lion, N.; Girault, H. H. Multitrack electrospray chips. *J. Mass Spectrom.* **2006**, *41*, 1484.

21. Burgreen, D.; Nakache, F. R. Electrokinetic flow in ultrafine capillary slits *J. of Phys. Chem.* **1964**, *68*, 1084.

22. Hu, J. S.; Chao, C. Y. H. A study of the performance of microfabricated electroosmotic pump. *Sens. Actuators, A: Phys.* **2007**, *135*, 273.

23. Rulison, A. J.; Flagan, R. C. Scale-up of electrospray atomization using linear arrays of taylor cones. *Rev. Sci. Instrum.* **1993**, *64*, 683.

24. Kelly, R. T.; Page, J. S.; Tang, K. Q.; Smith, R. D. Array of chemically etched fused-silica emitters for improving the sensitivity and quantitation of electrospray ionization mass spectrometry. *Anal. Chem.* **2007**, *79*, 4192.

25. Mellors, J. S.; Gorbounov, V.; Ramsey, R. S.; Ramsey, J. M. Fully integrated glass microfluidic device for performing high-efficiency capillary electrophoresis and electrospray ionization mass spectrometry. *Anal. Chem.* **2008**, *80*, 6881.